

Winter 2012

# Interaction between the coastal ocean and the estuarine systems

Shivanesh Arvinda Rao  
*University of New Hampshire, Durham*

Follow this and additional works at: <https://scholars.unh.edu/dissertation>

---

## Recommended Citation

Rao, Shivanesh Arvinda, "Interaction between the coastal ocean and the estuarine systems" (2012). *Doctoral Dissertations*. 704.  
<https://scholars.unh.edu/dissertation/704>

This Dissertation is brought to you for free and open access by the Student Scholarship at University of New Hampshire Scholars' Repository. It has been accepted for inclusion in Doctoral Dissertations by an authorized administrator of University of New Hampshire Scholars' Repository. For more information, please contact [nicole.hentz@unh.edu](mailto:nicole.hentz@unh.edu).

# INTERACTION BETWEEN THE COASTAL OCEAN AND THE ESTUARINE SYSTEMS

BY

SHIVANESH ARVINDA RAO

Bachelor of Science, University of the South Pacific, 2001  
Postgraduate Diploma, Department of Physics, 2002  
Master of Science, University of the South Pacific, 2005

DISSERTATION

Submitted to the University of New Hampshire  
in partial fulfillment of  
the requirements for the Degree of

Doctor of Philosophy

in

Earth and Environmental Science: Oceanography

December 2012

UMI Number: 3537826

All rights reserved

INFORMATION TO ALL USERS

The quality of this reproduction is dependent upon the quality of the copy submitted.

In the unlikely event that the author did not send a complete manuscript and there are missing pages, these will be noted. Also, if material had to be removed, a note will indicate the deletion.



UMI 3537826

Published by ProQuest LLC 2013. Copyright in the Dissertation held by the Author.

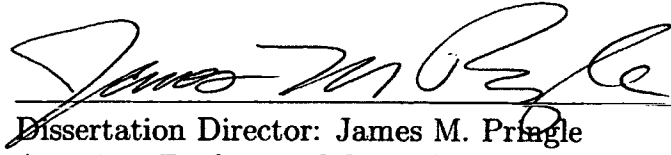
Microform Edition © ProQuest LLC.

All rights reserved. This work is protected against unauthorized copying under Title 17, United States Code.



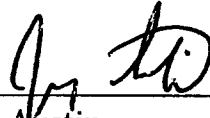
ProQuest LLC  
789 East Eisenhower Parkway  
P.O. Box 1346  
Ann Arbor, MI 48106-1346

This dissertation has been examined and approved.



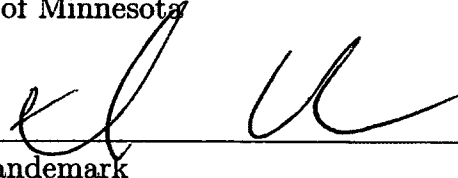
---

Dissertation Director: James M. Pringle  
Associate Professor of Earth Sciences  
Institute for the Study of Earth, Oceans, and Space  
University of New Hampshire



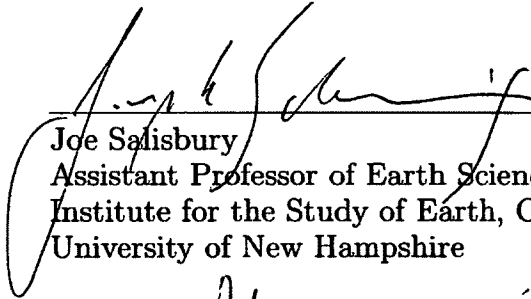
---

Jay A. Austin  
Associate Professor, Department of Physics  
Large Lake Observatory  
University of Minnesota



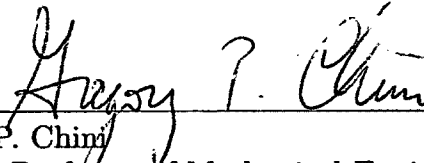
---

Douglas Vandemark  
Associate Professor of Earth Sciences  
Institute for the Study of Earth, Oceans, and Space  
University of New Hampshire



---

Joe Salisbury  
Assistant Professor of Earth Sciences  
Institute for the Study of Earth, Oceans, and Space  
University of New Hampshire



---

Gregory P. Chini  
Associate Professor of Mechanical Engineering  
Department of Mechanical Engineering  
University of New Hampshire

09/14/2012

---

Date



# ACKNOWLEDGMENTS

First and foremost, I would like to thank Professor Jamie Pringle for his guidance for this thesis. I sincerely appreciate his patience with my writing, and his advice and support through the course of the last six years, without which this thesis would not have been possible. I also like to thank Jamie, Zorana and Alex for their company on-campus and during family holiday celebrations.

I like to thank my dissertation committee members: Professor Jay Austin from the University of Minnesota, and from the University of New Hampshire: Professor Doug Vandemark, Professor Greg Chini, and Professor Joe Salisbury. I appreciate their time dedicated to reviewing the drafts of the thesis and offering valuable improvements.

My friends and colleagues at OPAL: Deb, Amanda P., Mimi, Olivia, Philip, Vincent, Michael, Amanda H., Ariel, Melika, and Megan; I sincerely appreciated their good company during classes and during weekend excursions. My stay in Babcock Hall and UNH would have been a much less exciting and confined to a 2 km radius around campus if it had not being for the opalites and my international friends.

I appreciate the teaching assistantship support provided by the Earth Science department and the research assistantship by the National Science Foundation Grant OCE 0453792, which provided my core support at UNH. I also like to thank Jen Bourgeault from NRESS for making sure I was meeting my program deadlines, Dovev Levine from Graduate School for reviewing my thesis, and Donna Thibault and Sue Clark for facilitating my stay at OPAL and Earth Sciences.

Finally, I would like to thank Mom, Dad, and my siblings Varun and Vrinda, for supporting me in all my studies and endeavors in Fiji and the US, and bearing with my six-year absence from home. This thesis, I dedicate to them as recompense.

# TABLE OF CONTENTS

ACKNOWLEDGMENTS . . . . .	iii
LIST OF TABLES . . . . .	vii
LIST OF FIGURES . . . . .	x
ABSTRACT . . . . .	xx
<b>1 Introduction</b>	<b>1</b>
1.1 How Estuarine Plumes Influence the Coastal Ocean . . . . .	3
1.2 How Fluctuating Winds and Coastal Ocean Influence the Estuary . . . . .	4
1.3 Outline . . . . .	6
<b>2 Upwelling Relaxation and Estuarine Plumes</b>	<b>10</b>
2.1 Abstract . . . . .	10
2.2 Introduction . . . . .	11
2.3 Description of Numerical Model . . . . .	15
2.3.1 Configuration of Numerical Model . . . . .	15
2.3.2 External Model Forcings . . . . .	18
2.3.3 The Response of the Base Case Numerical Experiment. . . . .	20
2.3.4 Observational Data . . . . .	22
2.4 Observations . . . . .	23
2.5 Derivation and Testing of our Predictor . . . . .	26
2.5.1 Testing Predictions Against Numerical Model . . . . .	31
2.6 Testing our Predictor Against Field Observations . . . . .	34
2.7 Discussion and Conclusions . . . . .	35

<b>3</b>	<b>Weather-Band Fluctuations In Wind Alters The Estuary-Ocean Exchange.</b>	<b>61</b>
3.1	Abstract . . . . .	61
3.2	Introduction . . . . .	61
3.3	Description of the Numerical Model . . . . .	63
3.3.1	External Model Forcing . . . . .	67
3.4	Equations for Salt Fluxes at Estuary Mouth . . . . .	69
3.5	Results . . . . .	70
3.5.1	How Fluctuating Winds Alter the Salt Exchange of Estuaries . . . . .	71
3.6	Discussion . . . . .	81
3.7	Conclusions . . . . .	84
<b>4</b>	<b>How Weather-Band Fluctuations in the Wind Alter the Steady State of an Estuary.</b>	<b>104</b>
4.1	Abstract . . . . .	104
4.2	Introduction . . . . .	105
4.3	Description of the Numerical Model . . . . .	107
4.3.1	External Model Forcing . . . . .	111
4.4	Steady State Balance . . . . .	112
4.5	Results . . . . .	115
4.5.1	Base Case with Winds both in the Estuary and Coastal Ocean . . . . .	115
4.5.2	Base Case with Winds only in the Coastal Ocean . . . . .	117
4.5.3	Well-Mixed Estuaries . . . . .	119
4.5.4	Other Estuarine and Coastal Conditions . . . . .	120
4.6	Discussion . . . . .	121
4.6.1	Adjustment Time . . . . .	123
4.6.2	Extension to other Estuaries . . . . .	124
4.7	Conclusions . . . . .	126

<b>5 Conclusions</b>	<b>141</b>
5.0.1 Future Direction of This Study . . . . .	144

# List of Tables

2.1	The range of variations used in our numerical experiments. . . . .	39
2.2	The base numerical experiment forcings and results as described in Sec. 2.3.3. . . . .	39
2.3	The predictions tested against the CoOP observations shows our predicted mechanism matches the observed mechanism for all seven events at Duck. When $L > 85$ km, then the plume is predicted to arrive at Duck first, otherwise the front returns to coast first. $\overline{\tau_{UW}}$ is the time-averaged wind stress over the duration of the upwelling winds, $t_{UW}$ is the duration of the upwelling winds, $\overline{\tau_{DW}}$ is the time-averaged downwelling wind stress, and $h$ is the cross-shore averaged plume thickness. $c_p$ is the speed of the plume under no wind forcing, $\bar{v}$ is the wind-induced alongshore flow, $v_{amb}$ is the ambient alongshore flow, and $L$ (Eq. 2.18) is the alongshore region where the plume arrives first. The last three columns show the mechanism predicted by $L$ to arrive nearshore at Duck, 85 km downwave of Chesapeake Bay, the mechanism observed in the CoOP observations, and if predicted and observed mechanisms match. PL indicates the plume arrives nearshore first and FR indicates the returning upwelled front is first. . . . .	40

2.4 The mean seasonal region,  $L$ , where the plume arrives nearshore first, for some common estuary-coastal ocean system. The length of the region is computed with the assumption that the mixed layer depth remains constant. The averages are for Delaware Bay 2006-2007; Chesapeake Bay 2006-2007; Hudson Bay 2005-2006; Columbia River 2008-2009 and Penobscot River 2008-2009. The plume speed  $c_p$  observations are from Yankovsky and Chapman (1997), the plume thickness are from Hickey et al. (1998); Pettigrew et al. (1998); Banas et al. (2009), and the remaining parameters are derived from NDBC stations 44009, ducn7, sgrn4, 46029 and 44033. Using  $r = 3 \times 10^{-4} \text{ m s}^{-1}$  and  $\rho = 1025 \text{ kg m}^{-3}$ .  $\overline{\tau^{UW}}$  and  $\overline{\tau^{DW}}$  are the average alongshore wind stress for wind events longer than an inertial period.  $t_{UW}$  is the duration of the upwelling winds after the front has formed. . . . . 41

3.1 The mean and standard deviation of the alongshore wind stress amplitude for several regions around the US coast. The data is averaged for the summer and winter seasons using 5 years of NDBC buoy historical observations from either 2000-2004 or 2005-2009. The orientation of the local coastline is used to determine the alongshore component of the fluctuating winds. The wind stress is estimated using  $\tau = \rho C_d u^2$ ; where  $\rho \sim 1.3 \text{ kg m}^{-3}$ ,  $C_d \sim 10^{-3}$ ,  $u$  is wind speed. . . . . 85

3.2 The net salt flux and depth-averaged and exchange salt fluxes averaged over the 30 days duration of (1<sup>st</sup> row) only coastal fluctuating winds. Also shown are the change in the average salinity of the estuary  $\delta \bar{s}_{est}$ , the residence time  $T_R$ , and the salinity difference between the estuary outflow and oceanic inflow  $\Delta S$  for different parameters of the estuary and the coastal ocean. The values in braces show the influence of only coastal winds. . . . . 86

3.3	Similar to Table 3.2, but showing the winds applied both and estuary and coastal ocean for different parameters of the estuary and the coastal ocean. The values in braces show the influence of only estuarine winds. . . . .	87
4.1	The range of parameters varied in the permutations of the numerical experiment. . . . .	128

# List of Figures

2-1	Cartoon of the upwelling mechanism transporting the upwelled front offshore with a cross-shore sectional view. The black dots indicate the nearshore and offshore moorings. . . . .	42
2-2	During wind-reversal, the onshore flow can transport the upwelled front back to the coast. The arrival of less dense water along the coast can be due to the front returning to the coast or the arrival of a plume from the upwave estuary. We predict the alongshore extent of the plume when the front returns to the coast near the southern boundary. . . .	43
2-3	The study area downwave of Chesapeake Bay, along North Carolina. The CoOP observations are centered at the Duck pier station and span from Chesapeake Estuary mouth to North of Cape Hatteras. The transects are T1, T2, T3, T4, T5, T6, and T7 in the downwave direction from estuary, see Lentz and Largier (2006). Triangles are CTD casts and circles are moored CT meters at Duck. . . . .	44
2-4	The schematics of the numerical model bathymetry. (A) The plan view of the model domain with the offshore boundary at 100 km. The upwave alongshore distance is 50 km while the downwave alongshore distance varies each numerical experiment with a minimum of 315 km. (B) The coastal ocean has a uniform alongshore bathymetry shown in the cross-section view. (C) The estuary has a uniform bathymetry with a length of 100 km and a width of 20 km approximating wide estuary systems. . . . .	45



2-5	(A) The stratification in the coastal ocean shown as a salinity profile. The temperature is constant. (B) The alongshore surface wind stress $\tau^{sx}$ is applied to the entire model domain. The ramping of the wind stress occurs over an inertial period. The downwelling wind continues until the end of the numerical simulation. . . . .	46
2-6	Alongshore salinity ( $\text{g kg}^{-1}$ ) at the coast as function of time in days. The vertical isohalines indicate the upwelled front moving offshore (upwelling) or onshore (downwelling). The dark shade along the coast at day 22 is the plume before upwelling winds. The sloping isohalines indicate the estuary plume progressing downwave with time. The front returns to the coast at day 27 and is seen in the plot as a decrease in surface salinity during the downwelling phase (between 150-250km), and the arrow shows the downwave position of the plume head at the time the upwelled front returns to the coast. The shaded region shows the freshwater plume from the estuary. . . . .	47
2-7	The cross-section of salinity ( $\text{g kg}^{-1}$ ) and tracer at 60 km downwave of the estuary. The darker shading shows the high tracer arriving with the plume. The sections are at times (A) 1 day before wind-reversal (B) onset of wind-reversal (C) 1 day after wind-reversal (D) 3 days after wind-reversal. The $32.5 \text{ g kg}^{-1}$ isohaline shows the position of the upwelled front. . . . .	48

- 2-8 (A) Coastal surface salinity ( $\text{g kg}^{-1}$ ) plot of the numerical model at the time the coastal halocline returns back to the coast wall, i.e., the upwelled front returns to the coast. The dashed lines are cross-sections upwave and downwave of the plume head. (B) Cross-shore slice upwave of the plume head shows the plume arrives nearshore before the front returns to the coast. (C) Cross-shore slice downwave of the plume head shows the front returning to the coast before the plume arrives. . . . 49
- 2-9 The time-series plot at the Duck pier station. (A) Low pass filtered (Flagg et al., 1976, PL33 filter) alongshore wind stress  $\tau^{sx}$  (Pa). Positive values are upwelling and negative values are downwelling. Near-surface and near-bottom salinity ( $\text{g kg}^{-1}$ ) time-series for moorings at (B) 1.5 km and (C) 5.5 km offshore. The dashed lines are the near-bottom salinity and the solid lines are the near-surface salinity. UWR1 indicates the period of upwelling wind relaxation [UWR] event 1. WR1P indicates the period of wind-reversal [WR] event 1 with plume-[P] arriving before front-[F]. The light shades show the upwelling relaxation duration and the darker shades show the duration of wind-reversal events. 50

2-10	(A-E) The cross-shore plots of salinity (psu), and (E-H) the cross-shore plots of sigma density ( $\text{kg m}^{-3}$ ) for the same periods at Duck pier station. The depth is in decibars, and the dark line is $\sigma_t=22 \text{ kg m}^{-3}$ . (A & E) On 16 August, the plume arrives before the front returns to coast. (B & F) The restart of the upwelling winds moved the plume offshore on 21 August. (C & G) After wind-reversal on 23 August, the less dense water nearshore is due to return of the upwelled front. (D & H) The plume arrives on 25 August after the front returned to the nearshore during downwelling winds. The temperature (not shown here) remained uniform during these events. The inverted triangles are cross-shore CTD shipboard cast locations and the dots are the locations of the 1.5 km and 5.5 km moorings of CT meters. . . . .	51
2-11	Same as Fig. 2-9 but for a shorter period 14-26 August. . . . .	52
2-12	Similar to Fig. 2-10. (A-B) The cross-shelf plots of salinity (psu) and (C-D) sigma density ( $\text{kg m}^{-3}$ ) for the same periods at Duck pier station. The depth is in decibars, and the dark line is $\sigma_t=22 \text{ kg m}^{-3}$ . (A & C) On 19 August the upwelling winds moved the surface layer offshore. (B & D) After the winds relax the less dense water nearshore is due to arrival of plume on 21 August. . . . .	53
2-13	The predictions of alongshore region $L$ , (km) where the plume arrives nearshore before the upwelled front, compared to numerical model results. The predictions and numerical results are in good agreement. The plot shows variations in the upwelling wind duration from 2.5-5 days, variations in the downwelling wind stress from 0.025-0.2 Pa, and variations in estuary salinity (hence plume density) from 5-25 $\text{g kg}^{-1}$ . . . . .	54

2-14	Similar as Fig. 2-13. Components of scaling from our theory are compared with numerical model experiments. (A) Offshore position of the upwelled front (B) onshore velocity of the upwelled front, (C) plume speed using Eq. 2.15 and the plume thickness at coast, and (D) the plume speed using the more complete form of the plume speed from Gill (1982) and the average plume thickness. . . . .	55
3-1	Our numerical experiments are modeled after the large estuaries and coastal ocean of the Mid-Atlantic Bight, including Chesapeake Bay and Delaware Bay. . . . .	88
3-2	The numerical domain used in our experiments (A) the plan view of the numerical domain; colors indicate the depth and the lattice structure shows the depth grid points. The blue arrows show spatially uniform fluctuating winds in the estuary and the coastal ocean, and the red arrows show spatially uniform fluctuating wind only in the coastal ocean. (B) The cross-sectional view into the estuary mouth, and (C) the cross-shore view of the coastal ocean; black is water and white is estuary bottom. . . . .	89
3-3	(A) The salinity profile for the coastal ocean in the base case numerical experiment. The profile represents summer conditions in the MAB. (B) The winds used in the base case numerical experiment. The winds ramp to maximum amplitude over a duration of a day. The winds are applied for a duration of 30 days, and has a time-averaged wind-stress amplitude of zero. . . . .	90
3-4	A cartoon of the along-estuary section. The salt exchange, i.e., net salt flux of the estuary is decomposed into two components; the depth-averaged salt flux, $F_D$ and the exchange salt flux, $F_{Ex}$ . . . . .	91

3-5	The change in the exchange salt flux, $F_{EX}$ , plotted against the change in the depth-averaged salt flux, $F_D$ , for fluctuating winds only in the estuary. The change in $F_{EX}$ due to fluctuating winds in the estuary are nearly always much larger than the change in $F_D$ . The dashed line is the 1:1 proportionality line. . . . .	92
3-6	The red line shows the influence of the coastal winds only, the blue lines shows the influence of both estuarine and coastal winds, and the black arrows show the influence of only estuarine winds. Positive y-axis means estuary is losing salt and negative means estuary is gaining salt. The salt exchange, i.e., net salt flux (averaged over 30 days of wind) plotted as a function of estuarine and coastal conditions: (A) wind-stress amplitude, (B) wind-stress period, (C) estuary angle; positive angle are above west direction and negative angles are below west direction, (D) coastal pycnocline depth, (E) estuary thalweg depth, (F) river discharge, (G) coastal bottom slope, (H) alongshore flow, and (I) wind-stress amplitude representative of different regions. When there are no winds, the time-averaged net salt flux is close to zero. . . . .	93
3-7	The percentage change in the volume exchange flux, $Q_{Ex}$ (pink bars) and $\Delta S$ (blue bars) for different estuarine and coastal conditions, for only estuarine winds are applied to the model run. Negative percentage indicates the $\Delta S$ is larger than the $\Delta S$ for the no wind model run of each parameter permutation. The percent change in $\Delta S$ is much larger than the change in $Q_{Ex}$ , so the wind influence on the salt exchange is mostly due to changes in $\Delta S$ . . . . .	94
3-8	Same as Figure 3-7, but for winds applied only in the coastal ocean. Positive percentage indicates the $\Delta S$ is smaller than the $\Delta S$ for the no wind model run of each parameter permutation. . . . .	95

3-9	The time-averaged net salt flux over 30 days of fluctuating winds as a function of the starting phase of the winds. The red line show winds only in the coastal ocean and the blue line show winds applied both on the ocean and the estuary, and the black arrows are the influence of winds only in the estuary. . . . .	96
3-10	A cartoon of how winds influence an estuary that is oblique to the coast and the coastal winds. The red arrows show the coastal wind directions and the depth-averaged flow caused by (A) coastal upwelling winds, and (B) down-welling winds, and the blue arrows show the depth-averaged flow forced by the along-estuary component of the coastal winds. For this orientation in the Northern hemisphere, the depth-averaged flows driven by the coastal and along-estuary winds counter each other (Garvine, 1985). . . . .	97
3-11	A cartoon of how alongshore flow, $v$ , changes the slope of the coastal pycnocline and sea-surface in the absence of winds, moving the deep salty coastal water (A) away from the estuary mouth, and (B) towards the estuary mouth. The dashed lines show pycnocline and sea-surface in absence of alongshore flow. . . . .	98
3-12	Cartoon of the across-estuary salt structure (A) narrow, and (B) wide estuaries. In the absence of winds, the wider estuary allows for Rossby adjustment, thus slumping the isopycnals across the estuary mouth and reducing the vertical stratification. . . . .	99
3-13	Time-averaged net salt flux as a function of the estuary width. Red line shows winds only in the coastal ocean and blue line shows the winds both in the estuary and coastal ocean. . . . .	100

4-1	Our numerical experiments are modeled after the large estuaries and coastal ocean of the Mid-Atlantic Bight, including the Chesapeake Bay and Delaware Bay. . . . .	129
4-2	The numerical domain used in our experiments (A) the plan view of the numerical domain; colors indicate the depth and the lattice structure shows the depth grid points. The blue arrows show spatially uniform fluctuating winds in the estuary and the coastal ocean, and the red arrows show spatially uniform fluctuating wind only in the coastal ocean. (B) The cross-sectional view into the estuary mouth, and (C) the cross-shore view of the coastal ocean; black is water and white is estuary bottom. . . . .	130
4-3	(A) The salinity profile for the coastal ocean in the base case numerical experiment. The profile represents summer conditions in the MAB. (B) The winds used in the base case numerical experiment. The winds ramp to maximum amplitude over a duration of a day. The winds are applied for a duration of 210 days, and has a time-averaged wind-stress amplitude of zero. . . . .	131
4-4	A cartoon of the along-estuary section. The salt exchange, i.e., net salt flux of the estuary is decomposed into two components; the depth-averaged salt flux, $F_D$ and the exchange salt flux, $F_{Ex}$ . . . . .	132

- 4-5 The tidally-averaged salt for the range of wind-stress amplitude in Table (4.1). The dotted lines are for winds only in coastal ocean and solid lines are winds on estuary and coastal ocean. The colored lines show the wind-stress for 0.05 Pa (red), 0.1 Pa (blue), 0.2 Pa (green). The influence of winds in the estuary shows a much larger change in average salinity than coastal winds alone. The fluctuations in the average salt are due the coastal winds fluctuating between upwelling and down-welling. . . . . 133
- 4-6 The along-estuary salt gradients ( $\times 10^{-5} \text{g kg}^{-1} \text{m}^{-1}$ ), when forced by fluctuating winds, as function of time. Solid line are winds applied both on estuary and coastal ocean, dashed lines are the winds applied only to the coastal ocean. (A) wind-stress amplitude (0.05Pa-red, 0.1Pa-blue, 0.2Pa-green), (B) wind-stress period (6day-red, 10day-blue, 30day-green), (C) well-mixed estuary (0.1Pa-red), (D) river discharge ( $200 \text{m}^3 \text{s}^{-1}$ -red,  $2 \times 10^3 \text{m}^3 \text{s}^{-1}$ -blue,  $20 \times 10^3 \text{m}^3 \text{s}^{-1}$ -green), (E) estuary thalweg depth (11m-red, 30m-blue, 45m-green), (F) estuary length (50km-red, 150km-blue, 300km-green), (G) coastal pycnocline depth (11m-red, 15m-blue, 45m-green), (H) time-integrated wind-stress amplitude (east-red, west-blue, steady-green), and (I) estuary orientation ( $-60^\circ$ -red,  $0^\circ$ -blue,  $60^\circ$ -green). . . . . 134
- 4-7 The evolution of the along-estuary salt gradient as a function of time. The starting phase of the fluctuating winds is upwelling when the legend label is positive, and down-welling when the legend label is negative. (A) Fluctuating winds applied both in estuary and coastal ocean for different wind-stress amplitude. (B) Fluctuating winds applied only in coastal ocean for different wind-stress amplitudes. The starting phase of the fluctuating has no significant influence on the adjustment. 135



4-8 The evolution of the along-estuary salt gradient as function of time, for different estuary widths. The fluctuating winds are applied both in the estuary and the coastal ocean. . . . . 136

4-9 The adjustment times for the range of conditions in Table (4.1). The dotted lines show the 1:2 and 2:1 proportionality lines. The predictions of the adjustment times are in line with numerical experiments. . . . 137

**ABSTRACT**

**INTERACTION BETWEEN THE COASTAL OCEAN  
AND THE ESTUARINE SYSTEMS**

by

Shivanesh Arvinda Rao

University of New Hampshire, December, 2012

Fluctuating winds change the interaction between an estuary and its adjacent coastal ocean. This change in the interaction determines how the wind-induced changes in the estuary influence the near-shore coastal ocean and vice-versa.

The first chapter examines the water properties in the near-shore coastal region close to estuaries after coastal upwelling. In regions where the time-integrated upwelling and down-welling wind stresses are comparable, there exists a region in the direction of a coastal Kelvin wave propagation from an estuary, where the arrival of the plume in the near-shore region prevents the upwelled front from returning to the coast. The weakened vertical stratification in the plume during down-welling winds allows vertical mixing, so the weak cross-shore flow in the plume stops the front from returning to the coast.

The second chapter examines the transient response of the interaction between an estuary and its adjoining coastal ocean, when forced by weather-band fluctuations in the wind. Over timescales shorter than the time taken for the estuary to adjust to a new steady state,  $T_{adj}$ , the initial stratification of an estuary and the coastal ocean control the influence of fluctuating winds on the salt exchange between the two regions. The wind-induced mixing in the estuary has by far the greatest effect on the salt exchange, compared to the coastal upwelling and down-welling. The changes in the salt exchange are largely due to changes in the salinity leaving and entering the estuary, and not the volume exchange.

The final chapter examines how the steady state of an estuary is altered, when forced by weather-band fluctuations in the wind. For timescales longer than  $T_{adj}$ , the influence of fluctuating winds on the stratification or the exchange of an estuary is not significant, but instead the fluctuating winds alter the salt intrusion length of the estuary. However, when  $T_{adj}$  (when forced by fluctuating winds) is short compared to the time of the initial change caused by the vertical mixing, the influence of fluctuating winds in a stratified estuary reduces the stratification and the exchange.

# CHAPTER 1

## Introduction

The estuary and the near-shore coastal ocean are highly productive areas: the runoff from land supplies a high flux of nutrients into the estuary, and the coastal upwelling and down-welling modulate the supply of nutrients from the bottom coastal ocean to the surface (e.g., Shanks et al. (2000); Shanks and Brink (2005); Shanks et al. (2002)). The supply of nutrients into these shallow, well-lit regions allow for primary productivity that provides food for many species. Since most of the residential and commercial activity in the world is located around these estuarine and coastal regions, the associated anthropogenic impact can adversely alter the health of the estuarine and near-shore coastal ecosystems (Scully, 2010; Cerco et al., 2004). This can lead to a potentially hazardous environment to developing larvae and juvenile species, as well as to humans. Understanding these impacts require a qualitative understanding of the state of the two regions, during their transient response to forcings and in steady state. The two regions are important because the changes in one region can influence the adjacent region, through the interaction between them.

The state of the estuary (Hansen and Rattray, 1965) and the state of the near-shore coastal ocean (Austin and Lentz, 2002) are governed by the interaction between an estuary and its adjacent coastal ocean. This interaction happens through the estuarine gravitational circulation, which depends on the along-estuary salinity gradient and the vertical stratification in an estuary, which are ultimately set by the freshwater inflow, oceanic salinity and the vertical mixing in the estuary (Hansen and Rattray, 1965; MacCready, 1999, 2007; Bowen and Geyer, 2003). In stratified estuaries, the circulation is exchange-dominated, where the landward component of the exchange

brings salty coastal water into the estuary and mixes with the freshwater discharge of the river, and then the seaward component of the exchange discharges the less salty surface estuarine water out of the estuary, onto the coastal shelf (Hansen and Rattray, 1965). The exchange mechanism can be significantly altered by forcings that include (but are not limited to): the daily tidal cycle, spring-neap tidal cycle, and winds. The studies presented in this thesis will focus on how fluctuating winds, varying between upwelling and down-welling, can alter the state of the estuary and the near-shore coastal ocean.

Numerous studies have shown the influence of winds on the estuary and coastal ocean. Hansen and Rattray (1965) provides the theoretical framework that has been used to study the wind-induced circulation in an estuary, and more recently MacCready (1999) derived analytical solutions that solve the estuarine circulation when there is a step change in the river or tidal forcing. Austin and Lentz (2002) provides the simplified framework that has been used to study the influence of separate upwelling and down-welling winds on a stratified coastal ocean. However, in the studies of the estuary the coastal ocean is often assumed a homogeneous body that is unaltered by the estuarine discharge (e.g., Hansen and Rattray (1965); MacCready (1999)), and in studies of coastal ocean the estuary is often a point source (Fong and Geyer, 2001, 2002). One of the contributions of our work is to consider a spatially resolved stratified estuary and stratified coastal ocean in our experiments (Rao et al., 2011). This allows us a qualitative understanding of the significance of the changes in the coastal ocean on the estuary, and vice versa.

Our studies are largely carried out by numerical experiments and where possible field observations. These experiments are modeled after the types of conditions found in the estuaries and coastal ocean along the Mid-Atlantic Bight (MAB). Although the model is based on the MAB to make use of the readily available coastal observations to support and test the model results, the core conditions of the MAB are common

with several other regions, which ensure wider applicability of our work.

These core conditions include a 2-layer type coastal stratification, an estuary with the along-estuary salinity decreasing from ocean salinity at the estuary mouth to freshwater at the head of the estuary, and wind-forcing with very weak mean along-shore fluctuating winds. Our analyses examine how these core conditions in the hydrography of an estuary and coastal ocean change due to fluctuating winds. Once we understand how the core conditions evolve, our results are extended to other conditions of the hydrography and meteorological forcing, such that the length of the estuary, coastal pycnocline depth, angle of the estuary, strength of the wind stress, etc.

## 1.1 How Estuarine Plumes Influence the Coastal Ocean

The influence of an estuary on the coastal ocean is due to the estuarine discharge onto the coastal shelf (e.g., Garvine (1999); Yankovsky and Chapman (1997)). This discharge forms a stationary rotating bulge and a buoyant coastal current along the coast (Fong and Geyer, 2002). The estuarine discharge onto the coastal shelf turns right after exiting the estuary mouth (in the northern hemisphere) forming a coastal current that propagates in the direction of a coastal Kelvin wave (Garvine, 2001). This behaviour has been observed in field observations (Rennie et al., 1999), numerical experiments (Garvine, 2001), and in the laboratory (Lentz and Helfrich, 2002). Garvine (1995) determined a system that separates the plume into different classes (i) where the rotational effects are important as the inertial effects and (ii) where rotation can be ignored. In our study, the effects of rotation are important.

The behavior of the plume can be further classed as surface-advected plumes where the plume does not contact the bottom, or bottom-advected plumes where the

plume contacts the bottom and bottom friction is important (Lentz and Helfrich, 2002; Yankovsky and Chapman, 1997). However, this classification can be altered by alongshore winds (Fong and Geyer, 2001). In the absence of external forcing such as winds, the coastal plume is surface-advected and in geostrophic balance, as it propagates along the coast (Lentz and Helfrich, 2002); this is supported by field observations (Rennie et al., 1999). However, external forcings such as tides and winds can alter the structure of the coastal plume. Alongshore winds such as upwelling winds force an offshore surface Ekman flow that spreads the plume offshore, finally detaching the plume from the coast and its estuarine source, thus stopping the alongshore movement of the plume (Fong and Geyer, 2001). In contrast, down-welling winds force a onshore surface Ekman flow that brings the coastal plume closer to the coast causing the cross-shelf density to intensify, causing the plume to propagate faster downwave (Fong and Geyer, 2001; Rao et al., 2011). Coastal and estuarine winds are usually continuous and often fluctuate between upwelling and down-welling, e.g., along the North Carolina coast (Austin and Lentz, 1999), that can cause the estuarine plume to move offshore during upwelling and then return when the wind direction reverses to down-welling. This study extends the above studies (e.g., Fong and Geyer (2001, 2002); Austin and Lentz (1999)) by examining the onshore transport of the upwelled coastal plume when forced by fluctuating winds, and the competing alongshore transport of a new estuarine coastal plume.

## **1.2 How Fluctuating Winds and Coastal Ocean Influence the Estuary**

Estuaries are regions where the salt water from the ocean mix with the fresh water of a river, thus setting the circulation in the estuary and the exchange between an estuary and a coastal ocean. The exchange depends on the along-estuary salinity

gradient and the vertical stratification in an estuary, which are ultimately set by the freshwater inflow, oceanic salinity and the vertical mixing in the estuary (Hansen and Rattray, 1965; MacCready, 1999, 2007; Bowen and Geyer, 2003). The oceanic salinity at the coast and thus at the estuary mouth is modulated by the coastal upwelling and down-welling (Austin and Lentz, 2002). Hansen and Rattray (1965) examines these important parameters that control the estuary circulation for exchange-dominated estuaries, and recently MacCready (1999) extended this work to include diffusion-dominated estuaries.

Understanding the initial response and adjustment of an estuary is important because the hydro-graphic structure in the estuary depends on these processes. The study by (MacCready, 1999) and others already examine what happens when there is increased vertical mixing in an estuary. In their studies, the background vertical mixing coefficient is altered in a step-change, which provides us with a robust understanding of how mixing (due to any mixing mechanism) would influence the estuary and its adjustment.

However, winds influence the estuary and coastal ocean in many significant ways, other than simple mixing. This includes (but are not limited to) (i) inducing Ekman transport in the estuary and coastal ocean, which could alter the volume exchange flow of the estuary, (ii) coastal upwelling and down-welling (Austin and Lentz, 1999), which can alter the salinity entering the estuary, (iii) driving depth-averaged flows in the estuary due to coastal sea surface setup by coastal Ekman transport (Garvine, 1985), and (iv) in cases of estuaries at an angle to the coast, the alongshore winds can tilt the sea-surface slope in the estuary, driving depth-averaged flow (Garvine, 1985). These wind-induced processes can significantly alter the estuary beyond the useful but simplified mixing approach of previous studies.

In our studies of the influence of fluctuating winds in the exchange between an estuary and a coastal ocean, we examine the above wind-induced processes, thus



providing a much more realistic evaluation of the influence of reversing alongshore winds on the estuary-ocean system. This approach used in our study fills a crucial gap in the knowledge of how the fluctuating winds, directly and by proxy, influence the initial response and the following adjustment to a new steady state.

The influence of fluctuating winds are examined at two timescales: (i) the transient time, which is the time taken for an initial change caused by fluctuating winds, this timescale helps us understand the unsteady response of the exchange of the estuary due to the influence of passing weather systems, and (ii) the steady state time, which is the time taken for the estuary to reach the new steady state; this timescale helps us understand how the steady state of an estuary changes as climate change alters the long-term variability in the weather. One of the contributions of this study is how fluctuating winds on a stratified coastal ocean can alter the exchange of the estuary.

### 1.3 Outline

The goal of this study is to examine influence of fluctuating winds on an estuary and a coastal ocean. In particular, the focus of this study is on examining how the fluctuating winds alter the salt structure in an estuary and the near-shore coastal ocean. In this thesis several theory length and timescales are derived and tested against numerical experiments and field observations where possible.

The outline of the thesis is as follow. In chapter 2, the evolution of the salt structure in the near-shore coastal ocean (down-wave of an estuary) is examined, when fluctuating winds upwell and then down-well the coastal plume towards the coast. The key result of this study is that there exists a near-shore region down-wave of an estuary where the upwelled coastal plume (“old” plume) does not reach when forced by down-welling winds. Instead this region is always influenced by the “new” coastal plume that propagates down-wave of the estuary, once the “old” plume

detaches from the estuary. In chapter 3, the influence of weather-band fluctuations in the winds on the net salt flux of an estuary is examined. In this study, we are interested in the transient response of the estuary to fluctuating winds. The timescale of this response is less than the time-taken for the estuary to reach its new steady state. The key result of this study is that the initial influence of wind-induced mixing (due to the fluctuating winds) in the estuary is to reduce the stratification and the net salt flux of the estuary. For a range of conditions, the wind-induced mixing in the estuary has a larger influence than the change in the coastal salinity drawn into the estuary. In chapter 4, the influence of weather-band fluctuations in the winds is examined again, but in this chapter the changes to the steady state of the estuary is examined. The key result of this study was the fluctuating winds in the estuary have little influence in altering the stratification of the estuary, but instead the estuary salt intrusion lengthens or shortens to adjust to the fluctuating winds. In both chapters 3 and 4, the changes in a stratified coastal ocean (due to fluctuating winds) has little influence on the net salt flux of an estuary, and these changes are only important when the estuary is already well-mixed or sheltered from estuarine winds. In chapter 5, the results of the thesis are summarised.

# Bibliography

- Austin, J. and S. Lentz, 1999: The Relationship Between Synoptic Weather Systems and Meteorological Forcing on the North Carolina Inner Shelf. *Journal of Geophysical Research-Oceans*, **104 (C8)**, 18 159–18 185.
- Austin, J. and S. Lentz, 2002: The Inner Shelf Response to Wind-Driven Upwelling and Downwelling. *Journal of Physical Oceanography*, **32 (7)**, 2171–2193.
- Bowen, M. and W. Geyer, 2003: Salt transport and the time-dependent salt balance of a partially stratified estuary. *Journal of Geophysical Research-Oceans*, **108 (C5)**, doi: 10.1029/2001JC001231.
- Cerco, C., M. Noel, and L. Linker, 2004: Managing for water clarity in Chesapeake Bay. *Journal of Environmental Engineering-ASCE*, **130 (6)**, 631–642, doi: 10.1061/(ASCE)0733-9372(2004)130:6(631).
- Fong, D. and W. Geyer, 2001: Response of a River Plume During an Upwelling Favorable Wind Event. *Journal of Geophysical Research-Oceans*, **106 (C1)**, 1067–1084.
- Fong, D. and W. Geyer, 2002: The alongshore transport of freshwater in a surface-trapped river plume. *Journal of Physical Oceanography*, **32 (3)**, 957–972, doi: 10.1175/1520-0485(2002)032<0957:TATOFI>2.0.CO;2.
- Garvine, R., 1985: A Simple-Model of Estuarine Subtidal Fluctuations Forced by Local and Remote Wind Stress. *Journal of Geophysical Research-Oceans*, **90 (NC6)**, 1945–1948, doi: 10.1029/JC090iC06p11945.
- Garvine, R., 1995: A Dynamical System For Classifying Buoyant Coastal Discharges. *Continental Shelf Research*, **15 (13)**, 1585–&, doi: 10.1016/0278-4343(94)00065-U.
- Garvine, R., 1999: Penetration of Buoyant Coastal Discharge onto the Continental Shelf: A Numerical Model Experiment. *Journal of Physical Oceanography*, **29 (8, Part 2)**, 1892–1909.
- Garvine, R., 2001: The impact of model configuration in studies of buoyant coastal discharge. *Journal of Marine Research*, **59 (2)**, 193–225, doi: 10.1357/002224001762882637.
- Hansen, D. and M. Rattray, 1965: Gravitational circulation in straits and estuaries. *Journal of Marine Research*, **23**, 104–122.
- Lentz, S. and K. Helfrich, 2002: Buoyant Gravity Currents Along a Sloping Bottom in a Rotating Fluid. *Journal of Fluid Mechanics*, **464**, 251–278.

- MacCready, P., 1999: Estuarine adjustment to changes in river flow and tidal mixing. *Journal of Physical Oceanography*, **29** (4), 708–726, doi: 10.1175/1520-0485(1999)029<0708:EATCIR>2.0.CO;2.
- MacCready, P., 2007: Estuarine adjustment. *Journal of Physical Oceanography*, **37** (8), 2133–2145, doi: 10.1175/JPO3082.1.
- Rao, S., J. Pringle, and J. Austin, 2011: Upwelling relaxation and estuarine plumes. *Journal of Geophysical Research-Oceans*, **116**, doi: 10.1029/2010JC006739.
- Rennie, S., J. Largier, and S. Lentz, 1999: Observations of a Pulsed Buoyancy Current Downstream of Chesapeake Bay. *Journal of Geophysical Research-Oceans*, **104** (C8), 18 227–18 240.
- Scully, M., 2010: The Importance of Climate Variability to Wind-Driven Modulation of Hypoxia in Chesapeake Bay. *Journal of Physical Oceanography*, **40** (6), 1435–1440, doi: 10.1175/2010JPO4321.1.
- Shanks, A. and L. Brink, 2005: Upwelling, Downwelling, and Cross-Shelf Transport of Bivalve Larvae: Test of a Hypothesis. *Marine Ecology-Progress Series*, **302**, 1–12.
- Shanks, A., J. Largier, L. Brink, J. Brubaker, and R. Hooff, 2002: Observations on the Distribution of Meroplankton During a Downwelling Event and Associated Intrusion of the Chesapeake Bay Estuarine Plume. *Journal of Plankton Research*, **24** (4), 391–416.
- Shanks, A. L., J. Largier, L. Brink, J. Brubaker, and R. Hooff, 2000: Demonstration of the Onshore Transport of Larval Invertebrates by the Shoreward Movement of an Upwelling Front. *Limnology and Oceanography*, **45** (1), 230–236, URL <http://www.jstor.org/stable/2670803>.
- Yankovsky, A. and D. Chapman, 1997: A Simple Theory for the Fate of Buoyant Coastal Discharges. *Journal of Physical Oceanography*, **27** (7), 1386–1401.

# CHAPTER 2

## Upwelling Relaxation and Estuarine Plumes

### 2.1 Abstract

After coastal upwelling, the water properties in the nearshore coastal region close to estuaries is determined by the race between the new estuarine plume travelling along the coast and the upwelled front (a marker for the old upwelled plume and the coastal pycnocline) returning to the coast under downwelling winds. Away from an estuary, downwelling winds can return the upwelled front to the coast bringing less dense water nearshore. Near the estuary, the estuarine plume can arrive along the coast and return less dense water to the nearshore region before the upwelled front returns to the coast. Where the plume brings less dense water to the coast first, the plume keeps the upwelled front from returning to the coast. In this region, only the plume and the anthropogenic input and larvae associated with the plume waters influence the nearshore after upwelling. We quantify the extent of the region where the plume is responsible for bringing less dense water to the nearshore and keeping the upwelled front from returning to the coast after upwelling. We successfully tested our predictions against numerical experiments and field observations of the Chesapeake plume near Duck, North Carolina. We argue that this alongshore region exists for other estuaries where the time-integrated upwelling and downwelling wind stresses are comparable.

## 2.2 Introduction

Coastal upwelling is a well-understood mechanism (Lentz, 1992; Austin and Lentz, 2002), but the physics of the upwelled front after the upwelling wind stops has received less attention (Send et al., 1987; Alessi et al., 1996; Dale et al., 2008). Upwelling-favorable alongshore winds (which blow with the coast on their left in the Northern Hemisphere) cause offshore Ekman transport in the surface mixed layer (Fig. 2-1). At the coast, this offshore transport can result in a displacement of the coastal pycnocline and, potentially, outcropping to the surface. This outcropping, the upwelled front, separates cold, salty upwelled water near the coast from warm, less-salty surface water offshore. Near estuaries, the surface coastal waters advected offshore also consist of the estuarine plume. On a shallow, stratified shelf, the upwelled front usually forms after about two inertial periods (Austin and Lentz, 2002); in this study we will focus on observations where the upwelled front has formed.

After the upwelling winds cease or reverse, the upwelled front moves shoreward as an ageostrophic buoyant gravity current for an inertial period (Csanady, 1971). When there are no winds, this onshore movement stops after a distance equal to the radius of deformation (Csanady, 1971). The onshore movement of the upwelled front stops after the Rossby adjustment, i.e., the shoreward ageostrophic pressure gradient is balanced by the Coriolis force resulting in an alongshore, geostrophic flow (Austin and Lentz, 2002). In the absence of downwelling winds or alongshore pressure gradients, the upwelled front can only return to coast if the offshore position of the front is closer than the radius of deformation. Using wind-reversal timescales for the east and west coast of US, Austin and Lentz (2002) predicts the upwelled front is usually much farther offshore, so the front does not return to coast as part of the Rossby adjustment process. If and when the upwelling winds reverse to downwelling, the shoreward surface Ekman flow forces the upwelled front towards the coast (Dale et al., 2008). In the absence of a nearby estuary, the return of the upwelled front

to the coast brings back the less dense surface water, initially moved offshore during upwelling, to the coast as the upwelled isopycnals return to their pre-upwelling state.

However, near estuaries, an estuarine plume can arrive along the coast from the estuary before the return of the upwelled front (Fig. 2-2). The plume propagates along the coast in the direction of a coastal Kelvin wave, the downwave direction, from the source estuary (Garvine, 1999; Fong and Geyer, 2001). The speed and distribution of the plume can be altered by the alongshore winds (Fong and Geyer, 2001). As we shall discuss below, the arrival of the plume nearshore keeps the front from returning to the coast. The plume is pushed against the coast during downwelling winds, forcing the plume isopycnals nearly upright and weakening the vertical stratification, similar to Williams et al. (2010). The weak vertical stratification in the plume permits vertical mixing, so the cross-shelf transport in the plume is weak. This is similar to the well-mixed nearshore region, ‘inner shelf’, described by Lentz et al. (1999), where the alongshore wind stress and pressure gradient are balanced by bottom friction. Numerical models have shown that this weak cross-shelf transport in the plume keeps the upwelled front and constituents trapped in it from returning to the coast (Austin and Lentz, 2002). As a result, where the plume arrives along the coast before the upwelled front, the salinity, larval inhabitants, terrestrial nutrient runoff, and pollutants in that region would be consistent with that of the estuary where the plume originated. Outside this region, where the upwelled front returns to the coast, the water properties would be influenced by both the estuarine plume and the coastal processes that affect the water during upwelling and downwelling.

There have been observations of alongshore plumes arriving first in the nearshore region. Along the east coast of US, Fong et al. (1997); Rennie et al. (1999); Cudaback and Largier (2001) show freshwater plumes arriving along the Maine coast and the North Carolina coast. Along the west coast, Send et al. (1987) shows a plume of warm water from the San Francisco Bay moving along the northern California coast.

However, there have also been observations of an upwelled front first returning to the coast during downwelling. In the east coast, Shanks et al. (2000, 2002); Marmorino et al. (2004); Shanks and Brink (2005) show the upwelled front returning to the North Carolina coast. In the west coast, Farrell et al. (1991); Miller and Emlet (1997); Dale et al. (2008) show the upwelled front returning to the California coast and the Oregon coast. What is not clear is where the plume or the upwelled front dominates. In this paper, we show that after upwelling there is a region downwave of an estuary where the plume is responsible for first bringing less dense water nearshore. This region will depend on the race between the alongshore propagating estuarine plume whose properties are primarily set by the estuary, and the shoreward returning upwelled front whose properties are set by the older upwelled low-salinity plumes and coastal processes.

We will focus on the role of the plume as the downwelling winds force the upwelled front shoreward. We derived an estimate of the region where the plume keeps the upwelled front from returning to the coast. This estimate is useful downwave of estuaries such as the Chesapeake Bay and Delaware Bay in the east coast of US or the Columbia River and Puget Sound in the west coast of US. The west coast has long upwelling periods followed by weak winds and a narrower shelf compared to the east coast, and while our focus is on the east coast (North Carolina, Fig. 2-3), we generalize our results to other coastal shelves in the discussion. We discuss where our estimate is applicable and how it will vary with the size and nature of the estuary and coastal regions.

Our work differs from prior studies (e.g., Garvine (1999); Simpson (1997)) because we estimate the length of the region close to an estuary where the plume can keep the upwelled front from returning to the coast after upwelling; our estimate is not the eventual length of a plume. Field observations show that an upwelled front arriving at the coast first does not stop the alongshore propagation of the plume



beyond that point (Rennie et al., 1999; Cudaback and Largier, 2001). The size of the plume derived by Garvine (1999) and the region of freshwater influence, ROFI, described by Simpson (1997) determines the eventual length of the plume along the coast from the source estuary. Furthermore, our work examines the advection of less dense, surface water into the nearshore region, which differs from the nearshore mixing-restratification studies on the ROFI (Linden and Simpson, 1988; Sharples and Simpson, 1993; Souza and Simpson, 1997; Burchard and Hofmeister, 2008); in these studies, the investigators examine when tidal, wind, and waves vertically mix the nearshore water column, and the subsequent restratification due to the seaward Rossby adjustment of the mixed water column during periods of low mixing. The dynamics in the ROFI, as discussed in the above literature, can tell us when the plume is vertically mixed during downwelling and our estimate works (i.e., the low cross-shelf transport in the mixed plume can prevent the upwelled front from reaching the coast), and when our estimate will fail.

The paper is organized as follows. Section 2 discusses the methods and configurations utilized for analysis of the numerical experiments and the observations. We examine the base case and tracer experiments and we also show that, as discussed in previous literature, the presence of the plume keeps the upwelled front from returning to the coast. In section 3, we use observations at Duck, NC, to identify periods after upwelling when the plume brings less dense water along the coast and when the front, forced by downwelling winds, brings less dense water along the coast. In section 4, we derive a predictor to estimate where the plume arrives along the coast before the returning upwelled front, and we test it against numerical experiments. In section 5, we test our predictions against CoOP field observations. In section 6, we apply our predictor to other estuaries, discuss in which systems our predictions are applicable, and extend our work to other systems.

## 2.3 Description of Numerical Model

### 2.3.1 Configuration of Numerical Model

#### Configuration of Numerical Model

The numerical model used in this study is the Regional Ocean Modeling System (ROMS). It is a primitive equation finite difference numerical model (Arakawa and Lamb, 1977). The vertical momentum balance is hydrostatic and a free surface is included. We define a constant horizontal eddy viscosity  $A_M$  of  $5.0 \text{ m}^2 \text{ s}^{-1}$  and a horizontal diffusivity  $A_H$  of  $0 \text{ m}^2 \text{ s}^{-1}$ . The background vertical eddy viscosity is  $\nu = 1.0 \times 10^{-5} \text{ m}^2 \text{ s}^{-1}$ . The Coriolis parameter  $f = 10^{-4} \text{ s}^{-1}$ . The vertical eddy viscosity  $K_M$  is computed by the Mellor-Yamada level 2.5 turbulence closure scheme (Mellor and Yamada, 1982) using the non-dimensional stability functions from Galperin et al. (1988) and Kantha and Clayson (1994). Some studies, e.g., Garvine (1999); Stacey et al. (1999); Fong and Geyer (2001), have shown that in strongly stratified conditions, the MY2.5 scheme underestimates the vertical eddy viscosity, while in weakly stratified conditions the vertical eddy viscosity is overestimated. Nevertheless, the MY2.5 scheme resolves the mixing accurate to first order, which is what we are interested in. The density is computed by a linear equation of state using a saline contraction coefficient of  $7.6 \times 10^{-4}$  and is a function of salinity alone. Temperature is kept constant in the model. A passive tracer is included in the estuarine water. This tracer configuration helps distinguish the estuarine plume from the returning upwelled front.

**Model Grids** The model utilizes a sigma coordinate system to resolve the vertical structure. We use 20 sigma levels with closer vertical spacing at the surface and bottom to resolve the boundary layers. The horizontal grid is a finite difference scheme with grid size ranging from 1 km (near northern boundary) to 4 km (near southern boundary). The higher resolution at the northern boundary minimizes the formation and downwave propagation of numerical artifacts into the study area. We

also use a higher horizontal resolution in the shallowest part of the domain to resolve the nearshore physics that we are examining. The shallowest region is along the coast (10 m), and the deepest region is along the offshore boundary (110 m). The domain in our base case numerical experiment has 174 points in the cross-shore direction and 179 points in the alongshore direction. The location of the boundaries are southern  $y = -315$  km, northern  $y = 50$  km, western  $x = -110$  km, and eastern  $x = 100$  km. The barotropic time step is 9 s, and the baroclinic time step is 180 s. A right-handed ‘east coast’ coordinate system is used where  $+x$  direction is offshore (‘seaward’),  $+y$  direction is northward (‘upwave’), and  $+z$  direction is upwards (‘skyward’).

**Boundary Conditions** The surface momentum boundary conditions are,

$$K_M \left. \frac{\partial (u, v)}{\partial z} \right|_{z=0} = \frac{(\tau^{sx, sy})}{\rho_o} \quad (2.1)$$

where  $\tau^{sx}$  and  $\tau^{sy}$  are cross-shore and alongshore surface wind stresses. In this study,  $\tau^{sx} = 0 \text{ N m}^{-2}$  while the alongshore wind stress is varied. The bottom momentum boundary condition is a linear bottom drag,

$$K_M \left. \frac{\partial (u, v)}{\partial z} \right|_{z=-H} = (ru_b, rv_b) \quad (2.2)$$

where the bottom drag coefficient is  $r = 3 \times 10^{-4} \text{ m s}^{-1}$  and  $(u_b, v_b)$  are the bottom velocity in the cross-shore and alongshore directions respectively. The bottom drag is chosen within the range observed by Lentz et al. (2001) for the North Carolina coast.

The northern open boundary conditions (OBC) are determined from numerical experiments using the same winds as the 3D model but in a 2D alongshore-uniform topography model. This 2D model is a cross-shore section at the northern boundary of the 3D model and has no alongshore variations. The northern OBC implies that the ocean outside the northern boundary can be approximated as an infinite coast with no alongshore variations in forcings or topography, as described in Gan and Allen (2005) and Pringle and Dever (2009). The southern and eastern edges are open boundaries with Sommerfeld radiation conditions. This radiation condition has the

least reflection at the boundary for the dominant wave mode but the other wave modes have higher reflection. To overcome this, the southern boundary also has a six grid-point wide sponge layer where the horizontal viscosity gradually increases in the southward direction. The sponge layer helps dissipate the energy of reflected waves preventing them from propagating along the southern open boundary. The western boundary is the coastal wall with free-slip condition. The free-slip imposes no friction between horizontal boundaries and the flow, and there is no normal flow into the wall. The western boundary also has a wide estuary with a freshwater river input into the model domain. Our model estuary has idealized dimensions similar to wide estuaries such as Chesapeake Bay and Delaware Bay.

**Bathymetry** The model domain is an idealized representation of the study area and has a wide estuary connected to a uniform alongshore bathymetry coastal ocean (Fig. 4-2A). The coastal ocean bathymetry (Fig. 2-4B) is given by

$$H(x) = H_o + \alpha x \quad 0 \leq x \leq L = 100 \times 10^3 \text{ m} \quad (2.3)$$

where  $H_o = 10$  m is the coastal wall depth,  $\alpha = 0.001$  is the bottom slope and  $x$  is the cross-shore distance. The estuary mouth is centered at  $[x, y] = [0, 0]$  km with a length of 100 km and a width of 20 km. The estuary has 10 m deep walls with a 11 m deep thalweg (Fig. 2-4C). The dimensions of the estuary are idealized and kept constant to prevent any variations in estuarine mixing. The details of the estuary are not first order important because the physics we are interested in depends on the density and thickness of the plume in the coastal ocean. The variations of these parameters are described later in this section.

**Stratification** The coastal ocean is modeled after the summer conditions at Duck, NC (Fig. 2-3) as a two layer system separated by a halocline (thickness of 10 m) centered at a depth of 15 m (Waldorf et al., 1995; Alessi et al., 1996). These dimensions of the halocline simplify the mixing dynamics at the estuary mouth by preventing the

coastal halocline from entering the estuary during the spin up. The initial density field is alongshore uniform and is a function of depth and salinity,

$$S(z) = 34 - 2 \tanh\left(\frac{z + 15}{3}\right) \text{ g kg}^{-1} \quad (2.4)$$

where the salinity is  $34 \text{ g kg}^{-1}$  at the halocline center, and  $z$  is the depth in metres (Fig. 4-3A). The salinity of the top layer of the coastal ocean is near  $32 \text{ g kg}^{-1}$ . We report the numerical model salinity using absolute salinity in units of  $\text{g kg}^{-1}$ , and the CoOP field observations (old data) are in units of psu, as defined in Millero et al. (2008). For our purposes, practical salinity and absolute salinity are essentially the same.

### 2.3.2 External Model Forcings

In our numerical experiments, three components are varied to test our prediction of the region where the plume arrives nearshore first: the duration of the upwelling wind, the downwelling wind stress, and the speed of the plume. The details of the variations of these components are described below. Each numerical experiment starts from an initial condition where the flow is at rest. The experiments run with no winds until steady state, and then a wind forcing is applied to the model domain. The experiment was run for two weeks after the onset of the wind forcing. Our analysis will focus on the evolution of the nearshore dynamics during and after the wind forcing.

**Wind Forcing** The surface forcing consists of uniform alongshore wind stress,  $\tau^{sy}$ . The wind stress begins 22 days into the numerical model run to allow the plume and exchange fluxes at the estuary mouth to stabilize. The wind forcing begins as an upwelling alongshore wind stress of  $\tau^{sy}$  lasting for an upwelling period of  $t_{UW}$ ; this period includes one inertial period ( $t_T = \frac{2\pi}{f}$ ) to ramp up and another inertial period to ramp down to zero wind stress (Fig. 4-3B). After the end of the upwelling period, the wind reverses and ramps up to a downwelling wind stress of  $B\tau^{sy}$  over an inertial

period. The downwelling wind stress remains at  $B\tau^{sy}$  for the remainder of the model run.  $t_{UW}$  controls the offshore position of the front and is varied from 2.5-5 days.  $B$  is a factor that controls the magnitude of the downwelling wind stress relative to the upwelling wind stress and is varied from 0.25-2. In all numerical experiments,  $\tau^{sy}=0.1$  Pa, roughly a  $8\text{ m s}^{-1}$  wind speed measured at height of 10 m (Fairall et al., 1996) and the changes in wind forcing in each numerical experiment is made through  $t_{UW}$  and  $B$ .

**River Forcing** The freshwater flux enters the model domain at the head of the estuary and is applied evenly over the depth. This inflow initiates at the start of the model simulation and is kept constant with time. The exchange flow at the estuary mouth has stabilized after 22 days. The freshwater inflow is fixed at  $2000\text{ m}^3\text{s}^{-1}$  in all our numerical experiments. The initial salinity along the estuary is,

$$S(x) = S_{co} + \frac{\partial S}{\partial x} x, \quad -100\text{ km} \leq x \leq 0\text{ km} \quad (2.5)$$

where the surface salinity of coastal ocean,  $S_{co} = 32\text{ g kg}^{-1}$  and the along-estuary salinity gradient,  $\frac{\partial S}{\partial x} = 0.2\text{ g kg}^{-1}\text{ km}^{-1}$  ( $\frac{\partial \rho}{\partial x} = 0.16\text{ kg m}^{-3}\text{ km}^{-1}$ ). This base case gradient is the stabilized along-estuary salinity gradient at the end of a 100-day simulation with the river flow alone. This helps shorten the spin up time for the estuary in the numerical model by starting the model close to the steady state. In order to change the plume speed, variations of the along-estuary salinity gradient ranging from  $0.05\text{-}0.25\text{ g kg}^{-1}\text{ km}^{-1}$  ( $\frac{\partial \rho}{\partial x} = 0.04\text{-}0.20\text{ kg m}^{-3}\text{ km}^{-1}$ ) are used to change the density of the buoyant estuarine plume leaving the estuary. In these density variations, the estuary salinity has reasonably adjusted such that the plume water at the estuary mouth varies between 2-10% over the last week before upwelling.

### 2.3.3 The Response of the Base Case Numerical Experiment.

The base case is configured such that there is 2.5 days of upwelling at a wind stress of  $\tau^{UW} = 0.1 \text{ Pa}$  followed by downwelling wind stress of  $\tau^{DW} = -0.1 \text{ Pa}$  until the end of the experiment. The upwelling duration of 2.5 days is chosen from the range of observed wind-reversal timescale in our study area (Austin and Lentz, 1999), so there is 1 more day of upwelling after the coastal halocline outcrops at the coast. The  $32.5 \text{ g kg}^{-1}$  isohaline, at the top of the coastal halocline, is used as a marker for the upwelled front. After the winds reverse to downwelling, the onshore speed of the front is the depth-averaged onshore velocity of the surface mixed layer. In the numerical model, the mixed layer is determined as the depth where the salinity is  $0.1 \text{ g kg}^{-1}$  higher than the surface salinity. The return of the upwelled front is associated with downwelling winds, and we define the return of the upwelled front to the coast when the bottom salinity at the coast (near the southern boundary) is fresher than  $34 \text{ g kg}^{-1}$  and the surface-bottom salinity difference is less than our tolerance of  $0.5 \text{ g kg}^{-1}$ . The  $34 \text{ g kg}^{-1}$  isohaline is the center of the model halocline returning back to intersect with the coastal wall, similar to the pre-upwelling salinity profile. For the base case configuration, the upwelled front returns to the coast on day 27 of the experiment or 2 days after onset of downwelling winds (marked in Fig. 2-6).

While the front is returning to the coast, the estuarine plume is also propagating alongshore as shown in the plot of alongshore surface salinity at the coastal wall versus experiment model time (Fig. 2-6). The vertical salinity contours indicate the upwelled front, and the alongshore distance-time gradient of the sloping salinity contours indicate the plume speed,  $c_T$ . We use the sloping  $31 \text{ g kg}^{-1}$  isohaline to determine the plume speed. The plume speed  $c_T$ , includes the downwelling wind-induced alongshore flow. The downwelling winds also push the plume against the coastal wall, narrowing the plume width and increasing the plume thickness, so the plume interacts with the coastal bottom slope.

**Base Case Tracer Experiment** A passive tracer is used in our base case numerical experiment to show that the upwelled front remains outside the plume boundary. At the onset of wind-reversal, a tracer is injected in the estuary while the rest of the model domain had no tracer. The cross-section shown in Fig. 2-7, is 60 km downwave of the estuary, in the region where the plume arrives nearshore first. The  $32.5 \text{ g kg}^{-1}$  isohaline marks the position of the upwelled front. During upwelling, 1 day before wind-reversal, we observe the upwelled front moving offshore (Fig. 2-7A) and replaced by the saltier bottom coastal water. When upwelling winds reverse to downwelling, the upwelled front moves shoreward (Fig. 2-7B), but 1 day after wind-reversal, we can observe the leading edge of the plume arriving nearshore before the upwelled front (Fig. 2-7C). We observed that 3 days after wind-reversal (Fig. 2-7D), the nearshore region occupied by the estuarine plume still had high tracer, and the returning front remained outside the plume boundary. This is important because the presence of the plume nearshore during downwelling is similar to an inner shelf, which keeps the returning upwelled front from returning to the coast, so the region where the plume arrives nearshore first is not influenced by the returning front.

We determine this region where the plume brings less dense water nearshore first and keeps the upwelled front from returning to the coast during downwelling winds. This alongshore extent of the plume is determined when the upwelled front returns back to the coast near the southern boundary. The surface salinity along the coast shows the alongshore extent of the plume when the upwelled front returns to the coast near the southern boundary (Fig. 2-8A). Closer to the estuary, the plume reaches the nearshore first (Fig. 2-8B) while farther downwave of the estuary the front returns first (Fig. 2-8C). We determined the base case magnitudes of the extent of the region where the plume arrive first, the offshore position of the upwelled front, onshore speed of the returning front, and the plume speed (listed in Table 2.2).



### 2.3.4 Observational Data

The observations we use to support our work are from the moorings and shipboard conductivity, temperature, and depth (CTD) data from the CoOP program in Duck, North Carolina (NC). The reasons for the selection of this site were the large volume of observations, background literature – those cited within Lentz and Largier (2006), and its alongshore bottom topography, which minimizes bathymetry induced alongshore variations (Fig. 2-3). The cross-shore array of moored conductivity and temperature (CT) sensors and current meters measured the hydrography from near-surface to near-bottom depths. The mooring measurements spanned from late August to early December 1994. The central mooring array consisted of moorings at the 4 m, 8 m, 13 m, 21 m, and 26 m isobaths ranging from 0.3 km to 16.5 km offshore. The observational data described in our analysis are from moored surface and bottom CT meters positioned cross-shore at 1.5 km and 5.5 km (known as the D1 and D2 moorings). There are mid depth sensors as well, but the surface and bottom moorings are the most useful in determining when the water column is mixed or stratified. The details are in Alessi et al. (1996); Lentz and Largier (2006). The shipboard CTD casts were made along cross-shore transects reaching as far as 50 km offshore. These CTD casts were made during the months of August and October in 1994. These transects are arranged in the downwave direction from the Chesapeake Bay mouth to north of Cape Hatteras (Fig. 2-3), and a full survey took 24 hours. In this time, the alongshore plume advection can travel 50 km, so these observational plots are not a snapshot of the system. The cross-shore sampling period for each transect of the array is much shorter (2-4 hours), so cross-shore advection of any water masses are small compared to the transect length and can be treated as a good snapshot of the cross-sectional hydrography. Details on the shipboard casts are given by Waldorf et al. (1995). The CoOP observations are old observations, so we report them in psu in line with Millero et al. (2008). This also makes it easy

to compare with prior studies which used CoOP observations. Several investigators (Rennie et al., 1999; Lentz et al., 1999; Shanks et al., 2000; Cudaback and Largier, 2001; Shanks et al., 2002; Lentz et al., 2003; Shanks and Brink, 2005) have identified the Chesapeake plume and the upwelled front in the CoOP observations.

## 2.4 Observations

Using the CoOP observations near Chesapeake Bay, we go a step further than prior studies by examining events when the plume arrives nearshore first, and when the returning upwelled front arrives nearshore first. The CoOP observations used were taken from 14 August to 14 October (Fig. 2-9).

If upwelling winds persist long enough, an upwelled front forms where the halocline is displaced to the surface near the coast and then moves offshore forced by the surface Ekman transport. Shoreward of the upwelled front, the difference between the surface and bottom salinities is small (Austin and Lentz, 2002). As an upwelled front moving offshore passes a mooring location, the water column at that location becomes well mixed.

After upwelling winds stop, two possible situations can occur. In the first situation, the upwelled front can return to the coast before the plume. When this happens, the moorings would show the less dense water in the upwelled front moving shoreward past them. Since there is no source of freshwater offshore, wind-induced mixing causes the salinity of the surface water moved offshore by upwelling winds to increase along with the thickness of the mixed layer (Pollard et al., 1973; Fong and Geyer, 2001). The increase in the mixed layer thickness can be large enough that when the upwelled front returns past the nearshore mooring, it influences both the surface and bottom salinity. Thus, when the upwelled front returns to the coast, we expect both the nearshore surface and bottom mooring to show the water freshening at the same

time.

In the second situation, the plume is the first to arrive nearshore bringing fresher water than the upwelled front returning to the coast. The Chesapeake plume usually causes the nearshore surface salinity to freshen by 4-6 psu while the bottom salinity remains mostly undisturbed (except during strong downwelling winds). In addition to the fresher plume water, the blunt wedge shape of the plume (Lentz and Helfrich, 2002) would bring fresh, less dense water at the nearshore mooring before the offshore (Fig. 2-2). With these heuristics, we can analyze the CoOP observations to determine when, after upwelling, the plume arrives nearshore before the upwelled front returns to the coast during downwelling winds.

In the CoOP observations, the upwelling winds often reversed before an upwelled front formed. In our analysis of the CoOP observations, we examined events where an upwelled front had formed. We divide these events into groups where upwelling winds reverse or relax. The upwelling wind-relaxation (UWR) events are defined as the upwelling wind stress becoming zero for at least a day. The wind-reversal (WR) events are defined as the upwelling winds reversing to downwelling winds. A suffix is attached to indicate if the plume (P) or the returning front (F) first reaches the nearshore region as determined with the heuristics discussed above, and the number indicates the period; WR2F is the second wind-reversal period and the upwelled front (F) returns nearshore before the plume. In the period when surface and bottom salinity data was being gathered, the CoOP observations contain seven upwelling events where an upwelled front was observed: five of which were followed by wind-reversals and two were followed by wind-relaxation (Fig. 2-9).

In three of the five wind-reversal events, saltier water than that moved offshore during upwelling arrives nearshore, and the difference between surface and bottom salinity at the nearshore mooring remained small as the nearshore water column became less salty, suggesting that the upwelled front returns to the coast first. The

wind-reversal period, WR2F, during 21-24 August is an example of the front returning to the coast before the plume arrives. By middle of 22 August the upwelling winds transported the front offshore forming an inner shelf (Fig. 2-10B). During the downwelling winds on 23 August, we observe saltier water nearshore (Fig. 2-10C) than that moved offshore by upwelling winds (Fig. 2-10B). This is consistent with the upwelled front returning to coast before the fresher plume; the plume arrival was observed a day later, early on 25 August (Fig. 2-10D).

In two of the five wind-reversal events, the nearshore surface salinity is much fresher than it would be if the upwelled front returned to the coast, and the nearshore surface salinity was freshening while the bottom salinity was mostly undisturbed giving a salinity difference of about 6 psu. The bottom salinity is undisturbed when the plume does not narrow and deepen significantly during weak downwelling wind stress. These observations are consistent with the arrival of the plume because the upwelled front returning back to the coast would be saltier due to wind-induced mixing (Pollard et al., 1973). The wind-reversal period, WR1P, during 14-17 August is an example of the plume arriving before the front returns to the coast. During the middle of 15 August the difference between the surface and bottom salinities is very small at the 1.5 km mooring (Fig. 2-11B) indicating the upwelling winds had transported the front past the mooring. Following the wind-reversal in the evening of 15 August, the nearshore region shows the arrival of much fresher water than that upwelled offshore (Fig. 2-10A). This suggests that the plume arrival brought the fresh, less dense water nearshore before the upwelled front.

In the case where the upwelling winds cease but do not reverse (Fig. 2-11A), UWR1, during 19-21 August, we observed that the nearshore mooring (Fig. 2-11B) and the offshore mooring (Fig. 2-11C) show the arrival of less dense water at the coast. This less dense water arrives at the nearshore mooring one day before the offshore mooring and is fresher than the water initially moved offshore; the minimum

nearshore salinity after upwelling was 31 psu (Fig. 2-12A), but after wind-relaxation we observe nearshore salinity of 29 psu (Fig. 2-12B). Since there is no source of freshwater offshore, this indicates that the less dense water at the coast is due to the alongshore propagation of freshwater from an upwave source. This is consistent with what is expected if the plume arrives at these stations and is also consistent with the conclusions of Austin and Lentz (2002) that during relaxation the upwelled front does not return to the coast. For the CoOP observations at Duck, the source of freshwater is the estuarine plume from Chesapeake Bay (Rennie et al., 1999).

The above examples of the wind-reversal and wind-relaxation events that followed the upwelling winds show that either the plume or the returning upwelled front during downwelling winds can bring less dense water nearshore along the coast. This suggests that at any point downwave of an estuary, the arrival of less dense water at the coast depends on the race between the alongshore propagation of the plume and the onshore return of the upwelled front during downwelling winds. In some region close to the estuary, the plume will win the race and is responsible for the less dense water nearshore. The arrival of the plume nearshore can keep the upwelled front from returning to the coast (as discussed in Sec. 2.3.3). In the following section, we derive a predictor to estimate the alongshore distance where the plume arrives along the coast first and keeps the upwelled front from returning to the coast.

## 2.5 Derivation and Testing of our Predictor

When upwelling winds reverse, the upwelled front moves towards the coast while the plume propagates downwave from the estuary (Fig. 2-2). First, we derive the time it would take for the front to return to the coast, and then we determine the distance the plume travels alongshore in this time. We define this alongshore distance  $L$ , as the region where the plume arrives nearshore before the upwelled front returns to

the coast under downwelling winds. Then, we test this length scale  $L$ , our predictor, using numerical experiments.

The offshore position of the upwelled front  $W$ , is determined by the upwelling Ekman velocity  $u_{UW}$ , and the duration of surface cross-shore transport  $t_{UW}$ ,

$$W = u_{UW}t_{UW} = u_{UW} (P_{UW} - t_{outcrop}) \quad (2.6)$$

where  $P_{UW}$  is the duration of the upwelling winds, and  $t_{outcrop}$  is the time needed for the divergence in cross-shore wind-driven transport to displace the isopycnals to the surface forming a front (Austin and Lentz, 2002). The outcropping time is determined using numerical experiments with successively longer durations of upwelling wind. The duration of upwelling  $P_{UW}$ , are plotted against the offshore positions of the front and extrapolated to find the time when the front is at the coast,  $x = 0$  km. This  $t_{outcrop}$  is determined to be 1.4 days, consistent with the range determined in Austin and Lentz (2002). This correction is only valid for our experiment since it may depend on the upwelling wind stress, stratification, the depth of the pycnocline, and the bottom slope (Austin and Lentz, 2002). However, this correction should be of similar magnitude for most upwelling systems with similar cross-shelf bathymetry, e.g., Northern California shelf (Lentz, 1987). We assume there are no alongshore variations in the position of the upwelled front due to eddies at the edge of the front (Barth, 1994). The upwelling surface velocity  $u_{UW}$ , is given by

$$u_{UW} = \frac{\tau^{UW}}{\rho_o h_{ml} f} \quad (2.7)$$

where  $\tau^{UW}$  is the alongshore upwelling wind stress,  $\rho_o = 1025 \text{ kg m}^{-3}$  is our reference density of sea water, and  $h_{ml}$  is the mixed layer depth in the coastal ocean. The surface mixed layer is assumed to be a flat slab moving offshore and onshore with a speed given by the Ekman velocity.

After the front has moved offshore, wind-reversal causes the front to move towards the coast under downwelling winds. The time for the front to return to the coast  $t_{DW}$ ,

under downwelling wind  $\tau^{DW}$ , is

$$t_{DW} = \frac{W}{u_{DW}} + \frac{2\pi}{f} \quad (2.8)$$

where  $\frac{2\pi}{f}$  is the inertial period for the downwelling surface Ekman transport to fully develop and  $u_{DW}$  is the downwelling Ekman velocity ( $\text{m s}^{-1}$ ) given by

$$u_{DW} = \frac{\tau^{DW}}{\rho_o h_{ml} f}. \quad (2.9)$$

The wind-induced mixing can erode stratification causing the surface mixed layer to deepen and become saltier (Pollard et al., 1973). The mixed layer depth is determined by the maximum surface mixed layer depth scaling from Pollard et al. (1973) (referred as PRT depth). If the downwelling wind stress is less than or equal to the preceding upwelling wind stress, then the surface mixed layer during the downwelling does not deepen. When the PRT depth is less than the initial mixed layer depth in the numerical model, the wind stress does not deepen the mixed layer. Pollard et al. (1973) notes that with sustained winds the mixed layer will continue to deepen beyond the PRT depth, but the rate of this secondary deepening is expected to be smaller.

In a 2 layer system (our configuration), the PRT depth is found by determining the new mixed layer depth whose velocity is given by Ekman dynamics and whose bulk Richardson number is critical,  $R_i = 1$ . The new mixed layer depth is the depth where the shear-induced turbulent mixing has stopped (Pollard et al., 1973; Fong and Geyer, 2001). The PRT depth predictions by (Pollard et al., 1973; Fong and Geyer, 2001, in their figure 5) compared well with field observations, to the first order of magnitude. Substituting Eqs. 2.11-2.13 into Eq. 2.10 for  $R_i = 1$  gives the new mixed layer depth (Eq. 2.14).

$$R_i = \frac{g\Delta\rho^{new}h_{ml}^{new}}{\rho_o(u)^2}, \quad (2.10)$$

$$u = \frac{\tau}{\rho_o h_{ml}^{new} f}, \quad (2.11)$$

$$\Delta\rho^{new} = \rho_{ml}^{new} - \rho_{bot}, \quad (2.12)$$

$$\rho_{ml}^{new} = \frac{\rho_{ml}^{old} h_{ml}^{old} + \rho_{bot} (h_{ml}^{new} - h_{ml}^{old})}{h_{ml}^{new}}, \quad (2.13)$$

where  $\rho_{ml}^{new}$  is the new mixed layer density,  $\rho_{ml}^{old}$  is the old mixed layer density,  $h_{ml}^{old}$  is the old mixed layer depth,  $\rho_{bot}$  is the bottom layer density (we assume the bottom layer is deep), and  $h_{ml}^{new}$  is the new mixed layer depth.

$$h_{ml}^{new} = \left( \frac{\tau^2}{g \Delta \rho^{old} h_{ml}^{old} \rho_o f^2} \right)^{\frac{1}{2}} \quad (2.14)$$

From Eq. 2.14, we determined that for all the wind stresses used in our numerical experiments (0.05-0.25 Pa) the new mixed layer depth is shallower than the old mixed layer. This means we expect little deepening of the mixed layer caused by the shear-induced turbulent mixing as a result of an increase in wind stress.

Next, we determine the alongshore distance propagated by the plume in the time,  $t_{DW}$  from Eq. 2.8, for the upwelled front to return to the coast. In the absence of ambient alongshore flow, the plume travels downwave at the speed  $c_p$ , given by

$$c_p = \sqrt{g' h_p} \quad (2.15)$$

where  $g' = \frac{\Delta \rho}{\rho_o} g$  is the reduced gravity,  $\Delta \rho$  is the density difference between plume and coastal ocean.  $c_p$  depends on the thickness of the plume at the coastal wall  $h_p$  (Lentz and Helfrich, 2002), however when a detailed cross-shore observation of the plume is available, then using the average plume thickness yields better predictions of the plume speed. We also assume in our theory that the reduced gravity in the plume is conserved. For the range of conditions we investigated, the mixing in the plume is a second order effect, however where mixing processes like tides, winds, and breaking waves are significant, as discussed in the ROFI literature (Linden and Simpson, 1988; Sharples and Simpson, 1993; Souza and Simpson, 1997; Burchard and Hofmeister, 2008), the plume density will erode, reducing the plume speed, thus decreasing the accuracy of our predictions. For simplicity in our theory, the influence of bottom friction on  $c_p$  is not considered; we examine the impact of this in our numerical modeling. Using the range of bottom friction found in Lentz et al. (2001) in our base



case experiment, we determined the changes in the plume speed is about 15%, so bottom friction is not a significant factor in our study.

Downwelling winds can increase the speed of the plume by driving an ambient downwave flow,  $\bar{v}$ . Over the shelf, the alongshore wind stress is balanced by the bottom friction  $r = 3 \times 10^{-4} \text{ m s}^{-1}$ , so the alongshore momentum balance during downwelling is,

$$\bar{v} = \frac{\tau^{DW}}{\rho_o r}. \quad (2.16)$$

This wind-induced depth-averaged alongshore flow  $\bar{v}$ , (Lentz et al., 1999) assists the plume speed  $c_p$ . In addition to the wind-induced alongshore flow, a large scale alongshore pressure gradient can also drive an ambient alongshore flow,  $v_{amb}$  (Lentz, 2008)(in our numerical experiments, we assume  $v_{amb} = 0 \text{ m s}^{-1}$ ). The plume speed,  $c_T$  is

$$c_T = c_p + \bar{v} = c_p + \frac{\tau^{DW}}{\rho_o r} + v_{amb}. \quad (2.17)$$

Using the plume speed, we determine the alongshore distance propagated by the plume in the time it takes for the upwelled front to return to the coast. This length scale  $L$ , is the region where the plume first arrives nearshore and keeps the upwelled front from returning to the coast.

$$L = t_{DW} c_T = \left( \frac{W}{u_{DW}} + \frac{2\pi}{f} \right) (c_p + \bar{v}) = \left( \frac{\tau_{UW} t_{UW}}{\tau_{DW}} + \frac{2\pi}{f} \right) \left( c_p + \frac{\tau^{DW}}{\rho_o r} + v_{amb} \right). \quad (2.18)$$

In our derivations above, we neglect the effects of mixing of the plume, but Garvine (1999) found that coastal mixing and the discharge strength of the estuary determine the eventual length of the plume. The Garvine (1999) length scale is the upper limit of all our predictions. In our experiments, all the predictions are smaller than the eventual length of the plume, 425 km, so mixing of the plume in the coast was not a significant factor. In the next sections we test our predictor, Eq. 2.18, using numerical experiments and field observations.

### 2.5.1 Testing Predictions Against Numerical Model

To test our predictions (Eq. 2.18), the numerical model is used to simulate the range of conditions observable in the typical coastal ocean, described in Sec.2.3.2, and determine the downwave distance where the plume arrives nearshore before the upwelled front. The predictions are tested in three sets of model runs (Table 2.1); in each set, only one parameter is varied while the others are fixed, allowing a rigorous testing of our predictor and its components such as the offshore position of the front, onshore velocity of the front, and the plume speed.

We varied the upwelling wind duration in the range of 2.5-5 days, variations in the downwelling wind stress are in the range of 0.025-0.20 Pa, and the variations in the estuary salinity (hence variations in plume density) relative to ambient coastal salinity are in the range of 5-25 g kg<sup>-1</sup>. Then the variations in our theory are compared with the results from the numerical experiments (Figs. 2-13 and 2-14). The predictions of the length scale,  $L$  are compared to the results from the numerical experiments in Fig. 2-13. The prediction of the components of our length scale such as the offshore position of front (inner shelf width), onshore velocity of the front, and the plume speed are compared to the results from the numerical experiments in Fig. 2-14. In the experiment where upwelling winds cease (downwelling wind is zero), the upwelled front remained offshore after upwelling inline with the numerical findings of Austin and Lentz (2002), and the estuarine plume brought less dense water downwave of the estuary, as expected from our predictions.

**Accuracy of the Prediction of our Length Scale** Next, we tested if our predictor  $L$  is reasonable for a range of variations in upwelling duration, downwelling wind stress, and plume density typical of coastal oceans. We can see in Fig. 2-13 that the relationship between our predictions and the results from the numerical experiment are, as expected, linear and accurate to the first order. The best fit

between our predictions of  $L$  and the numerical results is obtained when Eq. 2.18 is scaled by a factor of 0.6. To explain the magnitude of this factor, we analyze below the components of our predictor.

**Accuracy of the Predictions of the Offshore Position of the Front** In this experiment, we test the accuracy of our prediction of the offshore position of the front,  $W$ , for variations in the upwelling duration, downwelling wind stress, and the plume density. We determined that, as expected, the inner shelf width only changes significantly when the upwelling duration is varied (Fig. 2-14A). The offshore position of the front is not significantly changed when the downwelling wind stress or the plume density is varied. The response of our prediction of the inner shelf width matches well with the numerical model results.

**Accuracy of the Predictions of the Onshore Velocity of the Front** In this experiment, we test the accuracy of our prediction of the onshore velocity of the upwelled front,  $u_{DW}$ , for variations in the upwelling duration, downwelling wind stress, and the plume density. We determined that, as expected, the onshore velocity only changes significantly when the downwelling wind stress is varied (Fig. 2-14B). The onshore velocity is not significantly changed when the upwelling duration or the plume density is varied. The response of our prediction of the onshore velocity of the upwelled front is proportional to the numerical results; however, our predictions are about twice the numerical results (Fig. 2-14B). This is likely a combination of the mixed layer depth increasing beyond the maximum mixed layer depth described by Pollard et al. (1973) and part of the onshore Ekman transport occurring below the mixed layer depth (Lentz, 1992).

**Accuracy of the Predictions of Alongshore Plume Speed** In this experiment, we test the accuracy of our prediction of the plume speed,  $c_T$ , for variations in the

upwelling duration, downwelling wind stress, and the plume density. We determined that, as expected, the plume speed changes significantly when the plume density or the downwelling wind stress is varied (Fig. 2-14C). The plume speed is not significantly changed when the upwelling wind duration is varied; the small variation of plume speed with upwelling duration is due to the estuarine plume becoming saltier (and slower) over the course of the upwelling and downwelling wind event due to wind-induced mixing in the estuary. The response of the plume speed is influenced by downwelling winds because the downwelling winds determine the wind-induced alongshore flow,  $\bar{v}$ . The response of our prediction of the plume speed is proportional to the numerical results; however, our predictions are larger than the numerical results (Fig. 2-14C).

When we use a more complete form of the phase speed of an interfacial wave in a two layer fluid (Gill, 1982, pp.122) and the average plume thickness in our theory instead of the plume thickness at the coast, our predictions of the plume speed improves significantly (Fig. 2-14D). The average plume thickness can be determined from the cross-shore geometry of the plume. These changes give a more accurate plume speed, however, the average plume thickness is difficult to determine without detailed cross-shore field observations, and the Gill (1982) scaling is more complex and bulky. For simplicity in our prediction of plume speed, we use Eq. 2.15 and plume thickness at the coast. If detailed cross-shore plume observations are available then using the average plume depth yields better predictions. Our assumption of no mixing in the estuarine plume also overestimates the plume speed and can explain some of the second order difference in speed between the numerical model and our predictions, shown in Figs. 2-14C,D. Another factor that contributes to this second order difference is the increase in plume speed due to the intensification of the cross-shore density gradient due to downwelling winds ( $\approx 10-20\%$  of  $c_T$ ).

Our predictor, Eq. 2.18, agrees reasonably with the numerical experiment results

for the range of variations in each of its components. However, our theory makes several simplifying assumptions discussed in Sec.2.5, so some divergences between our prediction and the numerical model are expected. Next, we test our predictions against observational data from the Chesapeake Bay, and our predictor is applied to observational data from other estuaries to determine the region where the plume arrives nearshore first.

## 2.6 Testing our Predictor Against Field Observations

We predict when the plume brings less dense water nearshore before the returning front returns to the coast after upwelling winds. Then, we compare our predictions with what actually happens in the CoOP observations at Duck, which is 85 km downwave of the Chesapeake Bay. We selected periods in the observations when the nearshore mooring shows that an upwelled front has formed, moved offshore, and then the upwelling winds reversed or ceased. We find seven such periods from the observations at Duck (Fig. 2-9).

We predict where the plume arrives first along the coast using the time-averaged upwelling wind stress  $\overline{\tau_{UW}}$ , the upwelling wind duration  $t_{UW}$ , the time-averaged downwelling wind stress  $\overline{\tau_{DW}}$ , the cross-section averaged plume thickness  $h$ , the ambient alongshore coastal flow  $v_{amb}$ , the downwave plume speed  $c_p$ , and the wind-induced alongshore flow  $\bar{v}$  during each of the seven periods (Table 2.3).

The time-averaged upwelling wind stress,  $\overline{\tau_{UW}}$ , is the time-averaged wind stress over the duration of the upwelling winds; the time-averaged downwelling wind stress,  $\overline{\tau_{DW}}$ , is determined similarly. The duration of the upwelling winds,  $t_{UW}$ , is from the start of upwelling winds until the winds reverse. The cross-section averaged plume thickness is determined using the plume thickness at the coastal wall and a plume

width of 10 km, as determined by Rennie et al. (1999) for the CoOP observations. The speed of the plume is determined using the reduced gravity and average thickness of the plume (Eq. 2.15). The wind-induced alongshore flow,  $\bar{v}$ , is determined by Eq. 2.16 using the time-averaged downwelling wind stress and the bottom friction  $r = 3 \times 10^{-4} \text{ m s}^{-1}$ , in the range observed for North Carolina (Lentz et al., 2001). The ambient coastal flow near Chesapeake Bay is about  $0.04 \text{ m s}^{-1}$  in the southward direction (Valle-Levinson and Lwiza, 1997).

When the plume extent predicted by Eq. 2.18 is more than the 85 km from Chesapeake Bay to Duck, we expect the plume to be the first to arrive along the coast at Duck, bringing less dense water nearshore, otherwise the returning front reaches to the nearshore first. Next, we determined when the observations at Duck show the plume or the upwelled front arriving first nearshore for each of the seven periods. When the plume arrives first, we expect the nearshore water to be much fresher than the upwelled front returning to the coast. When the front returns to the coast first, we expect that the nearshore water is much saltier than that moved offshore during upwelling. These heuristics are described in detail in Sec. 2.4. To see if our prediction is successful, we compare the mechanism bringing less dense water nearshore in our observations with the mechanism predicted by Eq. 2.18. For each of the seven wind-reversal periods, shown in Table 2.3, the agreement between the observations and the predictions are good.

## 2.7 Discussion and Conclusions

Where the time-integrated upwelling and downwelling wind stresses are comparable, such as the east coast of US, there exists a region downwave of an estuary where the arrival of the plume in the nearshore region prevents the upwelled front from returning to the coast. This happens because the vertical stratification in the

plume weakens during downwelling winds and allows vertical mixing, so the weak cross-shore flow in the plume stops the front from returning to the coast. Close to the estuary, the plume arrives nearshore before the upwelled front, but far from the estuary, the upwelled front returns nearshore before the plume. We predicted the size of this region and successfully tested it against numerical experiments and field observations.

After upwelling has moved the surface coastal waters offshore, close to the estuary the plume always arrives nearshore and replaces the nearshore coastal water. The arrival of the plume blocks the upwelled surface coastal water from returning to the coast. Conversely, outside of the region the upwelled surface coastal water can return to the coast bringing back the pollutants, larvae, and nutrients that were moved offshore by upwelling. Thus, where the plume returns to the coast before the upwelling front, the salinity, temperature, larval inhabitants and the pollution next to the shelf are governed by water discharged from the estuary. Outside of this region, the properties of the nearshore waters are governed both by the estuarine discharge and the processes that alter the water as it moves along the coast, offshore during upwelling and onshore during downwelling.

**Limits to our Theory** In regions where the time-integrated downwelling wind stress is significantly less than the time-integrated upwelling wind stress, the upwelled front will not return to the coast. Some portions of the west coast of US have such regions where long periods of upwelling are separated by wind relaxation and weak downwelling winds (Send et al., 1987). In these regions, the plume propagates downwave until the next period of upwelling winds detaches the plume from the coast and moves it offshore, where it remains. Mixing processes like tides and breaking waves can (i) significantly deepen the surface mixed layer beyond the shear-induced turbulent mixed layer depth, and (ii) erode the plume density. This can decrease

the accuracy of our predictions, and furthermore, where these mixing processes are dominant, the nearshore water properties will be strongly dependent on the mixing, and this is when the ROFI literature can help us understand these nearshore dynamics in more detail (Linden and Simpson, 1988; Sharples and Simpson, 1993; Souza and Simpson, 1997; Burchard and Hofmeister, 2008).

**Relation to Prior Work and Extension to Other Estuaries** Our work provides new insight on results of prior studies like Shanks et al. (2002). Shanks et al. observed a cluster of estuarine organisms that entered the coastal region with the Chesapeake plume, but farther downwave they appeared to move from the plume to the coastal water. The region where the organisms appear to cross water masses is in the region where the plume arrives nearshore first and keeps the upwelled front from the coast; as a result, the organisms in the front, some of which are the same species of estuarine organisms as in the plume, passively remain offshore outside the plume boundary. This gives the appearance of the estuarine organisms in the plume actively crossing into the adjacent coastal water mass.

The comparisons to field observations and modeling above have been based on the Chesapeake estuary; however, estuaries will govern similar regions in other coastal oceans where there are comparable cycles of time-integrated upwelling and downwelling winds. The size of this region is estimated using the observed values of upwelling wind stress, upwelling duration, the plume speed, downwelling wind stress and the ambient alongshore flow. The monthly average of these parameters were used to determine the mean alongshore extent of the plume in summer and winter (Table 2.4). The plume speed observations are from Yankovsky and Chapman (1997), the thickness of plume are from Hickey et al. (1998); Pettigrew et al. (1998); Banas et al. (2009), the ambient alongshore flow are observations by (Valle-Levinson and Lwiza, 1997; Lentz, 2008, east coast) and (Berdeal et al., 2002, west coast), and



the rest of the parameters are derived from NDBC stations listed in Table 2.4. We defined the mean upwelling wind duration,  $\overline{t_{UW}}$ , as the average duration for all upwelling winds (greater than an inertial period) minus the time for an upwelled front to form (estimated as 1.4 days in our numerical experiments). The mean upwelling wind stress,  $\overline{\tau^{UW}}$ , is the average alongshore wind stress for all upwelling winds greater than an inertial period (similarly for downwelling,  $\overline{\tau^{DW}}$ ) while the plume speed is the sum of  $\sqrt{g'h}$  (Eq. 2.15), the alongshore flow  $\bar{v}$ , induced by the downwelling winds, and the ambient alongshore flow,  $v_{amb}$ . We also make the approximation that the surface mixed layer thickness remains constant during the upwelling and downwelling periods.

The predictions of the average alongshore extent of the plume near the east coast and west coast estuaries is in the range of 45-180 km (Table 2.4). The alongshore extent of the plume tends to be longer during winter compared to the summer. This was mainly due to relatively higher mean values of the upwelling wind duration, upwelling wind stress, and plume speed during winter. The above parameters are larger during winter, so the upwelled front moves farther offshore during upwelling, and the plume moves farther downwave in the time it takes for the front to return to the coast; this is seen in large estuaries, e.g., Delaware Bay and in smaller systems, e.g., Penobscot River.

**Conclusion** Close to an estuary, in the direction of a Kelvin wave, the nearshore hydrography, chemistry, and biology are controlled by the properties of the water leaving the estuary. We find the spatial extent of this region along the coast where the time-integrated upwelling and downwelling wind stresses are of comparable magnitude; this delimits the region most directly under the influence of the estuary, and where both the estuarine and coastal processes influence the nearshore water properties.

**Table 2.1:** The range of variations used in our numerical experiments.

Duration of Upwelling winds, $t_{UW}$	2.5-5 days
Downwelling wind stress, $\tau_{DW}$	0.025-0.20 Pa
Along-estuary salinity gradient over estuary length, $\frac{\partial S}{\partial x}$	5-25 g kg <sup>-1</sup>

**Table 2.2:** The base numerical experiment forcings and results as described in Sec. 2.3.3.

Upwelling wind stress, $\tau_{UW}$	0.1 N m <sup>-2</sup>
Upwelling wind duration, $t_{UW}$	2.5 days
Offshore position of the upwelled front, $W$	10.4 km
Downwelling wind stress, $\tau_{DW}$	-0.1 N m <sup>-2</sup>
Plume speed (no wind forcing), $c_p$	0.38 m s <sup>-1</sup>
Plume speed (under downwelling winds), $c_T$	0.59 m s <sup>-1</sup>
Onshore speed of front returning to coast, $u_{DW}$	0.05 m s <sup>-1</sup>
Length scale, $L$	104 km

**Table 2.3:** The predictions tested against the CoOP observations shows our predicted mechanism matches the observed mechanism for all seven events at Duck. When  $L > 85$  km, then the plume is predicted to arrive at Duck first, otherwise the front returns to coast first.  $\overline{\tau_{UW}}$  is the time-averaged wind stress over the duration of the upwelling winds,  $t_{UW}$  is the duration of the upwelling winds,  $\overline{\tau_{DW}}$  is the time-averaged downwelling wind stress, and  $h$  is the cross-shore averaged plume thickness.  $c_p$  is the speed of the plume under no wind forcing,  $\bar{v}$  is the wind-induced alongshore flow,  $v_{amb}$  is the ambient alongshore flow, and  $L$  (Eq. 2.18) is the alongshore region where the plume arrives first. The last three columns show the mechanism predicted by  $L$  to arrive nearshore at Duck, 85 km downwave of Chesapeake Bay, the mechanism observed in the CoOP observations, and if predicted and observed mechanisms match. PL indicates the plume arrives nearshore first and FR indicates the returning upwelled front is first.

Event	$\overline{\tau_{UW}}$ (Pa)	$t_{UW}$ (days)	$\overline{\tau_{DW}}$ (Pa)	$h$ (m)	$c_p$ (m s <sup>-1</sup> )	$\bar{v}$ (m s <sup>-1</sup> )	$v_{amb}$ (m s <sup>-1</sup> )	$L$ (km)	Pred	Obs	Match
WR1	0.03	4.75	0.02	4	0.46	0.06	0.04	291	PL	PL	Yes
WR2	0.03	2.46	0.04	6	0.43	0.13	0.04	81	FR	FR	Yes
WR3	0.03	1.42	0.05	6	0.51	0.17	0.04	46	FR	FR	Yes
WR4	0.01	6.54	0.03	4	0.42	0.08	0.04	140	PL	PL	Yes
WR5	0.04	1.54	0.05	6	0.25	0.17	0.04	33	FR	FR	Yes
UWR1	0.04	2.96	0.00	4	0.45	0.00	0.04	$\infty$	PL	PL	Yes
UWR2	0.01	2.17	0.00	4	0.45	0.00	0.04	$\infty$	PL	PL	Yes

**Table 2.4:** The mean seasonal region,  $L$ , where the plume arrives nearshore first, for some common estuary-coastal ocean system. The length of the region is computed with the assumption that the mixed layer depth remains constant. The averages are for Delaware Bay 2006-2007; Chesapeake Bay 2006-2007; Hudson Bay 2005-2006; Columbia River 2008-2009 and Penobscot River 2008-2009. The plume speed  $c_p$  observations are from Yankovsky and Chapman (1997), the plume thickness are from Hickey et al. (1998); Pettigrew et al. (1998); Banas et al. (2009), and the remaining parameters are derived from NDBC stations 44009, ducn7, sgrn4, 46029 and 44033. Using  $\tau = 3 \times 10^{-4} \text{ m s}^{-1}$  and  $\rho = 1025 \text{ kg m}^{-3}$ .  $\overline{\tau^{UW}}$  and  $\overline{\tau^{DW}}$  are the average alongshore wind stress for wind events longer than an inertial period.  $t_{UW}$  is the duration of the upwelling winds after the front has formed.

	Estuary	$\overline{\tau^{UW}}$ (Pa)	$t_{UW}$ (days)	$\overline{\tau^{DW}}$ (Pa)	$c_p$ ( $\text{m s}^{-1}$ )	$\bar{v}$ ( $\text{m s}^{-1}$ )	$v_{amb}$ ( $\text{m s}^{-1}$ )	$L$ (km)
Summer	Delaware Bay	0.02	0.95	0.03	0.38	0.09	0.04	61
	Chesapeake Bay	0.04	1.75	0.03	0.54	0.10	0.04	181
	Hudson Bay	<0.01	0.55	0.01	0.44	0.03	0.04	45
	Columbia River	0.02	0.45	0.02	0.56-0.69	0.05	0.05	68-82
	Penobscot River	0.01	0.55	0.01	0.73	0.02	0.05	90
Winter	Delaware Bay	0.05	0.95	0.03	0.28-0.38	0.09	0.04	83-103
	Chesapeake Bay	0.03	0.45	0.03	0.53	0.10	0.04	69
	Hudson Bay	0.01	0.95	0.01	0.43	0.02	0.04	72
	Columbia River	0.02	1.25	0.04	0.50-0.63	0.14	0.05	82-97
	Penobscot River	0.05	1.15	0.02	0.46	0.07	0.05	182

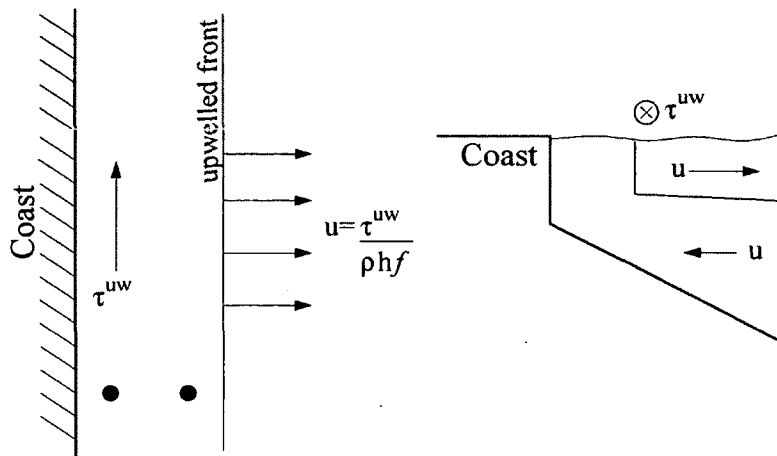


**Figure 2-1:** Cartoon of the upwelling mechanism transporting the upwelled front offshore with a cross-shore sectional view. The black dots indicate the nearshore and offshore moorings.

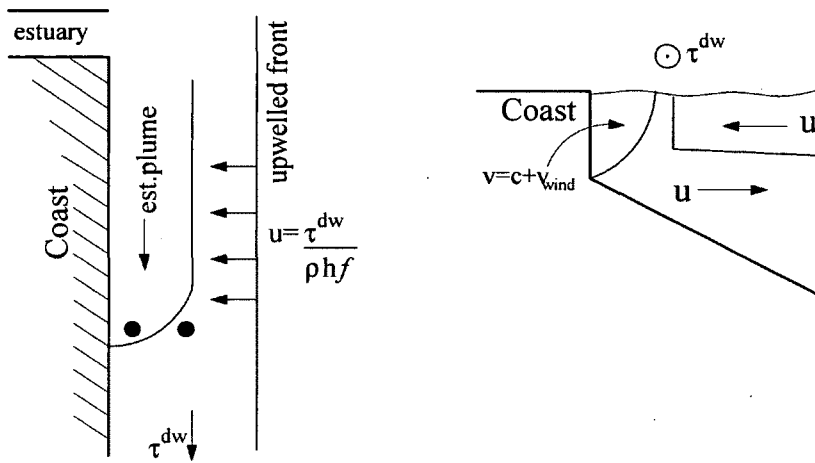


**Figure 2-2:** During wind-reversal, the onshore flow can transport the upwelled front back to the coast. The arrival of less dense water along the coast can be due to the front returning to the coast or the arrival of a plume from the upwave estuary. We predict the alongshore extent of the plume when the front returns to the coast near the southern boundary.

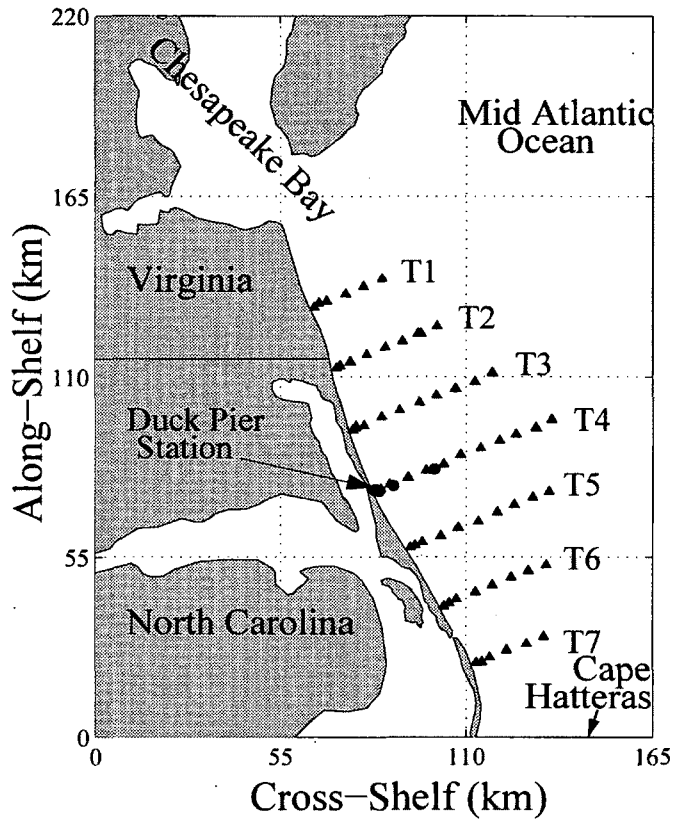


**Figure 2-3:** The study area downwave of Chesapeake Bay, along North Carolina. The CoOP observations are centered at the Duck pier station and span from Chesapeake Estuary mouth to North of Cape Hatteras. The transects are T1, T2, T3, T4, T5, T6, and T7 in the downwave direction from estuary, see Lentz and Largier (2006). Triangles are CTD casts and circles are moored CT meters at Duck.

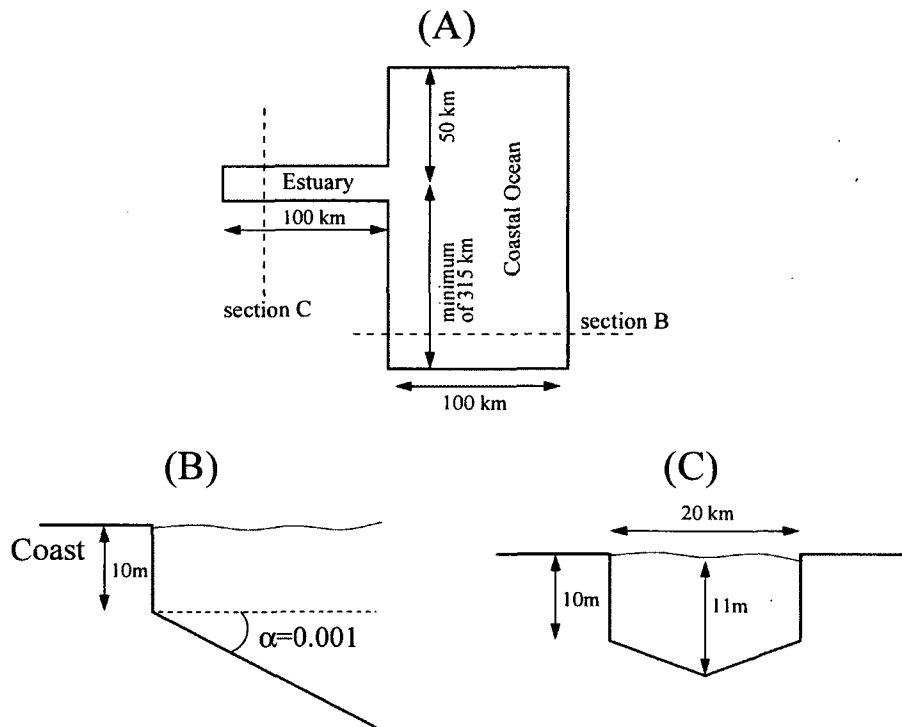


**Figure 2-4:** The schematics of the numerical model bathymetry. (A) The plan view of the model domain with the offshore boundary at 100 km. The upwave alongshore distance is 50 km while the downwave alongshore distance varies each numerical experiment with a minimum of 315 km. (B) The coastal ocean has a uniform alongshore bathymetry shown in the cross-section view. (C) The estuary has a uniform bathymetry with a length of 100 km and a width of 20 km approximating wide estuary systems.



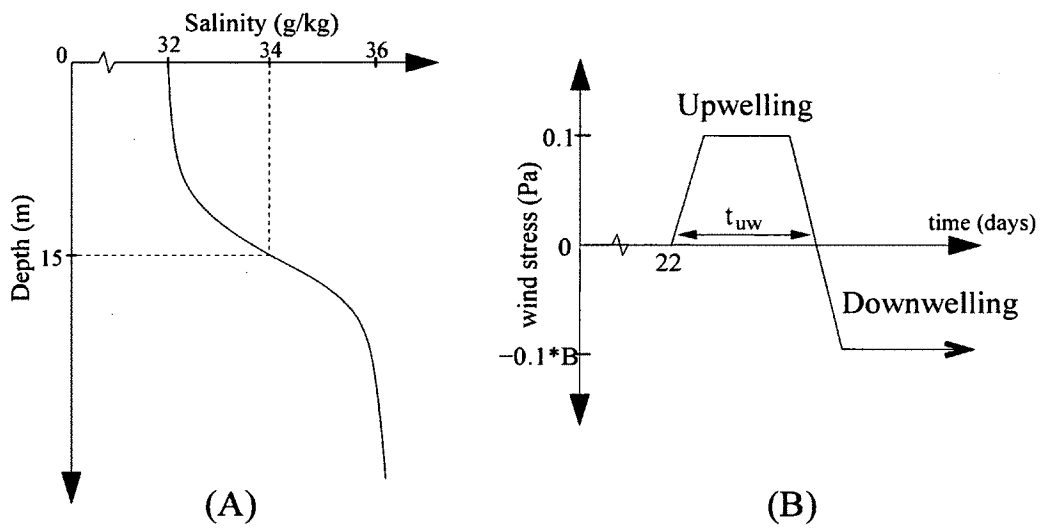


**Figure 2-5:** (A) The stratification in the coastal ocean shown as a salinity profile. The temperature is constant. (B) The alongshore surface wind stress  $\tau^{sx}$  is applied to the entire model domain. The ramping of the wind stress occurs over an inertial period. The downwelling wind continues until the end of the numerical simulation.

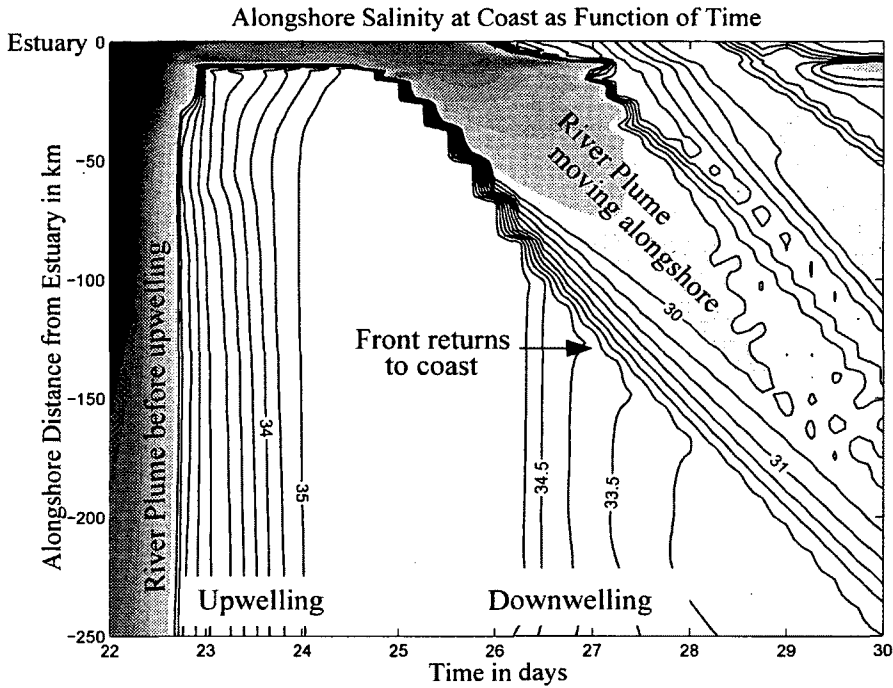


**Figure 2-6:** Alongshore salinity ( $\text{g kg}^{-1}$ ) at the coast as function of time in days. The vertical isohalines indicate the upwelled front moving offshore (upwelling) or onshore (downwelling). The dark shade along the coast at day 22 is the plume before upwelling winds. The sloping isohalines indicate the estuary plume progressing downwave with time. The front returns to the coast at day 27 and is seen in the plot as a decrease in surface salinity during the downwelling phase (between 150-250km), and the arrow shows the downwave position of the plume head at the time the upwelled front returns to the coast. The shaded region shows the freshwater plume from the estuary.

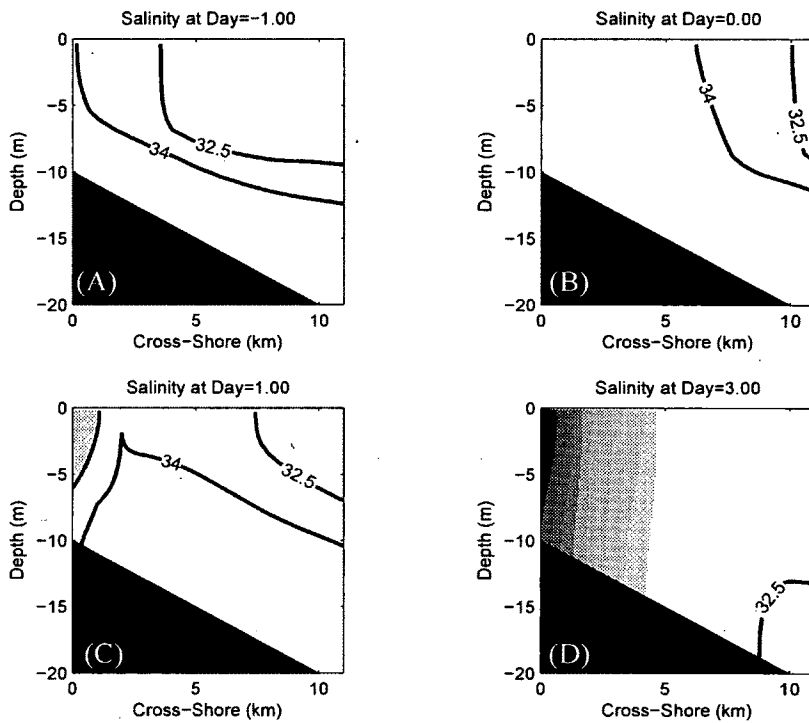


**Figure 2-7:** The cross-section of salinity ( $\text{g kg}^{-1}$ ) and tracer at 60 km downwave of the estuary. The darker shading shows the high tracer arriving with the plume. The sections are at times (A) 1 day before wind-reversal (B) onset of wind-reversal (C) 1 day after wind-reversal (D) 3 days after wind-reversal. The  $32.5 \text{ g kg}^{-1}$  isohaline shows the position of the upwelled front.

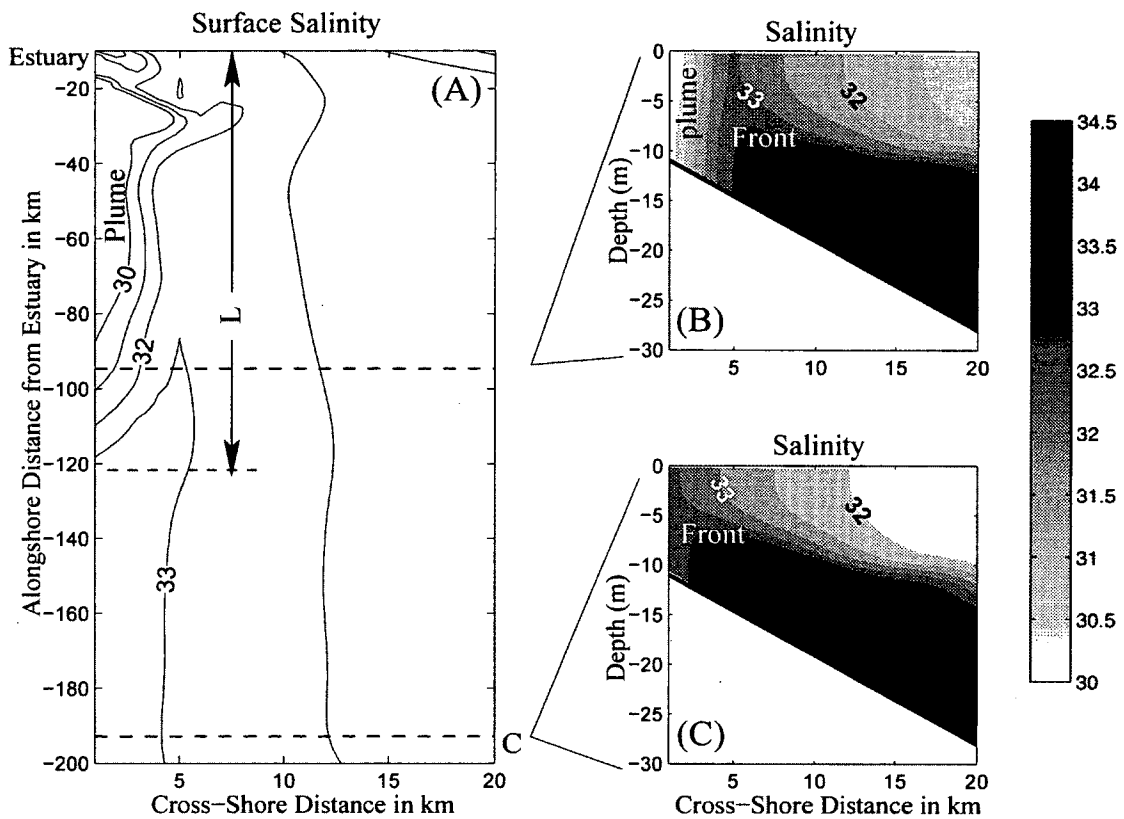


**Figure 2-8:** (A) Coastal surface salinity ( $\text{g kg}^{-1}$ ) plot of the numerical model at the time the coastal halocline returns back to the coast wall, i.e., the upwelled front returns to the coast. The dashed lines are cross-sections upwave and downwave of the plume head. (B) Cross-shore slice upwave of the plume head shows the plume arrives nearshore before the front returns to the coast. (C) Cross-shore slice downwave of the plume head shows the front returning to the coast before the plume arrives.

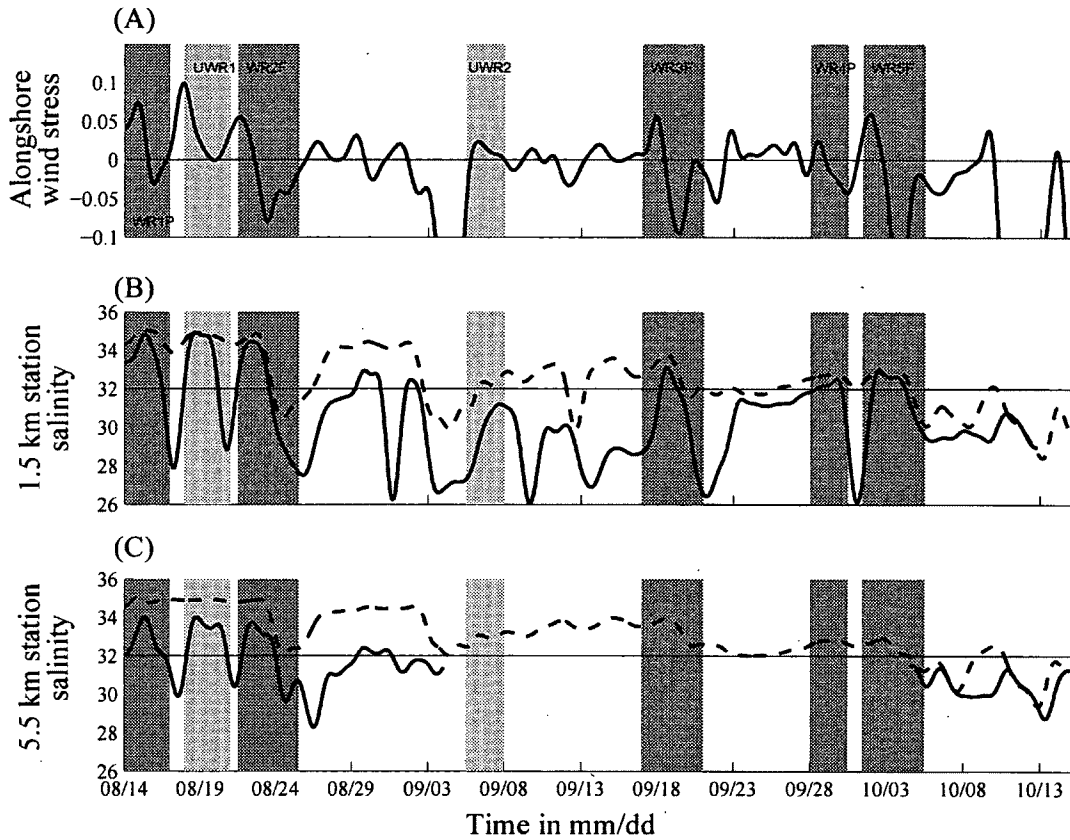


**Figure 2-9:** The time-series plot at the Duck pier station. (A) Low pass filtered (Flagg et al., 1976, PL33 filter) alongshore wind stress  $\tau^{sx}$  (Pa). Positive values are upwelling and negative values are downwelling. Near-surface and near-bottom salinity ( $\text{g kg}^{-1}$ ) time-series for moorings at (B) 1.5 km and (C) 5.5 km offshore. The dashed lines are the near-bottom salinity and the solid lines are the near-surface salinity. UWR1 indicates the period of upwelling wind relaxation [UWR] event 1. WR1P indicates the period of wind-reversal [WR] event 1 with plume-[P] arriving before front-[F]. The light shades show the upwelling relaxation duration and the darker shades show the duration of wind-reversal events.

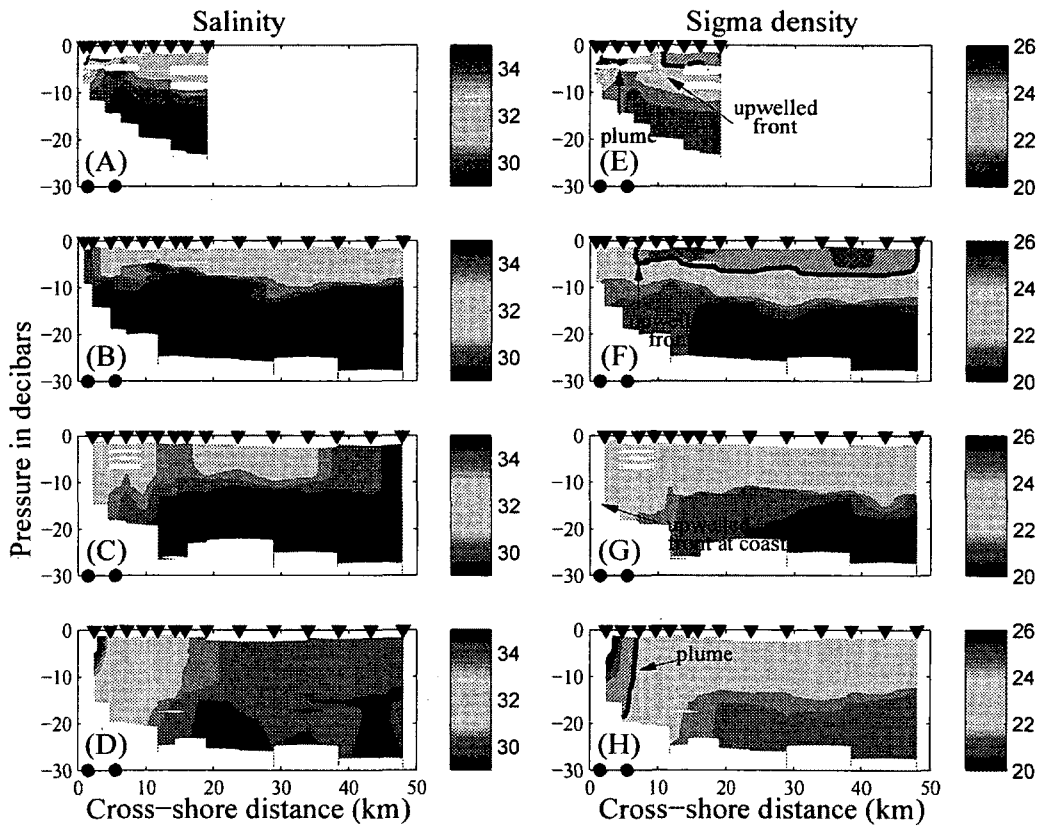


**Figure 2-10:** (A-E) The cross-shore plots of salinity (psu), and (E-H) the cross-shore plots of sigma density ( $\text{kg m}^{-3}$ ) for the same periods at Duck pier station. The depth is in decibars, and the dark line is  $\sigma_t = 22 \text{ kg m}^{-3}$ . (A & E) On 16 August, the plume arrives before the front returns to coast. (B & F) The restart of the upwelling winds moved the plume offshore on 21 August. (C & G) After wind-reversal on 23 August, the less dense water nearshore is due to return of the upwelled front. (D & H) The plume arrives on 25 August after the front returned to the nearshore during downwelling winds. The temperature (not shown here) remained uniform during these events. The inverted triangles are cross-shore CTD shipboard cast locations and the dots are the locations of the 1.5 km and 5.5 km moorings of CT meters.

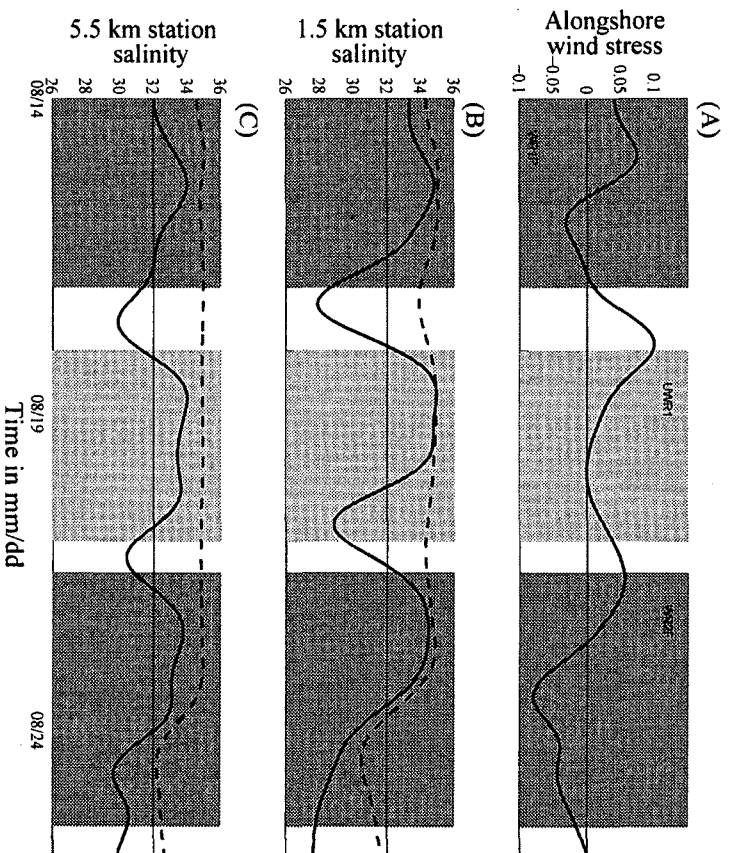
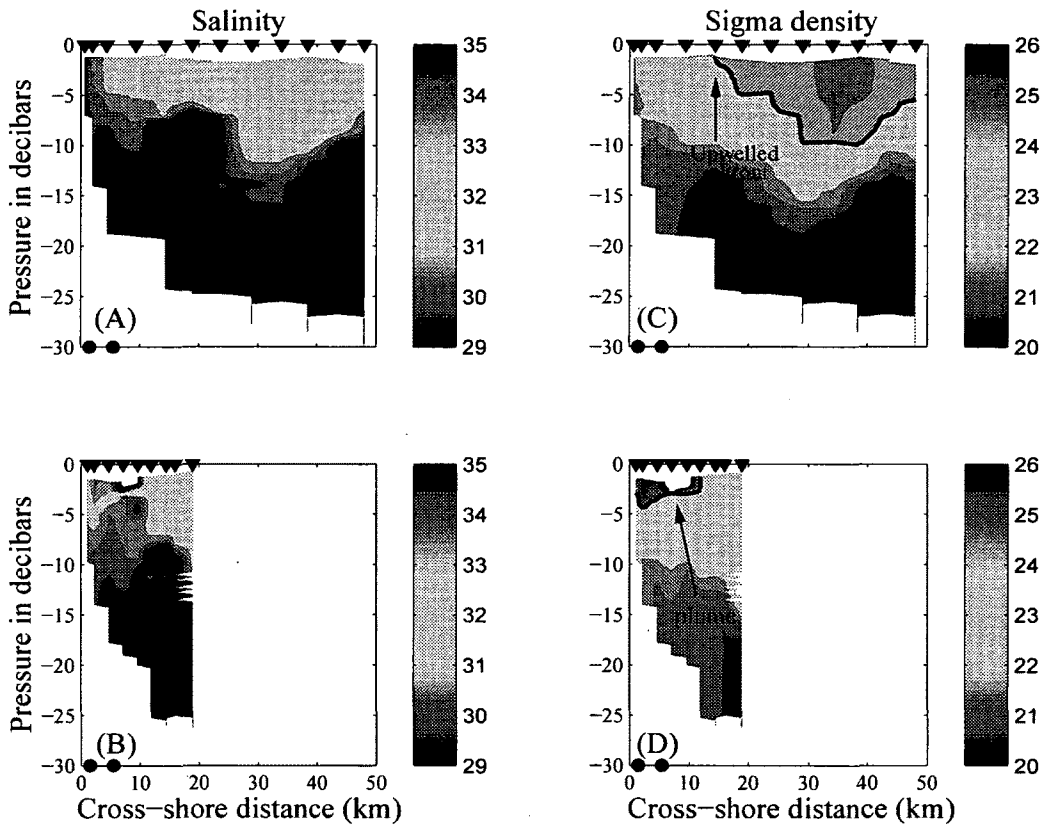
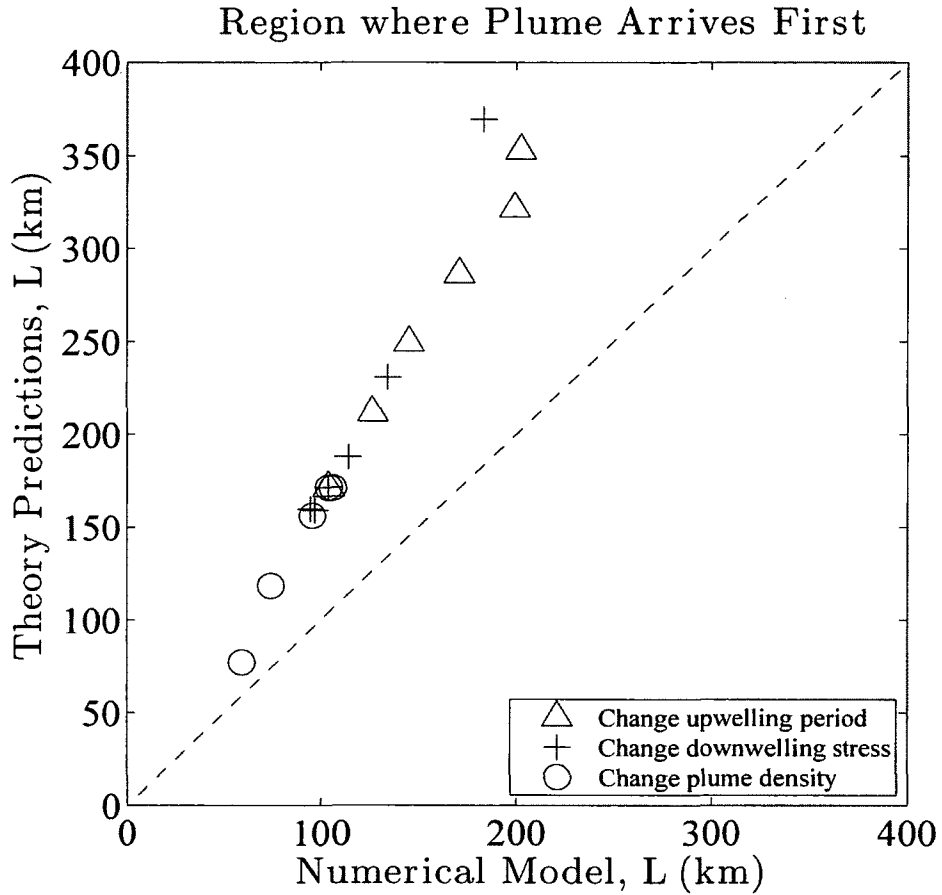


Figure 2-11: Same as Fig. 2-9 but for a shorter period 14-26 August.



**Figure 2-12:** Similar to Fig. 2-10. (A-B) The cross-shelf plots of salinity (psu) and (C-D) sigma density ( $\text{kg m}^{-3}$ ) for the same periods at Duck pier station. The depth is in decibars, and the dark line is  $\sigma_t=22 \text{ kg m}^{-3}$ . (A & C) On 19 August the upwelling winds moved the surface layer offshore. (B & D) After the winds relax the less dense water nearshore is due to arrival of plume on 21 August.





**Figure 2-13:** The predictions of alongshore region  $L$ , (km) where the plume arrives nearshore before the upwelled front, compared to numerical model results. The predictions and numerical results are in good agreement. The plot shows variations in the upwelling wind duration from 2.5-5 days, variations in the downwelling wind stress from 0.025-0.2 Pa, and variations in estuary salinity (hence plume density) from 5-25  $\text{g kg}^{-1}$ .

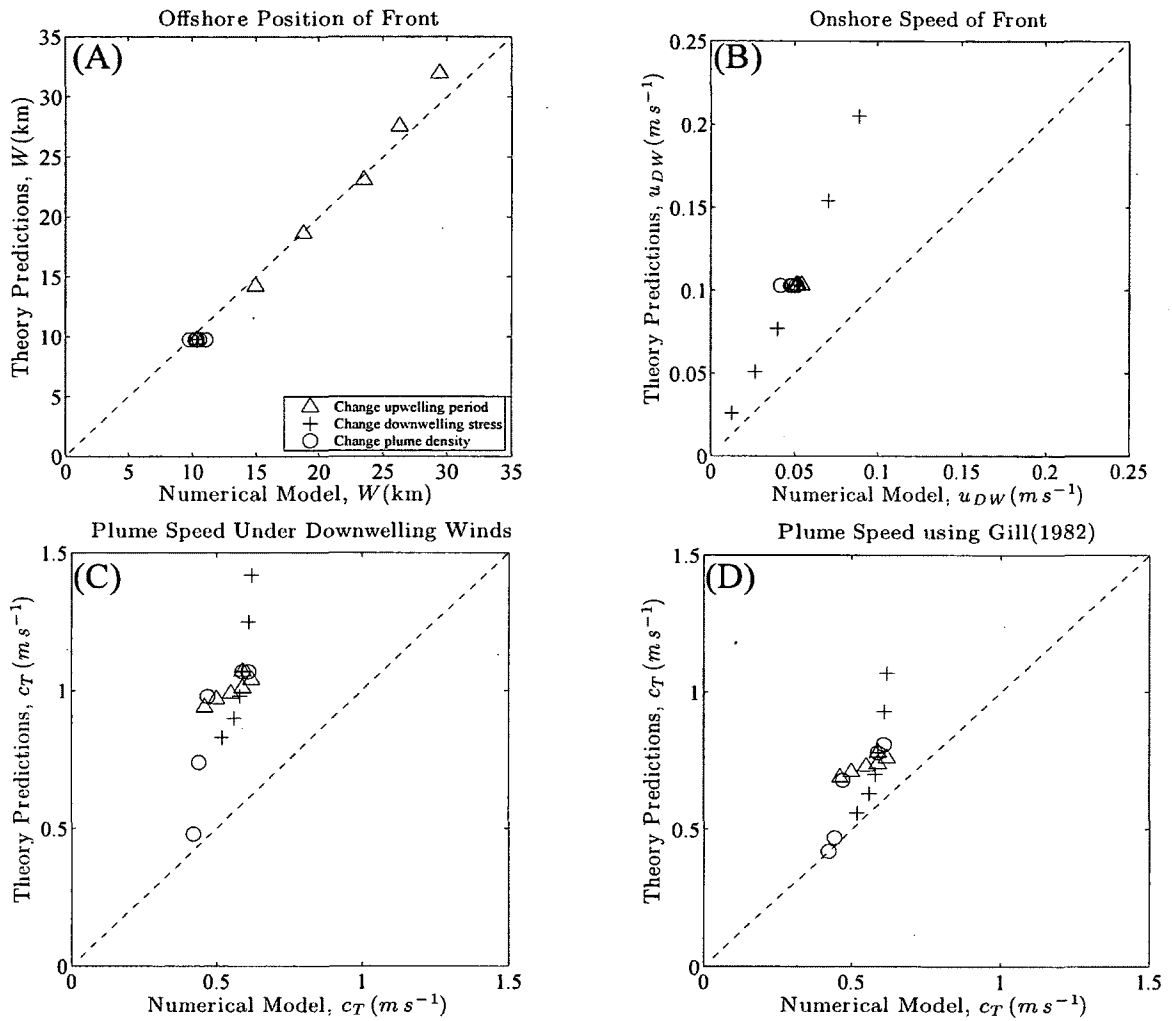


**Figure 2-14:** Similar as Fig. 2-13. Components of scaling from our theory are compared with numerical model experiments. (A) Offshore position of the upwelled front (B) onshore velocity of the upwelled front, (C) plume speed using Eq. 2.15 and the plume thickness at coast, and (D) the plume speed using the more complete form of the plume speed from Gill (1982) and the average plume thickness.

# Bibliography

- Alessi, C. A., S. J. Lentz, and J. A. Austin, 1996: Coastal Ocean Processes Inner-Shelf Study: Coastal and Moored Physical Oceanographic Measurements. *Woods Hole Oceanog. Inst. Tech. Rept.*, **WHOI-96-06** (-), 142.
- Arakawa, A. and V. Lamb, 1977: Computational Design and the Basic Dynamical Processes of the UCLA General Circulation Model. *Methods In Computational Physics*, **(17)**, 174–265.
- Austin, J. and S. Lentz, 1999: The Relationship Between Synoptic Weather Systems and Meteorological Forcing on the North Carolina Inner Shelf. *Journal of Geophysical Research-Oceans*, **104 (C8)**, 18 159–18 185.
- Austin, J. and S. Lentz, 2002: The Inner Shelf Response to Wind-Driven Upwelling and Downwelling. *Journal of Physical Oceanography*, **32 (7)**, 2171–2193.
- Banas, N., P. MacCready, and B. Hickey, 2009: The Columbia River Plume as Cross-Shelf Exporter and Along-Coast Barrier. *Continental Shelf Research*, **29 (1)**, 292 – 301, doi: DOI: 10.1016/j.csr.2008.03.011.
- Barth, J., 1994: Short-Wavelength Instabilities on Coastal Jets and Fronts. *Journal of Geophysical Research-Oceans*, **99 (C8)**, 16 095–16 115.
- Berdeal, I., B. Hickey, and M. Kawase, 2002: Influence of wind stress and ambient flow on a high discharge river plume. *Journal of Geophysical Research-Oceans*, **107 (C9)**, doi: 10.1029/2001JC000932.
- Burchard, H. and R. Hofmeister, 2008: A dynamic equation for the potential energy anomaly for analysing mixing and stratification in estuaries and coastal seas. *Estuarine Coastal and Shelf Science*, **77 (4)**, 679–687, doi: 10.1016/j.ecss.2007.10.025.
- Csanady, G., 1971: On the Equilibrium Shape of the Thermocline in a Shore Zone. *Journal of Physical Oceanography*, **1 (4)**, 263–270.
- Cudaback, C. and J. Largier, 2001: The Cross-Shelf Structure of Wind- and Buoyancy-Driven Circulation Over the North Carolina Inner Shelf. *Continental Shelf Research*, **21 (15)**, 1649–1668.
- Dale, A. C., J. A. Barth, M. D. Levine, and J. A. Austin, 2008: Observations of Mixed Layer Restratification by Onshore Surface Transport Following Wind Reversal in a Coastal Upwelling Region. *Journal of Geophysical Research-Oceans*, **113 (C1)**, doi: 10.1029/2007JC004128.

- Fairall, C., E. Bradley, D. Rogers, J. Edson, and G. Young, 1996: Bulk parameterization of air-sea fluxes for Tropical Ocean Global Atmosphere Coupled Ocean Atmosphere Response Experiment. *Journal of Geophysical Research-Oceans*, **101 (C2)**, 3747–3764.
- Farrell, T., D. Bracher, and J. Roughgarden, 1991: Cross-Shelf Transport Causes Recruitment to Intertidal Populations in Central California. *Limnology And Oceanography*, **36 (2)**, 279–288.
- Flagg, C., J. Vermersch, and R. Beardsley, 1976: MIT New England Shelf Dynamics Experiment (March, 1974) Data Report Part II; The Moored Array. *Woods Hole Oceanog. Inst. Tech. Rept.*, **WHOI-76-1**, 22.
- Fong, D. and W. Geyer, 2001: Response of a River Plume During an Upwelling Favorable Wind Event. *Journal of Geophysical Research-Oceans*, **106 (C1)**, 1067–1084.
- Fong, D., W. Geyer, and R. Signell, 1997: The wind-forced response on a buoyant coastal current: Observations of the western Gulf of Maine plume. *Journal of Marine Systems*, **12 (1-4)**, 69–81.
- Galperin, B., L. Kantha, S. Hassid, and A. Rosati, 1988: A Quasi-Equilibrium Turbulent Energy-Model For Geophysical Flows. *Journal of Atmospheric Sciences*, **45 (1)**, 55–62.
- Gan, H. and J. Allen, 2005: On Open Boundary Conditions for a Limited-Area Coastal Model off Oregon. Part 1: Response to Idealized Wind Forcing. *Ocean Modelling*, **8 (1-2)**, 115–133, doi: 10.1016/j.ocemod.2003.12.006.
- Garvine, R., 1999: Penetration of Buoyant Coastal Discharge onto the Continental Shelf: A Numerical Model Experiment. *Journal of Physical Oceanography*, **29 (8, Part 2)**, 1892–1909.
- Gill, A., 1982: *Atmosphere-Ocean Dynamics*. Academic Press, New York, 662 pp., URL <http://www.loc.gov/catdir/toc/els031/82008704.html>.
- Hickey, B., L. Pietrafesa, D. Jay, and W. Boicourt, 1998: The Columbia River Plume Study: Subtidal Variability in the Velocity and Salinity Fields. *Journal of Geophysical Research-Oceans*, **103 (C5)**, 10 339–10 368.
- Kantha, L. and C. Clayson, 1994: An Improved Mixed-Layer Model for Geophysical Applications. *Journal of Geophysical Research-Oceans*, **99 (C12)**, 25 235–25 266.
- Lentz, S., 1987: A Description of the 1981 and 1982 Spring Transitions over the Northern California Shelf. *Journal of Geophysical Research-Oceans*, **92 (C2)**, 1545–1567, 1549.
- Lentz, S., 1992: The Surface Boundary-Layer in Coastal Upwelling Regions. *Journal of Physical Oceanography*, **22 (12)**, 1517–1539.

- Lentz, S., 2008: Observations and a model of the mean circulation over the Middle Atlantic Bight continental shelf. *Journal of Physical Oceanography*, **38** (6), 1203–1221, doi: 10.1175/2007JPO3768.1.
- Lentz, S., M. Carr, and T. Herbers, 2001: Barotropic Tides on the North Carolina Shelf. *Journal of Physical Oceanography*, **31** (7), 1843–1859.
- Lentz, S., S. Elgar, and R. Guza, 2003: Observations of the Flow Field near the Nose of a Buoyant Coastal Current. *Journal of Physical Oceanography*, **33** (4), 933–943.
- Lentz, S., R. Guza, S. Elgar, F. Feddersen, and T. Herbers, 1999: Momentum Balances on the North Carolina Inner Shelf. *Journal of Geophysical Research-Oceans*, **104** (C8), 18 205–18 226.
- Lentz, S. and K. Helfrich, 2002: Buoyant Gravity Currents Along a Sloping Bottom in a Rotating Fluid. *Journal of Fluid Mechanics*, **464**, 251–278.
- Lentz, S. J. and J. Largier, 2006: The influence of wind forcing on the Chesapeake Bay buoyant coastal current. *Journal of Physical Oceanography*, **36** (7), 1305–1316.
- Linden, P. and J. Simpson, 1988: Modulated mixing and frontogenesis in shallow seas and estuaries. *Continental Shelf Research*, **8** (10), 1107–1127.
- Marmorino, G., A. Cooper, R. Mied, G. Lindemann, D. Trizna, and D. Porter, 2004: Onshore Propagation of a Buoyant Ocean Front Observed Using a Shore-Based Marine Radar. *Continental Shelf Research*, **24** (9), 951–964, doi: 10.1016/j.csr.2004.03.011.
- Mellor, G. and T. Yamada, 1982: Development of a Turbulence Closure-Model for Geophysical Fluid Problems. *Reviews of Geophysics*, **20** (4), 851–875.
- Miller, B. and R. Emlet, 1997: Influence of Nearshore Hydrodynamics on Larval Abundance and Settlement of Sea Urchins *Strongylocentrotus Franciscanus* and *Spurpuratus* in the Oregon Upwelling Zone. *Marine Ecology-Progress Series*, **148** (1-3), 83–94.
- Millero, F., R. Feistel, D. Wright, and T. McDougall, 2008: The composition of Standard Seawater and the definition of the Reference-Composition Salinity Scale. *Deep-Sea Research Part I-Oceanographic Research Papers*, **55** (1), 50–72, doi: 10.1016/j.dsr.2007.10.001.
- Pettigrew, N., D. Townsend, H. Xue, J. Wallinga, P. Brickley, and R. Hetland, 1998: Observations of the Eastern Maine Coastal Current and its Offshore Extensions in 1994. *Journal of Geophysical Research-Oceans*, **103** (C13), 30 623–30 639.
- Pollard, R., P. Rhines, and R. Thompson, 1973: Deepening of the Wind-Mixed Layer. *Geophysical & Astrophysical Fluid Dynamics*, **4** (1), 381–404.

- Pringle, J. M. and E. P. Dever, 2009: Dynamics of Wind-Driven Upwelling and Relaxation between Monterey Bay and Point Arena: Local-, Regional-, and Gyre-Scale Controls. *Journal of Geophysical Research-oceans*, **114**.
- Rennie, S., J. Largier, and S. Lentz, 1999: Observations of a Pulsed Buoyancy Current Downstream of Chesapeake Bay. *Journal of Geophysical Research-Oceans*, **104 (C8)**, 18 227–18 240.
- Send, U., R. Beardsley, and C. Winant, 1987: Relaxation from Upwelling in the Coastal Ocean Dynamics Experiment. *Journal of Geophysical Research-Oceans*, **92 (C2)**, 1683–1698.
- Shanks, A. and L. Brink, 2005: Upwelling, Downwelling, and Cross-Shelf Transport of Bivalve Larvae: Test of a Hypothesis. *Marine Ecology-Progress Series*, **302**, 1–12.
- Shanks, A., J. Largier, L. Brink, J. Brubaker, and R. Hooff, 2002: Observations on the Distribution of Meroplankton During a Downwelling Event and Associated Intrusion of the Chesapeake Bay Estuarine Plume. *Journal of Plankton Research*, **24 (4)**, 391–416.
- Shanks, A. L., J. Largier, L. Brink, J. Brubaker, and R. Hooff, 2000: Demonstration of the Onshore Transport of Larval Invertebrates by the Shoreward Movement of an Upwelling Front. *Limnology and Oceanography*, **45 (1)**, 230–236, URL <http://www.jstor.org/stable/2670803>.
- Sharples, J. and J. Simpson, 1993: Periodic frontogenesis in a region of fresh-water influence. *Estuaries*, **16 (1)**, 74–82.
- Simpson, J., 1997: Physical processes in the ROFI regime. *Journal of Marine Systems*, **12 (1-4)**, 3–15.
- Souza, A. and J. Simpson, 1997: Controls on stratification in the Rhine ROFI system. *Journal of Marine Systems*, **12 (1-4)**, 311–323.
- Stacey, M., S. Monismith, and J. Bureau, 1999: Observations of turbulence in a partially stratified estuary. *Journal of Physical Oceanography*, **29 (8, Part 2)**, 1950–1970, doi: 10.1175/1520-0485(1999)029<1950:OOTIAP>2.0.CO;2.
- Valle-Levinson, A. and K. Lwiza, 1997: Rapid Assessment of Current Velocities in the Coastal Ocean. In: *Rapid Environmental Assessment*, 131–135.
- Waldorf, B. W., J. L. Largier, S. Rennie, J. A. Austin, and G. C., 1995: Coastal Ocean Process (CoOP) Pilot Project Data Report: R/V Hatteras Shipboard Measurements. Underway, CTD and ADCP Data August 1994. *Scripps Inst. of Oceanog. Tech. Rept.*, **SIO-95-29 (-)**, –.
- Williams, W., T. Weingartner, and A. Hermann, 2010: Idealized Two-Dimensional Modeling of a Coastal Buoyancy Front, or River Plume, under Downwelling-Favorable Wind Forcing with Application to the Alaska Coastal Current. *Journal of Physical Oceanography*, **40 (2)**, 279–294, doi: 10.1175/2009JPO4206.1.

Yankovsky, A. and D. Chapman, 1997: A Simple Theory for the Fate of Buoyant Coastal Discharges. *Journal of Physical Oceanography*, **27** (7), 1386–1401.

# CHAPTER 3

## Weather-Band Fluctuations In Wind Alters The Estuary-Ocean Exchange.

### 3.1 Abstract

Winds fluctuating on weather-band time scales can alter the salt exchange between an estuary and the adjacent coastal ocean, changing the salinity and the residence time of the estuary. These changes are governed both by the impact of the wind on the estuary and the adjacent coastal ocean. In stratified estuaries, fluctuating winds mainly reduce the salt exchange by reducing the stratification of the estuary through mixing. When the estuary is well-mixed, fluctuating winds alter the salt exchange primarily by changing the salinity entering the estuary from the coastal ocean. In both stratified and well-mixed estuaries, the changes in the salinity entering and leaving the estuary have a larger effect on the salt exchange than changes in the volume of water exchanged between the estuary and the coastal ocean.

### 3.2 Introduction

The exchange between the estuary and the adjacent coastal ocean allows changes in the coastal ocean to alter the water-properties in the estuary, and the changes in the estuary to alter the near-shore coastal ocean. However, studies in the coastal ocean often represent the estuary as a freshwater point-source along the coastal wall (Fong and Geyer, 2001), and studies in the estuary often represent the coastal ocean



as a homogeneous water mass (MacCready, 1999); these assumptions are removed in our work to examine the influence of fluctuating winds on the exchange between the estuary and the coastal ocean. Large scale weather systems (Austin and Lentz, 1999) can influence both the estuary and the coastal ocean, changing the exchange between these two regions. Studies focusing on understanding the exchange between the estuary and the coastal ocean must simultaneously solve the dynamics in both the regions.

We examine how wind fluctuations influence the salt exchange of the estuary with the coastal ocean. These wind fluctuations can occur on a timescale of a few days (East coast of US) to a few weeks (West coast of US), and are referred to as weather-band fluctuations in the wind. The influence of these weather band fluctuations in the wind are examined over a duration of 30 days. The 30 days of fluctuating winds is much shorter than the time taken for an estuary to reach its new steady state. In large estuaries like the Chesapeake Bay, the steady state is reached in about 90 days (Austin, 2002). Examining the salt exchange of the estuary before the estuary has reached its new steady state helps us understand the immediate impact of storms on the salt exchange. Fluctuating winds can also alter the volume of water exchanged between an estuary and coastal ocean. The volume of the water exchanged governs the residence time of an estuary, i.e., the time a water parcel resides in the estuary. An estuary with a long residence time takes longer to flush out nutrients, pollutants, and other anthropogenic matter input via terrestrial runoff. This can cause water quality problems (Cerco et al., 2004) and create anoxic zones (Scully, 2010) in the estuaries.

Our study examines the net effect of the upwelling and down-welling winds on the estuary, ocean, and their exchange, rather than the effect of separate upwelling or down-welling winds. The wind fluctuations are examined for estuaries and coastal oceans typical of the Mid Atlantic Bight (MAB), and the results are extended to

other regions such as the West coast of US. This work is an extension of previous studies in (i) the coastal ocean where the influence of separate upwelling and downwelling winds on the near-shore circulation and water properties are studied (Austin and Lentz, 2002; Allen et al., 1995; Allen and Newberger, 1996); and (ii) estuaries where the influence of along-estuary or cross-estuary winds on the circulation and water properties are studied (Geyer, 1997; Chen et al., 2009).

This paper is organized as follows: section 2 describes the setup of the base case numerical experiment which was modeled after the Chesapeake Bay and the MAB. This includes a description of the different forcings applied to the permutations of the base case experiment to model the wind influence for a range of estuarine and coastal conditions observed in field data. In section 3, a Reynold's decomposition is used to identify the important parameters influenced by the wind fluctuations. Section 4 discusses how wind fluctuations influence the salt exchange for a range of estuarine and coastal conditions, and in section 5 our work is extended to other regions.

### 3.3 Description of the Numerical Model

Our base case numerical experiment is modeled after the Chesapeake Bay and the MAB coastal ocean (Figure 3-1). The parameters and forcings used in the base case experiment are described. The permutations of this base case experiment used to model the range of topography, estuarine, and coastal conditions are described as well.

The numerical model used in this study is the Regional Ocean Modeling System (ROMS). It is a primitive equation finite difference numerical model (Song and Haidvogel, 1994). The vertical momentum balance is hydrostatic and a free surface is included. A constant horizontal eddy viscosity,  $A_M$  of  $5.0 \text{ m}^2 \text{ s}^{-1}$  and a horizontal diffusivity,  $A_H$  of  $0 \text{ m}^2 \text{ s}^{-1}$  are set. The background minimum vertical eddy viscosity

is  $\nu = 1.0 \times 10^{-5} \text{ m}^2 \text{ s}^{-1}$ . Diurnal tides are included in the model and is a major source of vertical mixing in the background. The Coriolis parameter is  $f = 10^{-4} \text{ s}^{-1}$ . The vertical eddy viscosity  $K_M$  is computed by the Mellor-Yamada level 2.5 turbulence closure scheme (Mellor and Yamada, 1982) using the non-dimensional stability functions from Galperin et al. (1988) and Kantha and Clayson (1994). Some studies, e.g., Garvine (1999); Stacey et al. (1999); Fong and Geyer (2001), have shown that in strongly stratified conditions, the MY2.5 scheme underestimates the vertical eddy viscosity, while overestimating in weakly stratified conditions. Nevertheless, the MY2.5 scheme resolves the mixing accurate to first order. The density is computed by a linear equation of state using a saline contraction coefficient of  $7.6 \times 10^{-4}$  and is a function of salinity alone. Temperature is kept constant in the model.

**Model Grids** The model utilizes a terrain-following  $\sigma$  coordinate system to resolve the vertical structure. The horizontal grid is a finite difference scheme with grid size ranging from  $1 \text{ km} \times 1 \text{ km}$  (near the western and northern boundaries) to  $4 \text{ km} \times 4 \text{ km}$  (near the eastern and southern boundaries). The higher resolution at the northern boundary minimizes the formation and downwave propagation of numerical artifacts into the study area. The highest horizontal resolution of  $1 \text{ km} \times 1 \text{ km}$  is used in the estuary and the coastal region near the estuary mouth to resolve the salt and volume fluxes being examined.

The domain in the base case numerical experiment has 384 points in the cross-shore direction, 96 points in the alongshore direction, and 20 vertical  $\sigma$  levels. The location of the boundaries are southern  $y = -100 \text{ km}$ , northern  $y = 50 \text{ km}$ , western  $x = -320 \text{ km}$ , and eastern  $x = 100 \text{ km}$ . A right-handed ‘east coast’ coordinate system is used where  $+x$  direction is offshore (‘seaward’),  $+y$  direction is northward (‘upwave’), and  $+z$  direction is upwards (‘skyward’). In the numerical model, the baroclinic time step is 90 s and the model output is saved every 120 time steps to temporally resolve

the tides used in our model. The barotropic time step is 1/20 of the baroclinic time step. The model was run for half and double the grid spacing, and our results did not change significantly.

**Boundary Conditions** The surface momentum boundary conditions are,

$$K_M \frac{\partial (u, v)}{\partial z} \Big|_{z=0} = \frac{(\tau^{sx}, \tau^{sy})}{\rho_o} \quad (3.1)$$

where  $\tau^{sx}$  and  $\tau^{sy}$  are cross-shore and alongshore surface wind stresses. In this study,  $\tau^{sx} = 0$  Pa while the alongshore wind stress is varied. The bottom momentum boundary condition is a linear bottom drag,

$$K_M \frac{\partial (u, v)}{\partial z} \Big|_{z=-H} = (ru_b, rv_b) \quad (3.2)$$

where the bottom drag coefficient is  $r = 5 \times 10^{-4} \text{ ms}^{-1}$  and  $(u_b, v_b)$  are the bottom velocity in the cross-shore and alongshore directions respectively. The bottom drag is within the range observed by Lentz et al. (2001) for the North Carolina coast.

The northern open boundary conditions (OBC) are determined from numerical experiments using the same winds as the 3D model but in a 2D alongshore-uniform topography model. This 2D model is a cross-shore section of the 3D model and has no alongshore variations. The northern OBC implies that the ocean outside the northern boundary can be approximated as an infinite coast with no alongshore variations in forcings or topography, as described in Gan and Allen (2005) and Pringle and Dever (2009). The southern and eastern edges are open boundaries with Sommerfeld radiation conditions. This radiation condition has the least reflection at the boundary for the dominant wave mode but the other wave modes have higher reflection. To overcome this, the southern boundary also has a six grid-point wide sponge layer where the horizontal viscosity gradually increases in the southward direction. The sponge layer helps dissipate the energy of reflected waves preventing them from propagating along the southern open boundary. The western boundary is the coastal wall with free-slip condition. The free-slip imposes no friction between horizontal boundaries

and the flow, and there is no normal flow into the wall.

**Bathymetry** The model domain is an idealized representation of the Mid-Atlantic Bight and has a large estuary connected to a uniform alongshore bathymetry coastal ocean (Fig. 3-2). The coastal ocean bathymetry is given by

$$H(x) = H_o + \alpha x \quad 0 \leq x \leq 100 \times 10^3 \text{ m} \quad (3.3)$$

where  $H_o = 10$  m is the coastal wall depth,  $x$  is the cross-shore distance, and  $\alpha$  is the bottom slope. The  $\alpha$  was varied between  $(0.5 - 5) \times 10^{-3}$  to examine the influence of wind fluctuations for different coastal slope. In the base case experiment,  $\alpha$  was  $1 \times 10^{-3}$ , typical of the MAB.

Our model estuary has idealized dimensions similar to large estuaries such as Chesapeake Bay and Delaware Bay (Fig. 3-2B). The estuary mouth is centered at  $[x, y] = [0, 0]$  km with a length of 300 km and a width of 20 km. The length of the estuary is selected to prevent tidal resonance in the estuary. The estuary has 10 m deep walls. In the base case experiment, the estuarine thalweg was 30 m and the estuary thalweg was varied between 11-45 m to examine the influence of winds for different estuary depths. The angle of the estuary was varied between  $-60^\circ$  to  $60^\circ$  to examine the influence of fluctuating winds for different estuary orientations. In the base case experiment, the estuary was perpendicular to the coastal ocean, i.e.,  $\theta = 0^\circ$ . Positive angles mean the head of the estuary is northward of the estuary mouth.

**Coastal Stratification** The stratification is modeled after the summer conditions at Duck, NC as a two layer system separated by a halocline centered at a depth of  $h_{hc}$  and has a halocline thickness of  $\Delta z = 11$  m (Waldorf et al., 1995; Alessi et al., 1996). The  $h_{hc}$  was varied between 10-45 m to examine the influence of winds at different pycnocline depths; in the base case experiment, the  $h_{hc}$  was 15 m. The initial density field is uniform alongshore and is a function of depth and salinity,

$$S(z) = 33 - \Delta S_{hc} \tanh\left(\frac{z + h_{hc}}{3}\right) \text{ g kg}^{-1} \quad (3.4)$$

where the salinity is  $33 \text{ g kg}^{-1}$  at the halocline center,  $z$  is the depth in metres,  $\Delta S_{hc} = 2 \text{ g kg}^{-1}$  (Figure 3-3A). The denominator of the  $\tanh()$  function sets the  $\Delta z$  and is kept constant for all model runs. The salinity of the top layer of the coastal ocean is near  $31 \text{ g kg}^{-1}$ . The numerical experiment salinity is reported using absolute salinity in units of  $\text{g kg}^{-1}$  (Millero et al., 2008).

### 3.3.1 External Model Forcing

Each numerical experiment starts from an initial condition where the flow is at rest. The experiments run with tides and river discharge but no winds, until day 200 when steady state is reached. Then the wind forcing is applied to the model for 30 days because it is shorter than the adjustment time of our estuary but longer than the observed weather-band timescales being examined. Our analysis will focus on the estuary exchange during the 30 days of fluctuating winds.

**Wind Forcing** The surface forcing consists of alongshore wind-stress,  $\tau^{sy}$  which is uniform across the numerical domain and fluctuates between upwelling and downwelling (Fig. 3-3B). The winds begin with an upwelling wind-stress of  $\tau^{sy}$  lasting for a period of  $t_{UW}$  days, followed by a down-welling wind-stress of  $-\tau^{sy}$  lasting  $t_{DW}$  days. A wind-stress of  $\tau^{sy} = 0.1 \text{ Pa}$  is a wind speed of about  $8 \text{ m s}^{-1}$  measured at height of 10 m (Fairall et al., 1996). Both the periods  $t_{UW}$  and  $t_{DW}$  include one day for the wind to ramp to  $\tau^{sy}$  and another day to ramp back to zero wind-stress. Only complete wind-reversal cycles,  $t_{UW} + t_{DW}$ , that fit in the 30 day duration are used.

The wind-stress amplitude and period was varied between 0.05-0.3 Pa and 6-30 days respectively; in the base case experiment these were 0.1 Pa and 6 days. The time-averaged wind-stress over the 30 days wind is zero for all the experiments presented in this study, unless otherwise stated. The alongshore winds fluctuating about zero mean wind stress amplitude is a common occurrence in the coastal wind forcing.

Statistical analyses of several coastal regions show that the average of the alongshore component of the wind stress amplitude is often close to zero (Table 3.1). Furthermore, the fluctuation, i.e., standard deviation, from the mean wind is often much larger (often by an order of magnitude) than the mean wind stress amplitude. This is shown by the small ratio between the mean and the standard deviation (Table 3.1).

However, there are regions along the US coasts where the mean wind stress amplitude in this component is comparable to the standard deviations. We observe that this occurs for our defined West coast region, Buzzards Bay, and sometimes the Chesapeake Bay during summer. In these regions where the mean and the standard deviation are comparable, the results from our study, which use zero mean alongshore wind-stress amplitude has to be modified.

**River Forcing** The freshwater discharge enters the model at the head of the estuary and is applied evenly over the depth. The freshwater discharge has a salinity of  $0 \text{ g kg}^{-1}$ . The river discharge range of  $(0.2 - 20) \times 10^3 \text{ m}^3 \text{ s}^{-1}$  is used to examine the influence of winds at different discharge rates; the base case discharge rate was  $2 \times 10^3 \text{ m}^3 \text{ s}^{-1}$ , similar to Austin (2002). This inflow initiates at the start of the model simulation and is kept constant with time. The initial salinity along the estuary is,

$$S(x) = S_{co} + \frac{\partial S}{\partial x} x, \quad -300 \text{ km} \leq x \leq 0 \text{ km} \quad (3.5)$$

where the surface salinity of the coastal ocean,  $S_{co} = 31 \text{ g kg}^{-1}$  and the along-estuary salinity gradient,  $\frac{\partial S}{\partial x} = 0.1 \text{ g kg}^{-1} \text{ km}^{-1}$  ( $\frac{\partial \rho}{\partial x} = 0.08 \text{ kg m}^{-3} \text{ km}^{-1}$ ). In order to reduce the computer time for each model run, the estuary salinity is initiated closer to the steady state. The exchange flow at the estuary mouth has stabilized by 200 days.

**Tides** The inclusion of tides in the numerical model sets a more realistic background estuarine mixing. Tidal forcing included in the numerical model is achieved by imposing the fluctuations of the sea surface height and current associated with a 12-hour tide at the offshore (eastern) boundary of the domain. The fluctuations

of the sea surface height and current at this offshore boundary is the sum of the initial coast-ward moving tidal wave and the tidal wave reflected from the coast, as described by Das and Middleton (1997). Their solution was used to determine the magnitude of the fluctuations in the sea surface height and currents at the offshore boundary. These offshore tidal boundary conditions are then tuned to get the tides at the coastal wall to be similar to observed tidal fluctuations along the MAB coast.

### 3.4 Equations for Salt Fluxes at Estuary Mouth

In order to examine how fluctuating winds alter the salt exchange between an estuary and an adjacent coastal ocean, i.e., the net salt flux, we decompose the salt exchange into simpler components. A positive net salt flux indicates the estuary is losing salt, and a negative net salt flux indicates the estuary is gaining salt. The net salt flux is examined over weather-band timescales to find how the estuary initially responds to fluctuating winds. Over longer duration of fluctuating winds when the estuary has reached steady state, the net salt flux is zero; our estuary does not reach steady state over the 30 days of fluctuating winds.

The net salt flux across the estuary mouth of cross-sectional area,  $A$  is,

$$F_{net}(t) = \int_0^A u(x, y, z, t) \cdot s(x, y, z, t) \cdot dA \quad (3.6)$$

The velocity,  $u$ , and salinity,  $s$ , are the tidal averages for time,  $t$ , for each point  $(x, y, z)$  along the cross-section of the estuary mouth.

The net salt flux is broken down using the following decompositions, similar to MacCready (1999),

$$u(x, y, z, t) = \bar{u}(t) + u'(x, y, z, t) \quad (3.7)$$

$$s(x, y, z, t) = \bar{s}(t) + s'(x, y, z, t) \quad (3.8)$$

$\bar{u}(t)$  and  $\bar{s}(t)$  are the velocity and salinity, averaged across the cross-sectional area



of the estuary mouth. While,  $u'(x, y, z, t)$  and  $s'(x, y, z, t)$  are the deviation of the velocity and salinity from the cross-sectional averages of velocity and salinity. Using the decompositions from equations 3.7 & 3.8 in equation 3.6 gives,

$$F_{net}(t) = \underbrace{\bar{u}(t) \bar{s}(t) A(t)}_{F_D} + \underbrace{\int_0^A u'(x, y, z, t) s'(x, y, z, t) dA}_{F_{Ex}} \quad (3.9)$$

The first term on the right hand side is the cross-sectional average of the net salt flux across the estuary (hereafter referred as the depth-averaged salt flux,  $F_D$ ), and the second term is the deviation of the net salt flux from the depth-averaged salt flux (hereafter referred as the exchange salt flux,  $F_{Ex}$ ).

The depth-averaged salt flux describes the salt flux caused by the depth-averaged volume flow due to (i) the river volume discharge, and (ii) the change in estuarine volume due to the sea-level change at the estuary mouth driven by coastal Ekman transport (Garvine, 1985), and the average salinity across the estuary mouth. The exchange salt flux is described by the difference in the average salinity of the water leaving,  $S_{out}$ , and entering the estuary,  $S_{in}$ , and the volume exchange flux between the estuary and the coastal ocean,  $Q_{Ex}$  (Figure 3-4).

$$F_{Ex} = \Delta S \cdot Q_{Ex}, \quad (3.10)$$

where  $\Delta S = S_{out} - S_{in}$ . The  $S_{out}$  and  $S_{in}$  are the salinity deviations from the salinity averaged across the estuary. The exchange fluxes and parameters described above are averaged over the 30 days duration of fluctuating winds. Positive  $F_{Ex}$  indicate the estuary loses salt and negative  $F_{Ex}$  indicate the estuary gains salt.

### 3.5 Results

The salt exchange between an estuary and a coastal ocean is the sum of the depth-averaged and exchange salt fluxes. On timescales short compared to the estuary adjustment time, the depth-averaged salt flux changes little (Figure 3-5). The depth-averaged salt flux is the product of the river discharge rate and the average salinity

at the estuary mouth (Equation 3.9). The river discharge rate was kept constant in our model runs while the average salinity adjusts on timescales much longer than the 30 days of fluctuating winds. Thus most of the rapid response to the fluctuating winds will be caused by the exchange salt flux. This is seen in all model runs (Figure 3-5). The exchange salt flux is the product of the exchange volume flux,  $Q_{Ex}$ , and the salinity difference,  $\Delta S$ . The changes in the salt exchange are primarily due to the larger percent changes in  $\Delta S$ , and less to the smaller fractional changes in  $Q_{Ex}$  (Figure 3-7 & 3-8). The percent changes in  $\Delta S$  and  $Q_{Ex}$  shown in these figures are relative to no wind model runs for each parameter setting used. The volume exchange flux does not change significantly because it is driven by the along-estuary salinity gradient (Hansen and Rattray, 1965), which adjusts on a timescale longer than the 30 days of fluctuating winds. The fluctuating winds can alter  $\Delta S$  by changing the estuarine processes that alter the salinity of the water leaving the estuary, or coastal processes that alter the salinity entering the estuary.

The influence of fluctuating winds on the salt exchange are examined for different conditions that can alter the  $\Delta S$ . These conditions include the river discharge rates, coastal pycnocline depth, alongshore wind-stress amplitude and period, estuary orientation, estuary thalweg depth, the coastal bottom slope, and geostrophic alongshore flow.

### **3.5.1 How Fluctuating Winds Alter the Salt Exchange of Estuaries**

#### **Influence of Wind-Stress**

When the wind-stress amplitude or period is changed, there can be changes in the stratification of an estuary, and changes in the coastal upwelling and down-welling. The amplitude and period of the wind-stress is varied from 0.05-0.3 Pa and 6-30 days

to examine how the wind-stress alters the salt exchange between an estuary and a coastal ocean.

For this range of wind-stress amplitude and period, the fluctuating winds in the estuary cause a larger change in the salt exchange, compared to the change caused by fluctuating winds in the coastal ocean. This was examined by comparing the salt exchange of models runs made of uniform winds over both the estuary and coastal ocean (blue arrows in Figure 3-2A), and model runs made of winds only over the coastal ocean (red arrows in Figure 3-2A). The difference between these model runs can be attributed to the effect of winds in the estuary. This comparison of the salt exchange is seen in Figure 3-6. The black arrows show the salt exchange, i.e., net salt flux, caused by fluctuating winds only in the estuary, and the red line shows the salt exchange caused by fluctuating winds only in the coastal ocean. These changes in the salt exchange are primarily due to changes in  $\Delta S$ , as discussed above.

As the wind-stress amplitude and period increases, fluctuating winds in the estuary cause more mixing, reducing the estuarine stratification, increasing the surface salinity leaving the estuary and thus reducing the magnitude of  $\Delta S$  and the salt exchange flux (Figure 3-7A,B). The influence of fluctuating winds in the estuary is dependent on the initial estuarine stratification. When the estuary is initially stratified, the wind-induced mixing in the estuary reduces the magnitude of  $\Delta S$  and changes the salt exchange. This is seen in all our model runs (black arrows in Figure 3-6). When the estuary is initially well-mixed (or sheltered from wind by topography), the wind-induced mixing has no significant effect on  $\Delta S$  ( $\frac{0.01}{-0.70} \approx -1\%$ ) and the salt exchange ( $\frac{63}{-3.94e4} \approx -0.1\%$ ) (Table 3.3).

In the above section, the fluctuating winds start in the upwelling phase causing the coastal pycnocline to upwell, bringing deep salty water to the estuary mouth, thus changing the net salt flux. However, if the winds start in the down-welling phase, then the coastal pycnocline is initially pushed away from the estuary and the upwelling

winds would bring the coastal pycnocline back to its initial condition. The influence of the phase shift is that the movement of the coastal pycnocline is altered in the numerical experiments, i.e., upwelling would no longer bring the coastal pycnocline to the estuary mouth, but would return the coastal pycnocline close to its initial condition.

For timescales much shorter than the time taken for the estuary to adjust to the winds, and when wind-induced mixing in the estuary is important, the initial response of the net salt flux of the estuary depends on (i) the wind-induced mixing in the estuary which removes salt from the estuary, and (ii) the influence of the coastal ocean which depends on how the fluctuating winds move the coastal pycnocline vertically. When the fluctuating winds move the coastal pycnocline to the surface, the coastal ocean adds salt to the estuary, as described earlier in this section. However, when the fluctuating winds move the coastal pycnocline below its initial depth, the coastal ocean removes salt from the estuary (Figure 3-9).

When the influence of the wind-induced mixing in the estuary is in concert with the influence of the coastal down-welling in removing salt from the estuary, the change in the net salt flux is larger compared to when the influence of these mechanisms on the net salt flux are in opposition (blue line in Figure 3-9).

The influence of fluctuating winds in the coastal ocean has an important but secondary effect on the salt exchange. As the wind-stress amplitude and period increases, fluctuating winds upwell deep salty water at the coast increasing the salinity entering the estuary, and thus increasing the magnitude of  $\Delta S$  (Figure 3-8A,B). However, once the upwelling is sufficient to outcrop the coastal pycnocline to the surface, further upwelling does not produce saltier water at the estuary mouth, so the salt exchange does not change much. This is seen in model runs where longer wind periods result in smaller fractional changes in the salt exchange (red line in Figure 3-6B). In a coastal ocean with continuous vertical stratification, upwelling

caused by fluctuating winds keep increasing the salinity entering the estuary because there is always saltier deep water upwelling, so the magnitude of  $\Delta S$  and the salt exchange would increase uniformly with more upwelling. When the coastal ocean is homogeneous, the upwelling caused by fluctuating winds do not change the salinity entering the estuary, so the  $\Delta S$  and salt exchange do not change.

When only the winds in the coastal ocean are important, i.e., the estuary is well-mixed, the influence of the coastal ocean on the initial net salt flux depends on how the fluctuating winds move the coastal pycnocline vertically. When the fluctuating winds move the coastal pycnocline to the surface, the coastal ocean adds salt to the estuary, as discussed earlier in this section. However, when the fluctuating winds move the coastal pycnocline below its initial depth, the coastal ocean removes salt from the estuary. This can be seen in our experiments (red line in Figure 3-9).

In our experiments, when the starting phase of the fluctuating winds is upwelling winds, the coastal pycnocline moves to the surface and the coastal ocean adds salt to the estuary. When the starting phase of the fluctuating winds is down-welling winds (i.e., we use a phase shift in the winds), the coastal pycnocline moves away from the surface and the coastal ocean removes salt from the estuary. This is because the salinity at the estuary mouth decreases as the deep salty water is moved away from the coast by wind-induced Ekman transport. This decreases the salinity difference  $\Delta S$ , between the water entering and leaving the estuary reducing the exchange salt flux, so the estuary loses salt (red line in Figure 3-9).

### **Influence of Estuary Orientation**

When the orientation of an estuary is oblique to the direction of a fluctuating wind, there can be changes in the depth-averaged flow due to the along-estuary wind component. The orientation of the estuary is varied from  $-60^\circ$  to  $60^\circ$  to examine how the orientation of the estuary alters the salt exchange between the estuary and

the ocean due to fluctuating winds.

The orientation of an estuary has an important but secondary effect on the depth-averaged salt flux in an estuary. The fluctuating winds in the estuary have the largest influence on the depth-averaged salt flux when the orientation of the estuary is such that a component of coastal upwelling winds blow along the estuary toward the head of the estuary (Figure 3-10). The depth-averaged salt flux changes by 17% from the no wind case of the same orientation (Table 3.3). For this orientation, the depth-averaged velocity forced by the along-estuary winds opposes the depth-averaged velocity forced by the sea-level setup due to the coastal Ekman transport at the estuary mouth. For these estuary orientations, i.e., positive angles, the along-estuary winds and coastal winds both set up the sea-level at the estuary mouth, enhancing the depth-averaged velocity so the change in the depth-averaged salt flux is large. This change in the depth-averaged salt flux is still only about 33% of the change in the exchange salt flux (Table 3.3). For other estuary orientations, i.e., negative angles, the along-estuary winds set up sea-level but the coastal winds set down the sea-level at the estuary mouth, reducing the depth-averaged velocity so the change in the depth-averaged salt flux is small. This change in the depth-averaged salt flux is about 12% of the change in the exchange salt flux for the parameters used in the base case model run (Table 3.3).

For fluctuating winds only in the coastal ocean, the angle of the estuary does not significantly alter the salt exchange. This is seen by the small change in the salt exchange for the large range of estuary orientations (red line in Figure 3-6C). The above results are consistent with the solutions of Garvine (1985).

### **Influence of Coastal Pycnocline Depth**

When the coastal pycnocline depth is increased, it takes a larger upwelling wind-stress amplitude or duration to upwell deep salty water at the estuary mouth and

alter the salt exchange of the estuary. The pycnocline depth of the coastal ocean is varied between 10–45 m to examine how the change in the depth of the pycnocline alters the salt exchange between the estuary and the coastal ocean due to fluctuating winds.

When the coastal pycnocline depth is increased, the fluctuating winds in the coastal ocean have an important but secondary influence on the salt exchange. Fluctuating winds in a coastal ocean with a deeper pycnocline decreases the salt exchange flux into the estuary, so the estuary loses salt (red line in Figure 3-6D). This is because as the depth of the coastal pycnocline is increased, it takes longer to upwell the same deep salty water from below the coastal pycnocline to the estuary mouth (Csanady, 1977). As a result, for a given upwelling wind-stress, if the coastal pycnocline is deeper, the salinity entering the estuary is less salty, reducing the magnitude of  $\Delta S$  (Figure 3-8D).

When the depth of the coastal pycnocline is changed, it alters the relationship between the upwelling period of fluctuating winds and the salt exchange, discussed in sec. 3.5.1.

### **Influence of the Estuary Thalweg**

In the absence of winds, as the depth of an estuary thalweg is increased, more salty water can enter the estuary, increasing the initial stratification in the estuary (Hansen and Rattray, 1965). We examine how these changes, due to the increase in the estuary thalweg depth, alter the salt exchange due to fluctuating winds in the estuary and coastal ocean. The estuary thalweg depth is varied from 11–45 m for this study. This range of thalweg depth are typical of large estuaries such as Chesapeake Bay and similar to the range used in estuarine studies, e.g, (MacCready, 1999).

As the thalweg depth increases, the fluctuating winds in an estuary have a decreasing influence on the salt exchange due to a decrease in the wind-induced mixing

in the estuary (black arrows in Figure 3-6E). This decrease in the wind-induced mixing is due to the initial stratification in the estuary becoming stronger as the thalweg deepens. As a result, for a given wind-stress amplitude, there is less wind-induced mixing in the estuary and thus the change in the  $\Delta S$  becomes smaller as the thalweg depth increases (Figure 3-7E).

The fluctuating winds in a coastal ocean do not alter the influence on the salt exchange for the range of estuary thalweg depths studied (red line in Figure 3-6E). This is because the thalweg depths set in our study are close to or deeper than the coastal pycnocline, so for a given upwelling wind-stress the deep salty water from below the pycnocline was always able to enter the estuary mouth. If the coastal pycnocline were much deeper than the estuary thalweg, then fluctuating winds in the coastal ocean would have little influence on the salt exchange because the deep salty water would not reach the estuary mouth, except for extended upwelling winds.

### **Influence of River Discharges**

In the absence of winds, when the river discharge increases, two things can happen: (i) the volume exchange,  $Q_{Ex}$ , becomes larger (Hansen and Rattray, 1965), so small changes in  $\Delta S$  can cause large changes in the magnitude of the salt exchange. The changes in  $Q_{Ex}$  discussed here are due to the river discharge and not due to the adjustment of the estuary to the winds; (ii) there is fresher water on the surface estuary, so the initial estuarine stratification is stronger (Hansen and Rattray, 1965) and the discharged coastal plume is fresher (Garvine, 1999). We examine how these changes due to river discharge alter the salt exchange due to fluctuating winds in an estuary and a coastal ocean. The freshwater input at the head of the estuary is varied from  $(0.02 - 2) \times 10^4 \text{ m}^3\text{s}^{-1}$  and is spun up for 200 days before fluctuating winds are applied.

When the river discharge increases, the fluctuating winds in an estuary have an



increasing influence on the salt exchange (black arrows in Figure 3-6F). As the river discharge increases, the initial estuarine stratification is stronger, so the wind-induced mixing in the estuary decreases, reducing the change in the magnitude of  $\Delta S$  (Figure 3-7F). However, the increase in the volume exchange (associated with the increase in the river discharge) is much larger than the decrease in the change in  $\Delta S$ , so the magnitude of the salt exchange increases (black arrows in Figure 3-6F).

When the river discharge increases, the fluctuating winds in a coastal ocean have an increasing influence on the salt exchange (red line in Figure 3-6F). The fluctuating winds in a coastal ocean bring deep salty coastal water into the estuary during upwelling, and a portion of the fresh surface coastal plume water into the estuary during down-welling. As the river discharge increases, the salinity of the plume drawn into the estuary during coastal down-welling decreases, causing a decrease in  $\Delta S$  that is large enough to counter the increase in  $\Delta S$  during coastal upwelling. As a result, over the duration of the fluctuating winds the change in the magnitude of  $\Delta S$  (relative to the no wind model run at each river discharge rate) becomes small (Figure 3-8F). However, the increase in the volume exchange is much larger than the decrease in the change in  $\Delta S$ , so the magnitude of the salt exchange increases (red line in Figure 3-6F).

Increasing the river discharge decreases the effect of the period of fluctuating winds on the salt exchange, discussed in sec. 3.5.1.

### **Influence of Coastal Slopes**

When the slope of a coastal ocean is increased, the deep salty coastal water is closer to the estuary mouth. Thus, for a given upwelling wind-stress, the deep salty water upwell faster at the estuary mouth and alter the salt exchange of the estuary (Csanady, 1977). The slope of the coastal ocean,  $\alpha$ , is varied between  $(0.5-5) \times 10^{-3}$  to examine how the change in the coastal slope alters the salt exchange due to fluctuating

winds in an estuary and a coastal ocean.

The fluctuating winds in a coastal ocean cause an increase in the salt exchange, as the coastal bottom slope increases (Figure 3-6G). When the coastal bottom slope increases, the deep salty water upwells to the estuary mouth faster, for a given upwelling wind-stress, increasing the salinity of the water drawn into the estuary and causing the  $\Delta S$  to increase in magnitude (Figure 3-8G). In our model runs, the steeper coastal slope ( $\alpha = 5 \times 10^{-3}$ ) upwells the center of the coastal pycnocline to the bottom of estuary mouth a day earlier than the gentle coastal slope ( $\alpha = 1 \times 10^{-3}$ ), for the same upwelling wind.

The influence of fluctuating winds in the estuary do not change significantly as the coastal slope increases (black arrows in Figure 3-6G). This is because the coastal slope does not alter the stratification in an estuary (Hansen and Rattray, 1965), so for a given wind-stress amplitude, the wind-induced mixing in the estuary and the change in  $\Delta S$  are similar for our range of coastal slopes (Figure 3-7G).

### **Influence of Coastal Alongshore Flows**

In the absence of winds, when the alongshore flow is opposite of the direction of a coastal trapped Kelvin wave, two things can happen: (i) a portion of the fresh coastal plume water re-circulates in a bulge outside the estuary mouth (Hickey et al., 1998; Fong and Geyer, 2002), so fresh plume water is drawn back into the estuary, making the estuary fresher and reducing the initial estuarine stratification (Hansen and Rattray, 1965); and (ii) the alongshore flow induces a cross-shore slope in the coastal pycnocline that moves the deep salty coastal water closer to the coast (Figure 3-11), similar to Lentz (2008). The cross-shore slope in coastal pycnocline can change how fast the deep water upwells and alter the salinity at the estuary mouth.

The alongshore flow in the coastal ocean is varied between  $-0.1$  to  $0.1 \text{ m s}^{-1}$  to examine how an alongshore flow alters the salt exchange driven by fluctuating winds

in an estuary and a coastal ocean. These model runs are spun up with geostrophic alongshore flow for 200 days then the fluctuating winds are applied for 30 days. The negative alongshore velocities are in the direction of a coastal trapped Kelvin wave.

As the alongshore flow becomes more positive, the fluctuating winds in an estuary have less influence on the salt exchange (black arrows in Figure 3-6H). As the alongshore flow becomes more positive, the fresh coastal plume is drawn back into the estuary making the estuary well-mixed (Hansen and Rattray, 1965). As a result, the wind-induced mixing has little effect in the estuary and the change in  $\Delta S$  becomes small (Figure 3-7H).

As the alongshore flow becomes more positive, the fluctuating winds in the coastal ocean have more influence on the salt exchange (red line in Figure 3-6H). As the alongshore flow becomes more positive (Figure 3-11B), the deep salty water is closer to the estuary mouth. Thus, for a given upwelling wind-stress, the deep salty water upwells faster, causing a large increase in  $\Delta S$  (Figure 3-8H). For the positive alongshore flow, the initial stratification of the estuary is weak while the change in salinity drawn into the estuary during upwelling is large, so the fractional change in  $\Delta S$  is larger than other alongshore flows (Figure 3-8H).

### **Influence of Estuary Width**

When the width of an estuary is increased, there is reduced vertical stratification in the estuary because the isopycnals in the estuary relax across the estuary width due to the Rossby adjustment. This alters the influence of mixing by fluctuating winds in the estuary and alters the salt exchange. The estuary width is increased from 6-80km to examine how the change in the estuary width alters the salt exchange between the estuary and the coastal ocean due to fluctuating winds.

When the width of the estuary is increased, the influence on the salt exchange due to the wind-induced mixing in the estuary becomes smaller such that the influence of

the coastal upwelling and down-welling has a greater influence on the salt exchange (Figure 3-13). This is because as the estuary width increases, the salinity structure across the estuary mouth changes from a vertically stratified estuary to a vertically mixed estuary (but whose cross-estuary salt gradient is significant, see cartoon in Figure 3-12).

As a result, for wide estuaries wind-induced mixing has a small influence on changing the salinity of the water leaving the estuary, so the influence of wind-induced mixing on the salt exchange becomes smaller while the coastal ocean has a greater influence, as the estuary width increases (Figure 3-13).

### 3.6 Discussion

Over shorter than seasonal timescales, the initial stratification of an estuary and an adjacent coastal ocean control the influence that fluctuating winds have on the salt exchange of the estuary. When both regions are well-mixed, the fluctuating winds have no significant influence on the salt exchange. When both regions are stratified, the fluctuating winds have a significant influence on the salt exchange by (i) increasing the surface salinity leaving the estuary due to wind-induced mixing, and (ii) changing the salinity of the water drawn into the estuary mouth during coastal upwelling and down-welling. When both the coastal ocean and the estuary are stratified and when the winds are strong in both the regions, then the mixing in the estuary has by far the greatest effect on the salt exchange, on shorter than the seasonal timescales. The changes in the salt exchange are largely due to changes in the salinity leaving and entering the estuary, and not the volume exchange; this remains true for a range of estuarine and coastal conditions. However, when the angle of the estuary is such that an along-estuary component of the coastal upwelling winds blows toward the head of the estuary (Figure 3-10), the change in the depth-averaged flow in the estuary due to

along-estuary winds also contributes significantly to the change in the salt exchange.

The exchange dynamics discussed above suggest the influence of fluctuating winds depend on the condition of the estuary as the seasons change. For estuaries oblique to the coast, such as the Chesapeake and Delaware Bay, during winter the estuaries are well-mixed due to winter cooling, so the change in the salt exchange caused by fluctuating winds is primarily due to the depth-averaged flow driven by the along-estuary winds and the coastal upwelling and down-welling. While during spring/summer the estuaries are stratified (Officer et al., 1984), the change in the salt exchange caused by fluctuating winds is primarily due to wind-induced mixing in the estuary and the depth-averaged flow driven by along-estuary winds.

Over shorter than seasonal timescales, the fluctuating winds alter the salt exchange of the estuary thus changing the average salinity in the estuary, but over longer timescales when the estuary has reached steady state, the salt exchange must be zero. Studies on the longer than seasonal influence of fluctuating winds must focus on how the dynamics in the estuary change to return the salt exchange to zero and the estuary to steady state.

**Extension to Other Regions** The results discussed above were derived for wind-stress conditions typical of the East coast of US. In the East coast, the fluctuating winds are such that time-integrated upwelling and down-welling wind-stress have similar magnitudes, so the time-averaged wind-stress amplitude is weak or zero (Austin and Lentz, 1999). However, there are regions where the time-integrated upwelling and down-welling wind-stress are not of similar magnitudes, so the time-averaged wind-stress amplitude is strong (Pickett and Schwing, 2006, their Fig.3). Two such regions examined are: (i) where the upwelling wind is followed by weak or cessation of wind, such as the West coast of US, and (ii) where the upwelling winds persist during the seasonal timescale.

For both weak and strong time-averaged wind-stress regions, the wind-induced mixing in the estuary remains more important than changes in the water drawn into the estuary (Figure 3-6I). The initial stratification and amplitude of the wind-stress which control the wind-induced mixing are identical for these model runs, thus the mixing in the estuary is similar, so the change in  $\Delta S$  are similar (Figure 3-7 I). The change in the salt exchange due to mixing in the estuary ranges from  $(2.21 - 2.80) \times 10^4 \text{ g kg}^{-1} \text{ m}^3 \text{ s}^{-1}$  as the time-averaged wind-stress increases towards upwelling (Table 3.3).

As the time-averaged wind-stress is increased towards upwelling favorable, two things happen: (i) the change in the salt exchange due to coastal upwelling becomes larger in magnitude (red line in Figure 3-6I). This is because as the time-averaged wind-stress increases the near-shore coastal ocean remains largely in an upwelled state, so the deep salty water from below the pycnocline is always present at the estuary mouth. This causes the salinity entering the estuary to increase thus increasing the magnitude of  $\Delta S$  (Figure 3-8I); (ii) the change in the salt exchange due to the depth-averaged salt flux out of the estuary also becomes larger. This is due to the near-shore coastal ocean largely being in an upwelled state, which sets down the coastal sea-surface at the estuary mouth driving a depth-averaged volume flow out of the estuary (Garvine, 1985). As the time-averaged wind-stress is increased towards upwelling favorable, the change in the salt exchange due to the coastal upwelling ( $-2.48 \times 10^4 \text{ g kg}^{-1} \text{ m}^3 \text{ s}^{-1}$ ) and depth-averaged flow ( $1.95 \times 10^4 \text{ g kg}^{-1} \text{ m}^3 \text{ s}^{-1}$ ) become roughly as large as the change in the salt exchange due to mixing in the estuary (Table 3.2&3.3). This indicates that in regions with strong time-averaged upwelling wind-stress, the depth-averaged flow out of the estuary and the change in salinity of the water drawn into the estuary become as significant as the wind-induced mixing in the estuary.

There are regions where a stratified estuary is sheltered from winds by the surrounding topography such as the Merrimack River. During fluctuating winds, in

these regions the change in the salinity of the water drawn into the estuary from the coastal ocean and the change in the depth-averaged flow control the salt exchange of the estuary.

### 3.7 Conclusions

This study demonstrates that over shorter than seasonal timescales, the initial stratification in an estuary strongly controls the influence that fluctuating winds have on the salt exchange between an estuary and a coastal ocean. Fluctuating winds in the estuary have little influence on the salt exchange for well-mixed estuaries, while for stratified estuaries the influence is significant on the salt exchange. The change in the salt exchange is caused largely by the fluctuating winds changing the salinity difference between the water entering and leaving the estuary, but does not significantly alter the volume exchange. In the case of estuaries oblique to the coast, an along-estuary depth-averaged flow is introduced that contributes to the salt exchange. In regions where the time-averaged upwelling wind-stress is large and upwelling favorable, the wind-induced mixing in the estuary, the coastal upwelling, and the depth-averaged flow cause comparable changes in the salt exchange.

The fluctuating winds in the estuary decrease the average salinity in the estuary indicating that the freshwater reside longer in the estuary. Thus, the fluvial pollutants carried into the estuary by the freshwater runoff from land also reside longer in the estuary, before being discharged and diluted in the coastal ocean. When there are weather-band fluctuations in the wind lasting less than seasonal timescales, the exchange dynamics discussed above show that pollutants accumulate in the estuary.

**Table 3.1:** The mean and standard deviation of the alongshore wind stress amplitude for several regions around the US coast. The data is averaged for the summer and winter seasons using 5 years of NDBC buoy historical observations from either 2000-2004 or 2005-2009. The orientation of the local coastline is used to determine the alongshore component of the fluctuating winds. The wind stress is estimated using  $\tau = \rho C_d u^2$ ; where  $\rho \sim 1.3 \text{ kg m}^{-3}$ ,  $C_d \sim 10^{-3}$ ,  $u$  is wind speed.

Region	Season	Year	Wind Stress	Wind Stress	$\bar{\tau} : \tau'$
			Mean, $\bar{\tau}$ (Pa)	Deviation, $\tau'$ (Pa)	
Chesapeake Bay (CHLV2)	Winter	2000	0.00	0.06	0.0
		2001	0.00	0.06	0.0
		2002	0.00	0.06	0.0
		2003	0.00	0.06	0.0
		2004	0.00	0.07	0.0
	Summer	2000	0.00	0.04	-0.1
		2001	0.00	0.04	-0.1
		2002	0.00	0.04	-0.1
		2003	-0.02	0.03	-0.7
		2004	0.00	0.03	-0.1
Gulf of Maine (IOSN3)	Winter	2000	0.00	0.04	0.0
		2001	0.00	0.03	-0.1
		2002	0.00	0.05	0.0
		2003	0.00	0.06	0.0
		2004	0.00	0.04	0.0
	Summer	2000	0.00	0.04	-0.1
		2001	-0.01	0.03	-0.2
		2002	0.00	0.04	0.0
		2003	-0.01	0.03	-0.2
		2004	0.00	0.03	-0.2
West Coast (ANVC1)	Winter	2006	0.00	0.01	-0.2
		2007	0.00	0.01	0.0
		2008	0.00	0.01	-0.1
		2009	0.00	0.01	-0.3
		2010	0.00	0.01	-0.5
	Summer	2006	0.00	0.04	0.5
		2007	0.00	0.03	0.4
		2008	0.00	0.04	0.8
		2009	0.00	0.03	0.8
		2010	0.00	0.03	0.4
Buzzards Bay (BUZM3)	Winter	2000	-0.02	0.06	-0.3
		2001	-0.02	0.04	-0.4
		2002	-0.03	0.05	-0.5
		2003	-0.02	0.07	-0.2
		2004	-0.02	0.05	-0.3
	Summer	2000	0.00	0.04	-0.1
		2007	-0.01	0.02	-0.4
		2008	-0.01	0.03	-0.2
		2009	-0.01	0.03	-0.3
		2010	0.00	0.03	-0.1



**Table 3.2:** The net salt flux and depth-averaged and exchange salt fluxes averaged over the 30 days duration of (1<sup>st</sup> row) only coastal fluctuating winds. Also shown are the change in the average salinity of the estuary  $\delta\bar{s}_{est}$ , the residence time  $T_R$ , and the salinity difference between the estuary outflow and oceanic inflow  $\Delta S$  for different parameters of the estuary and the coastal ocean. The values in braces show the influence of only coastal winds.

Coast Winds	$F_{net}$ ( $\text{g kg}^{-1} \text{m}^3 \text{s}^{-1}$ )	$F_D$ ( $\text{g kg}^{-1} \text{m}^3 \text{s}^{-1}$ )	$F_{Ex}$ ( $\text{g kg}^{-1} \text{m}^3 \text{s}^{-1}$ )	$\delta\bar{s}$ ( $\text{g kg}^{-1}$ )	$\Delta S$ ( $\text{g kg}^{-1}$ )
<b>Wind Stress</b>					
0 Pa	-4.70E+03 (0.E+0)	4.52E+04 (0.E+0)	-4.99E+04 (1.81E-1)	0.1878 (0.00)	-0.55 (0.00)
0.05 Pa	-4.47E+02 (4.26E+3)	4.48E+04 -(4.12E+2)	-4.52E+04 (4.67E+3)	0.082 -(0.11)	-0.62 -(0.07)
0.1 Pa	-3.39E+03 (1.32E+3)	4.37E+04 -(1.56E+3)	-4.70E+04 (2.87E+3)	0.1766 -(0.01)	-0.63 -(0.08)
0.2 Pa	-1.50E+04 -(1.03E+4)	4.76E+04 (2.4E+3)	-6.26E+04 -(1.27E+4)	0.5842 (0.40)	-0.68 -(0.13)
0.3 Pa	-1.89E+04 -(1.42E+4)	4.47E+04 -(5.02E+2)	-6.36E+04 -(1.36E+4)	0.6021 (0.41)	-0.64 -(0.09)
<b>Wind Period</b>					
3 day	-3.39E+03 (1.32E+3)	4.37E+04 -(1.56E+3)	-4.70E+04 (2.87E+3)	0.1766 -(0.01)	-0.63 -(0.08)
5 day	-1.85E+04 -(1.38E+4)	4.50E+04 -(2.13E+2)	-6.35E+04 -(1.36E+4)	0.7525 (0.56)	-0.74 -(0.19)
7.5 day	-2.71E+04 -(2.24E+4)	4.54E+04 (2.1E+2)	-7.25E+04 -(2.26E+4)	1.0845 (0.90)	-0.80 -(0.24)
15 day	-3.03E+04 -(2.56E+4)	4.63E+04 (1.11E+3)	-7.66E+04 -(2.67E+4)	1.2426 (1.05)	-0.83 -(0.28)
Mixed Est.	-1.57E+03 (1.27E+3)	3.78E+04 -(4.53E+2)	-39414.7795 (1.72E+3)	0.1093 (0.08)	-0.7138 -(0.10)
<b>Est.Angle</b>					
-60°	-8.88E+03 -(6.71E+3)	4.42E+04 -(8.96E+3)	-5.31E+04 (2.24E+3)	0.1374 (0.08)	-0.44 (0.13)
0°	-3.39E+03 (1.32E+3)	4.37E+04 -(1.56E+3)	-4.70E+04 (2.87E+3)	0.1766 -(0.01)	-0.63 -(0.08)
+60°	-1.67E+03 -(8.17E+3)	6.07E+04 -(3.02E+3)	-6.24E+04 -(5.14E+3)	0.1913 (0.10)	-1.02 (0.24)
<b>Pycnocline Depth</b>					
10 m	3.34E+03 (7.85E+3)	4.57E+04 (5.02E+3)	-4.24E+04 (2.83E+3)	-0.0801 -(0.01)	-0.58 -(0.07)
15 m	-3.39E+03 (1.32E+3)	4.37E+04 -(1.56E+3)	-4.70E+04 (2.87E+3)	0.1766 -(0.01)	-0.63 -(0.08)
30 m	3.38E+03 (2.31E+3)	4.36E+04 -(1.98E+3)	-4.02E+04 (4.29E+3)	-0.0323 -(0.13)	-0.55 (0.01)
45 m	1.27E+04 (8.95E+3)	4.62E+04 (1.42E+2)	-3.35E+04 (8.81E+3)	-0.2593 -(0.32)	-0.49 (0.09)
<b>Thalweg Depth</b>					
11 m	-3.85E+03 (8.74E+2)	3.83E+04 (7.6E+3)	-4.21E+04 -(6.72E+3)	0.5195 (0.28)	-0.61 (0.16)
30 m	-3.39E+03 (1.32E+3)	4.37E+04 -(1.56E+3)	-4.70E+04 (2.87E+3)	0.1766 -(0.01)	-0.63 -(0.08)
45 m	-9.93E+03 -(6.28E+3)	4.47E+04 -(8.47E+3)	-5.47E+04 (2.2E+3)	0.0619 -(0.02)	-0.64 (0.04)
<b>River Discharge</b>					
200 $\text{m}^3/\text{s}$	-1.07E+04 -(3.03E+3)	-3.36E+02 -(1.46E+3)	-1.04E+04 -(1.57E+3)	0.387 (0.16)	-0.19 -(0.08)
2000 $\text{m}^3/\text{s}$	-3.39E+03 (1.32E+3)	4.37E+04 -(1.56E+3)	-4.70E+04 (2.87E+3)	0.1766 -(0.01)	-0.63 -(0.08)
20000 $\text{m}^3/\text{s}$	3.25E+04 (2.25E+4)	3.76E+05 -(5.13E+4)	-3.43E+05 (7.37E+4)	-1.2062 -(1.06)	-3.54 (0.24)
<b>Coastal Slope</b>					
0.0005	-8.20E+03 (8.35E+2)	2.94E+04 -(1.65E+4)	-3.76E+04 (1.74E+4)	-0.2383 -(0.35)	-0.46 (0.04)
0.001	-3.39E+03 (1.32E+3)	4.37E+04 -(1.56E+3)	-4.70E+04 (2.87E+3)	0.1766 -(0.01)	-0.63 -(0.08)
0.005	9.80E+03 -(2.5E+3)	6.48E+04 (5.09E+3)	-55034.3345 -(7.59E+3)	0.4063 (0.12)	-0.9284 -(0.06)
0.01	-8.82E+03 -(5.09E+2)	3.03E+04 (3.78E+3)	-3.92E+04 -(4.29E+3)	0.0626 (0.07)	-0.83 -(0.18)
<b>Along Shore Flow</b>					
-0.1 m/s	-5.05E+03 (5.47E+2)	5.27E+04 -(3.56E+3)	-5.78E+04 (4.1E+3)	0.4413 -(0.04)	-0.71 -(0.05)
0 m/s	-3.39E+03 (1.32E+3)	4.37E+04 -(1.56E+3)	-4.70E+04 (2.87E+3)	0.1766 -(0.01)	-0.63 -(0.08)
+0.1 m/s	8.85E+03 -(1.62E+4)	5.68E+04 -(7.78E+3)	-4.80E+04 -(8.41E+3)	-0.1981 (0.64)	-0.263 -(0.18)
East Coast	-3.39E+03 (1.32E+3)	4.37E+04 -(1.56E+3)	-4.70E+04 (2.87E+3)	0.18 -(0.01)	-0.63 -(0.08)
West Coast	-2.17E+04 -(1.7E+4)	4.82E+04 (3.04E+3)	-7.00E+04 -(2.01E+4)	1.02 (0.84)	-0.87 -(0.32)
Steady Upwelling	-1.89E+04 -(1.42E+4)	5.58E+04 (1.06E+4)	-7.47E+04 -(2.48E+4)	1.14 (0.95)	-0.93 -(0.38)

**Table 3.3:** Similar to Table 3.2, but showing the winds applied both and estuary and coastal ocean for different parameters of the estuary and the coastal ocean. The values in braces show the influence of only estuarine winds.

Estuary & Coastal Winds	$F_{net}$ ( $\text{g kg}^{-1} \text{m}^3 \text{s}^{-1}$ )	$F_D$ ( $\text{g kg}^{-1} \text{m}^3 \text{s}^{-1}$ )	$F_{Ex}$ ( $\text{g kg}^{-1} \text{m}^3 \text{s}^{-1}$ )	$\delta\bar{s}$ ( $\text{g kg}^{-1}$ )	$\Delta S$ ( $\text{g kg}^{-1}$ )
Wind Stress					
0 Pa	-4.70E+03 (0.E+0)	4.52E+04 (0.E+0)	-4.99E+04 (0.E+0)	0.1878 (0.00)	-0.55 (0.00)
0.05Pa	1.85E+04 (1.9E+4)	4.83E+04 (3.54E+3)	-2.98E+04 (1.54E+4)	-0.592 -(0.67)	-0.47 (0.15)
0.1Pa	2.24E+04 (2.58E+4)	4.73E+04 (3.68E+3)	-2.49E+04 (2.21E+4)	-0.7783 -(0.95)	-0.41 (0.23)
0.2 Pa	2.34E+04 (3.84E+4)	5.37E+04 (6.05E+3)	-3.02E+04 (3.24E+4)	-0.8176 -(1.40)	-0.35 (0.34)
0.3 Pa	2.47E+04 (4.36E+4)	5.16E+04 (6.92E+3)	-2.69E+04 (3.67E+4)	-0.9353 -(1.54)	-0.28 (0.36)
Wind Period					
3 day	2.24E+04 (2.58E+4)	4.73E+04 (3.68E+3)	-2.49E+04 (2.21E+4)	-0.7783 -(0.95)	-0.41 (0.23)
5 day	1.68E+04 (3.53E+4)	5.17E+04 (6.66E+3)	-3.49E+04 (2.87E+4)	-0.5205 -(1.27)	-0.45 (0.30)
7.5day	1.22E+04 (3.93E+4)	5.39E+04 (8.45E+3)	-4.17E+04 (3.08E+4)	-0.2837 -(1.37)	-0.49 (0.30)
15 day	9.79E+03 (4.E+4)	5.46E+04 (8.26E+3)	-4.48E+04 (3.18E+4)	-0.1749 -(1.42)	-0.53 (0.30)
Mixed Est.	-4.08E+02 (1.17E+3)	3.89E+04 (1.1E+3)	-39351.7692 (6.3E+1)	0.043 -(0.07)	-0.7021 (0.01)
Est. Angle					
-60°	2.09E+04 (2.98E+4)	4.04E+04 -(3.77E+3)	-1.95E+04 (3.36E+4)	-1.0879 -(1.23)	-0.18 (0.27)
0°	2.24E+04 (2.58E+4)	4.73E+04 (3.68E+3)	-2.49E+04 (2.21E+4)	-0.7783 -(0.95)	-0.41 (0.23)
+60°	5.25E+04 (5.41E+4)	7.12E+04 (1.05E+4)	-1.88E+04 (4.36E+4)	-1.4116 -(1.60)	-0.31 (0.71)
Pycnocline Depth					
10 m	2.91E+04 (2.58E+4)	5.01E+04 (4.4E+3)	-2.10E+04 (2.14E+4)	-0.9948 -(0.91)	-0.36 (0.22)
15 m	2.24E+04 (2.58E+4)	4.73E+04 (3.68E+3)	-2.49E+04 (2.21E+4)	-0.7783 -(0.95)	-0.41 (0.23)
30 m	2.66E+04 (2.33E+4)	4.84E+04 (4.77E+3)	-2.17E+04 (1.85E+4)	-0.8848 -(0.85)	-0.34 (0.20)
45 m	3.45E+04 (2.19E+4)	5.08E+04 (4.65E+3)	-1.63E+04 (1.72E+4)	-1.0706 -(0.81)	-0.28 (0.21)
Thalweg Depth					
11 m	3.63E+04 (4.02E+4)	5.27E+04 (1.45E+4)	-1.64E+04 (2.57E+4)	-1.1216 -(1.64)	-0.28 (0.33)
15 m	2.24E+04 (2.58E+4)	4.73E+04 (3.68E+3)	-2.49E+04 (2.21E+4)	-0.7783 -(0.95)	-0.41 (0.23)
45 m	4.94E+03 (1.49E+4)	4.59E+04 (1.18E+3)	-4.10E+04 (1.37E+4)	-0.4201 -(0.48)	-0.57 (0.07)
River Discharge					
200 $\text{m}^3/\text{s}$	-4.94E+03 (5.77E+3)	1.44E+03 (1.78E+3)	-6.38E+03 (3.99E+3)	0.1652 -(0.22)	-0.12 (0.07)
2000 $\text{m}^3/\text{s}$	2.24E+04 (2.58E+4)	4.73E+04 (3.68E+3)	-2.49E+04 (2.21E+4)	-0.7783 -(0.95)	-0.41 (0.23)
20000 $\text{m}^3/\text{s}$	1.03E+05 (7.07E+4)	3.96E+05 (2.05E+4)	-2.93E+05 (5.01E+4)	-3.6735 -(2.47)	-3.21 (0.33)
Coastal Slope					
0.0005	1.50E+04 (2.32E+4)	3.56E+04 (6.16E+3)	-2.06E+04 (1.7E+4)	-0.9971 -(0.76)	-0.29 (0.17)
0.001	2.24E+04 (2.58E+4)	4.73E+04 (3.68E+3)	-2.49E+04 (2.21E+4)	-0.7783 -(0.95)	-0.41 (0.23)
0.005	4.03E+04 (3.05E+4)	7.28E+04 (7.94E+3)	-32490.1671 (2.25E+4)	-0.5521 -(0.96)	-0.684 (0.24)
0.01	2.36E+04 (3.24E+4)	4.00E+04 (9.67E+3)	-1.64E+04 (2.27E+4)	-1.0491 -(1.11)	-0.51 (0.32)
Alongshore Flow					
-0.1 m/s	3.13E+04 (3.63E+4)	6.03E+04 (7.58E+3)	-2.90E+04 (2.88E+4)	-0.8851 -(1.33)	-0.42 (0.29)
0 m/s	2.24E+04 (2.58E+4)	4.73E+04 (3.68E+3)	-2.49E+04 (2.21E+4)	-0.7783 -(0.95)	-0.41 (0.23)
0.1 m/s	1.84E+04 (9.56E+3)	5.53E+04 -(1.54E+3)	-3.69E+04 (1.11E+4)	-0.4863 -(0.29)	-0.252 (0.01)
East Coast	2.24E+04 (2.58E+4)	4.73E+04 (3.68E+3)	-2.49E+04 (2.21E+4)	-0.78 -(0.95)	-0.41 (0.23)
West Coast	1.35E+04 (3.53E+4)	5.66E+04 (8.34E+3)	-4.31E+04 (2.69E+4)	-0.18 -(1.21)	-0.59 (0.29)
Steady Upwelling	1.80E+04 (3.69E+4)	6.47E+04 (8.86E+3)	-4.67E+04 (2.8E+4)	-0.23 -(1.37)	-0.62 (0.31)

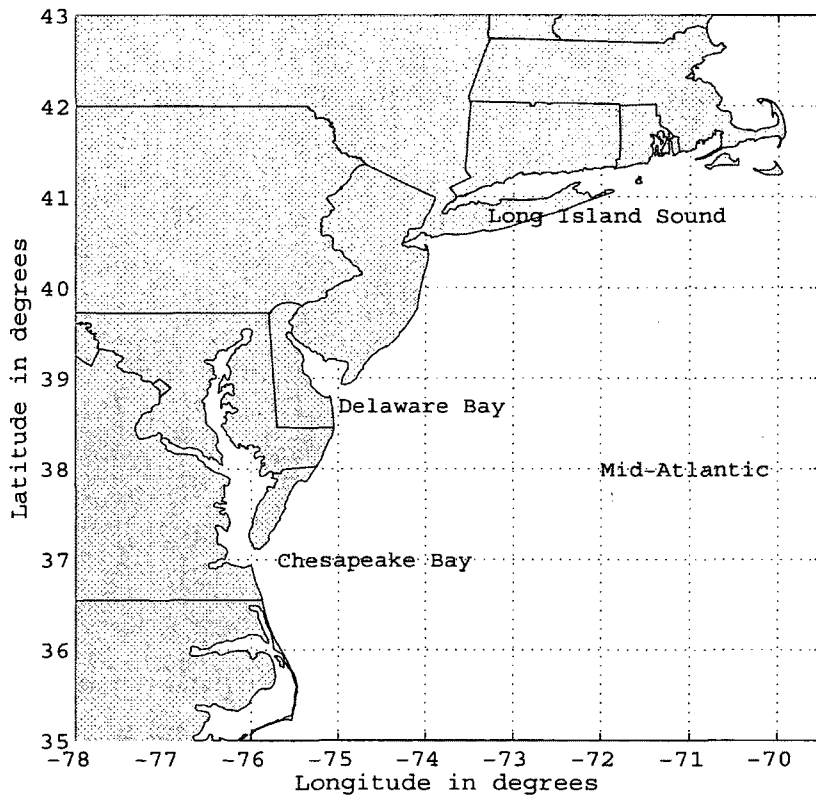


**Figure 3-1:** Our numerical experiments are modeled after the large estuaries and coastal ocean of the Mid-Atlantic Bight, including Chesapeake Bay and Delaware Bay.

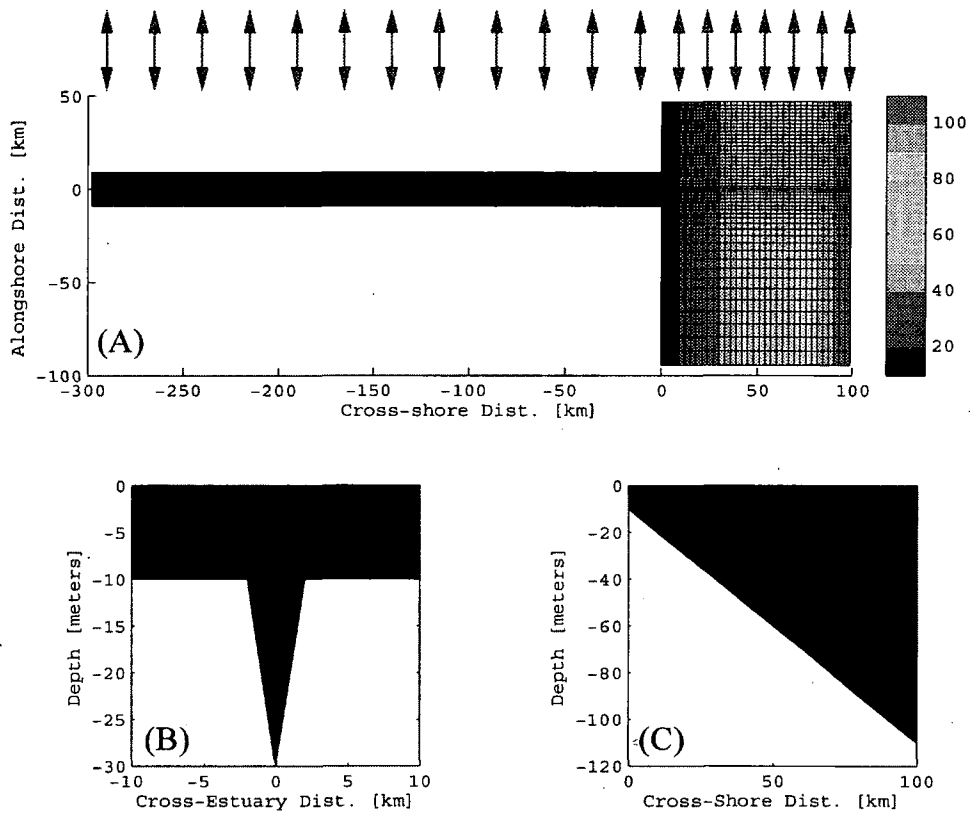


**Figure 3-2:** The numerical domain used in our experiments (A) the plan view of the numerical domain; colors indicate the depth and the lattice structure shows the depth grid points. The blue arrows show spatially uniform fluctuating winds in the estuary and the coastal ocean, and the red arrows show spatially uniform fluctuating wind only in the coastal ocean. (B) The cross-sectional view into the estuary mouth, and (C) the cross-shore view of the coastal ocean; black is water and white is estuary bottom.

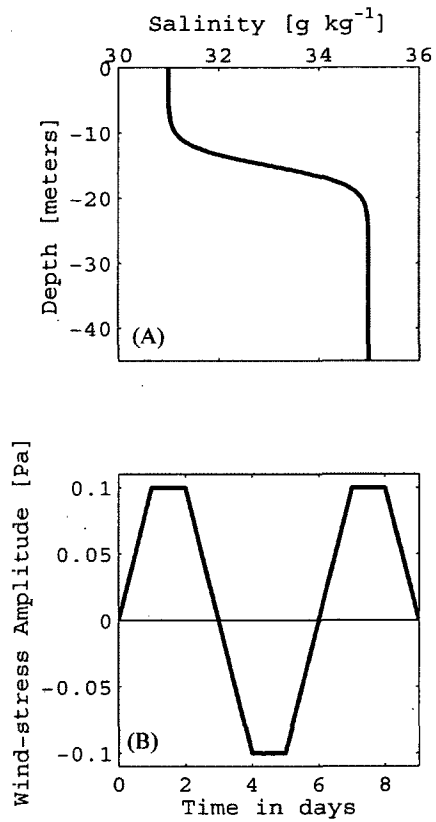


**Figure 3-3:** (A) The salinity profile for the coastal ocean in the base case numerical experiment. The profile represents summer conditions in the MAB. (B) The winds used in the base case numerical experiment. The winds ramp to maximum amplitude over a duration of a day. The winds are applied for a duration of 30 days, and has a time-averaged wind-stress amplitude of zero.

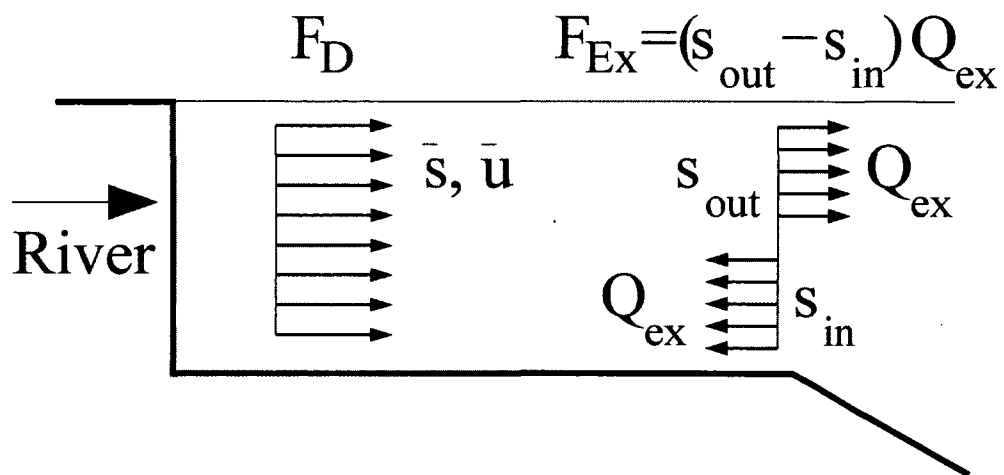


**Figure 3-4:** A cartoon of the along-estuary section. The salt exchange, i.e., net salt flux of the estuary is decomposed into two components; the depth-averaged salt flux,  $F_D$  and the exchange salt flux,  $F_{Ex}$ .

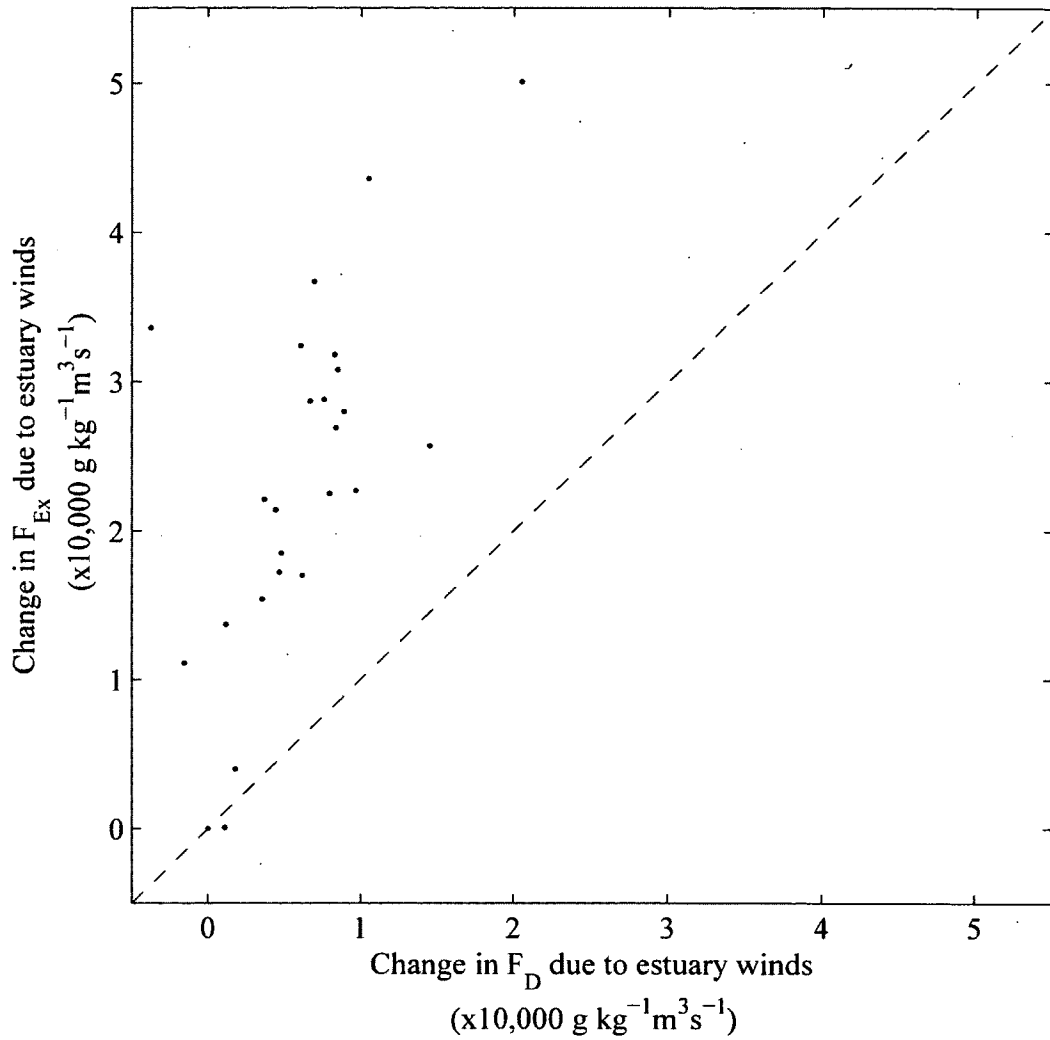


**Figure 3-5:** The change in the exchange salt flux,  $F_{EX}$ , plotted against the change in the depth-averaged salt flux,  $F_D$ , for fluctuating winds only in the estuary. The change in  $F_{EX}$  due to fluctuating winds in the estuary are nearly always much larger than the change in  $F_D$ . The dashed line is the 1:1 proportionality line.

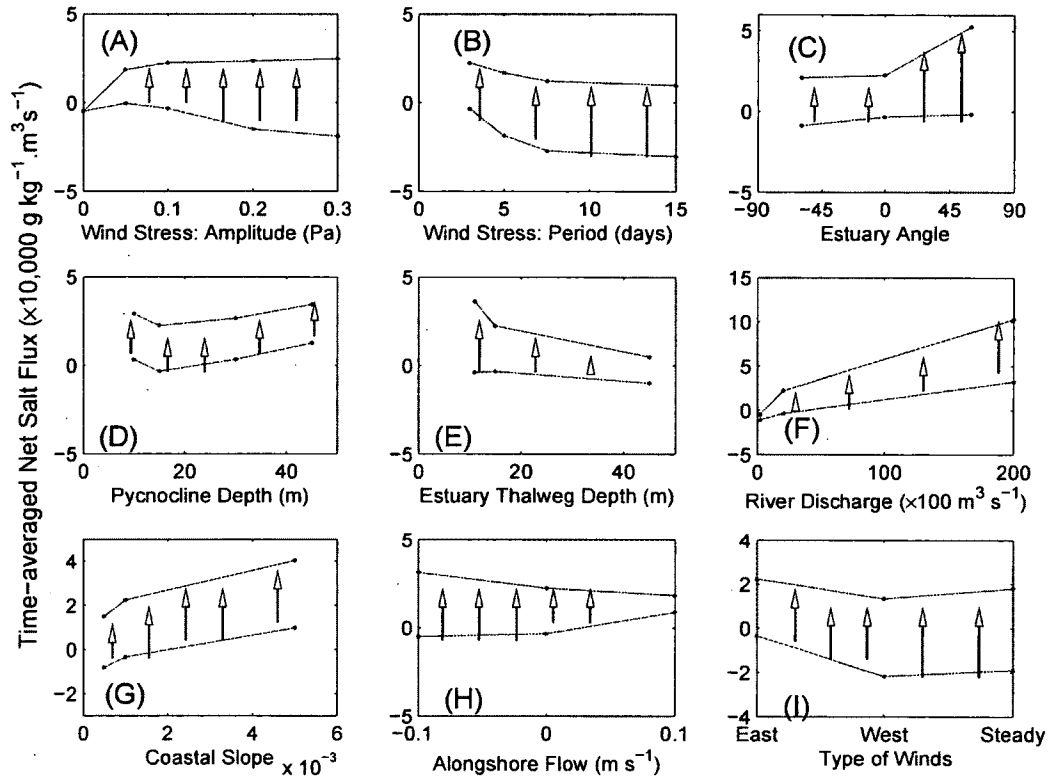


**Figure 3-6:** The red line shows the influence of the coastal winds only, the blue lines shows the influence of both estuarine and coastal winds, and the black arrows show the influence of only estuarine winds. Positive y-axis means estuary is losing salt and negative means estuary is gaining salt. The salt exchange, i.e., net salt flux (averaged over 30 days of wind) plotted as a function of estuarine and coastal conditions: (A) wind-stress amplitude, (B) wind-stress period, (C) estuary angle; positive angle are above west direction and negative angles are below west direction, (D) coastal pycnocline depth, (E) estuary thalweg depth, (F) river discharge, (G) coastal bottom slope, (H) alongshore flow, and (I) wind-stress amplitude representative of different regions. When there are no winds, the time-averaged net salt flux is close to zero.



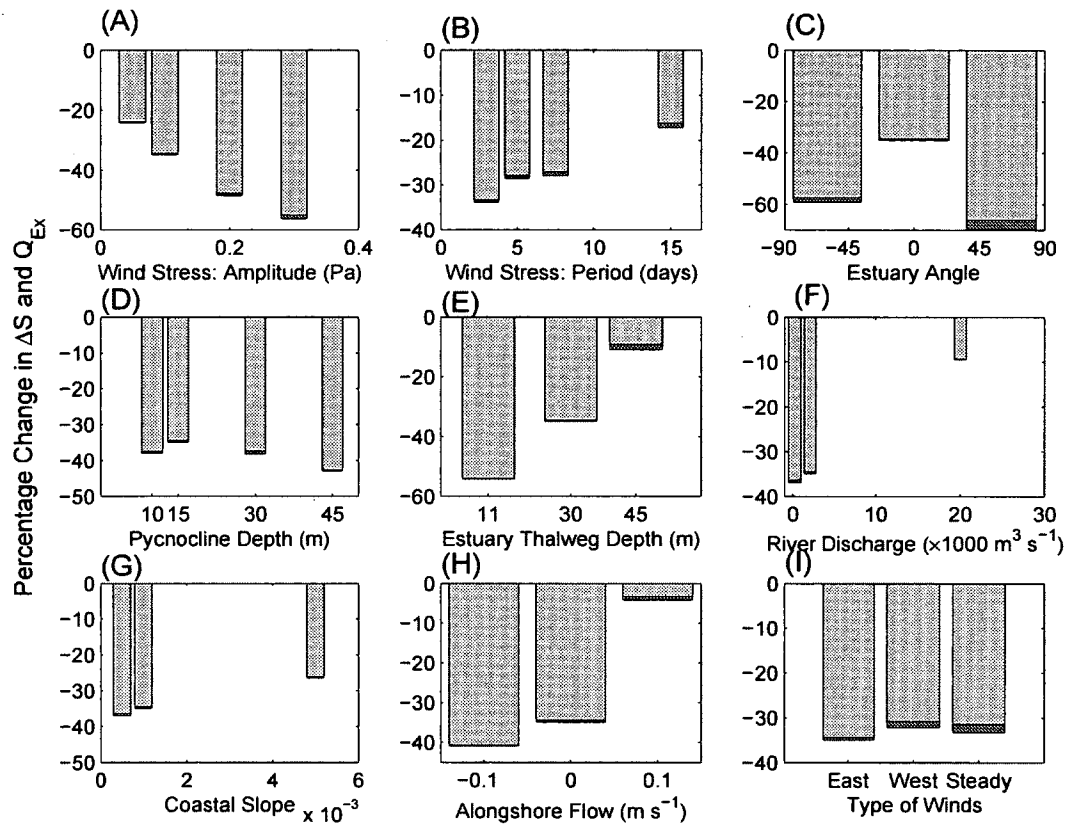


**Figure 3-7:** The percentage change in the volume exchange flux,  $Q_{Ex}$  (pink bars) and  $\Delta S$  (blue bars) for different estuarine and coastal conditions, for only estuarine winds are applied to the model run. Negative percentage indicates the  $\Delta S$  is larger than the  $\Delta S$  for the no wind model run of each parameter permutation. The percent change in  $\Delta S$  is much larger than the change in  $Q_{Ex}$ , so the wind influence on the salt exchange is mostly due to changes in  $\Delta S$ .

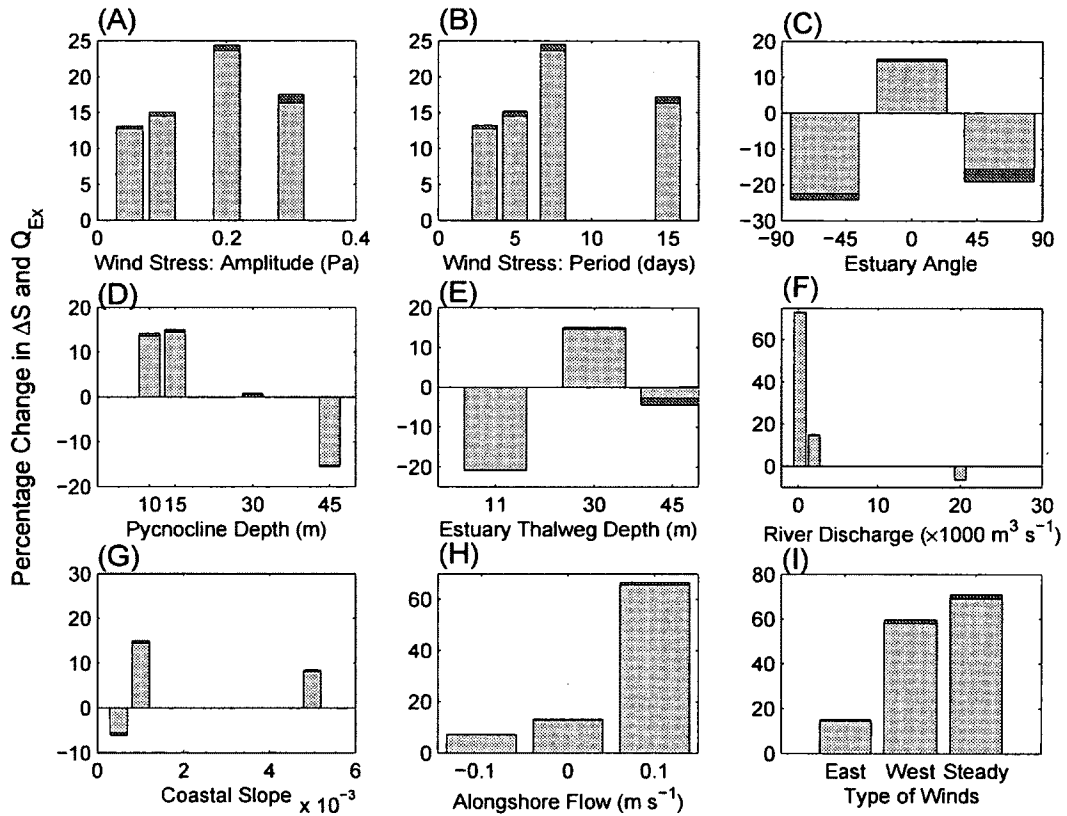


**Figure 3-8:** Same as Figure 3-7, but for winds applied only in the coastal ocean. Positive percentage indicates the  $\Delta S$  is smaller than the  $\Delta S$  for the no wind model run of each parameter permutation.

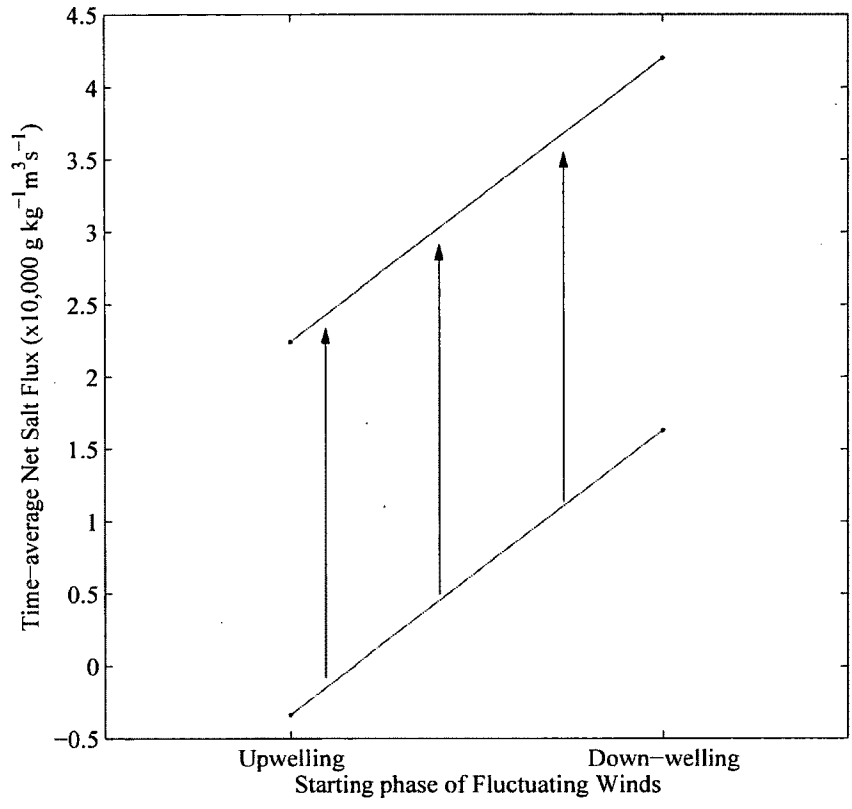


**Figure 3-9:** The time-averaged net salt flux over 30 days of fluctuating winds as a function of the starting phase of the winds. The red line show winds only in the coastal ocean and the blue line show winds applied both on the ocean and the estuary, and the black arrows are the influence of winds only in the estuary.

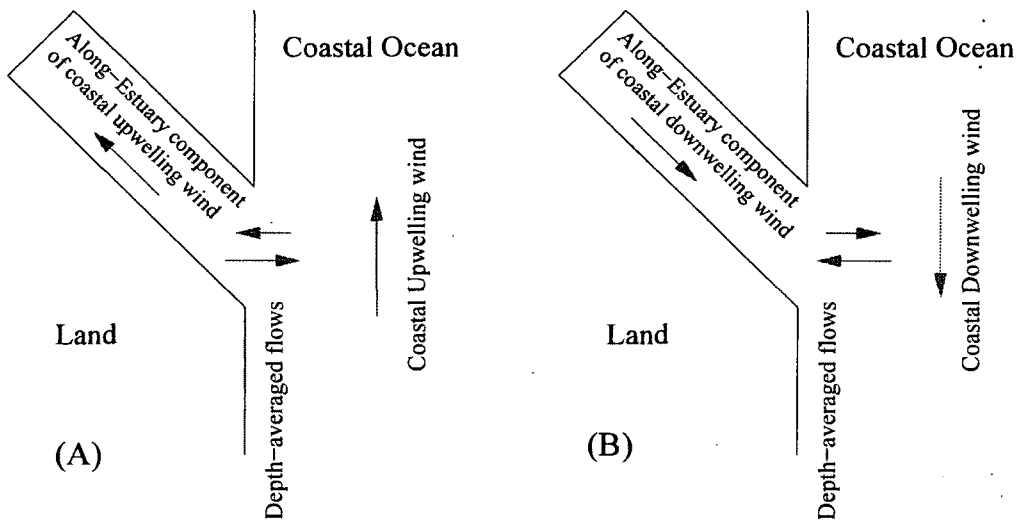


**Figure 3-10:** A cartoon of how winds influence an estuary that is oblique to the coast and the coastal winds. The red arrows show the coastal wind directions and the depth-averaged flow caused by (A) coastal upwelling winds, and (B) down-welling winds, and the blue arrows show the depth-averaged flow forced by the along-estuary component of the coastal winds. For this orientation in the Northern hemisphere, the depth-averaged flows driven by the coastal and along-estuary winds counter each other (Garvine, 1985).

For Northern Hemisphere

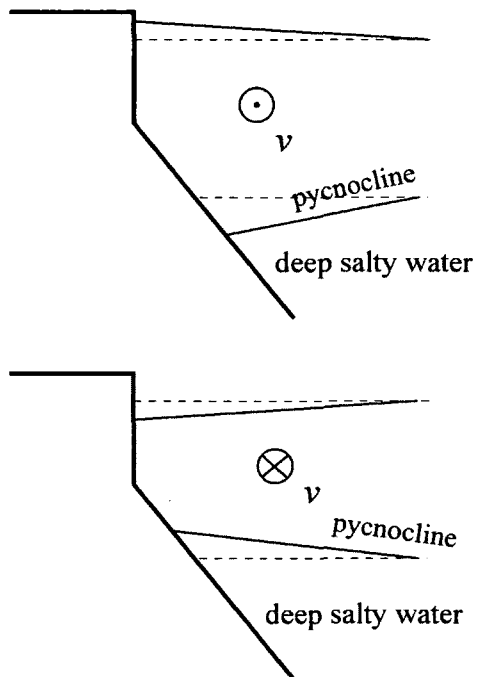
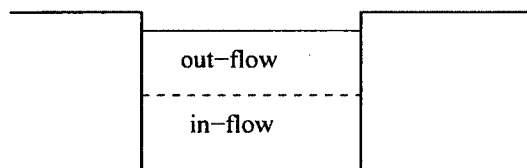
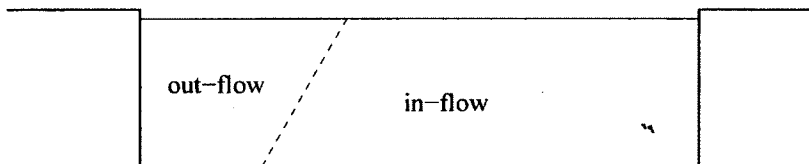


**Figure 3-11:** A cartoon of how alongshore flow,  $v$ , changes the slope of the coastal pycnocline and sea-surface in the absence of winds, moving the deep salty coastal water (A) away from the estuary mouth, and (B) towards the estuary mouth. The dashed lines show pycnocline and sea-surface in absence of alongshore flow.



(A)



(B)

**Figure 3-12:** Cartoon of the across-estuary salt structure (A) narrow, and (B) wide estuaries. In the absence of winds, the wider estuary allows for Rossby adjustment, thus slumping the isopycnals across the estuary mouth and reducing the vertical stratification.

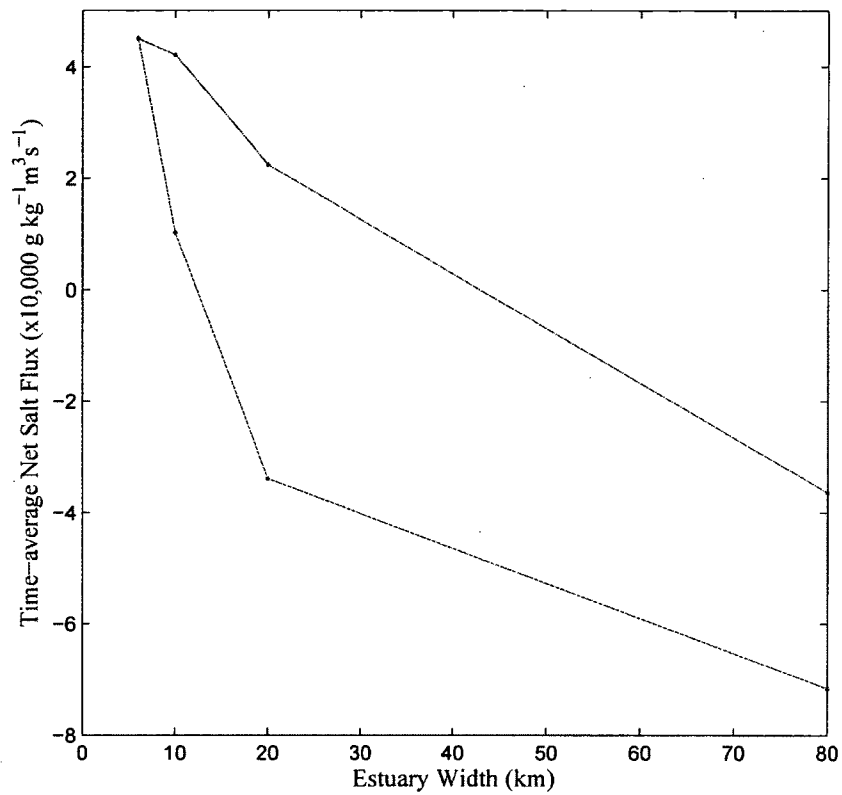


**Figure 3-13:** Time-averaged net salt flux as a function of the estuary width. Red line shows winds only in the coastal ocean and blue line shows the winds both in the estuary and coastal ocean.

## Bibliography

- Alessi, C. A., S. J. Lentz, and J. A. Austin, 1996: Coastal Ocean Processes Inner-Shelf Study: Coastal and Moored Physical Oceanographic Measurements. *Woods Hole Oceanog. Inst. Tech. Rept.*, **WHOI-96-06 (-)**, 142.
- Allen, J. and P. Newberger, 1996: Downwelling circulation on the Oregon continental shelf .1. Response to idealized forcing. *Journal of Physical Oceanography*, **26 (10)**, 2011–2035, doi: 10.1175/1520-0485(1996)026<2011:DCOTOC>2.0.CO;2.
- Allen, J., P. Newberger, and J. Federiuk, 1995: Upwelling circulation on the Oregon continental shelf .1. Response to idealized forcing. *Journal of Physical Oceanography*, **25 (8)**, 1843–1866, doi: 10.1175/1520-0485(1995)025<1843:UCO-TOC>2.0.CO;2.
- Austin, J., 2002: Estimating the mean ocean-bay exchange rate of the Chesapeake Bay. *Journal of Geophysical Research-Oceans*, **107 (C11)**, doi: 10.1029/2001JC001246.
- Austin, J. and S. Lentz, 1999: The Relationship Between Synoptic Weather Systems and Meteorological Forcing on the North Carolina Inner Shelf. *Journal of Geophysical Research-Oceans*, **104 (C8)**, 18 159–18 185.
- Austin, J. and S. Lentz, 2002: The Inner Shelf Response to Wind-Driven Upwelling and Downwelling. *Journal of Physical Oceanography*, **32 (7)**, 2171–2193.
- Cerco, C., M. Noel, and L. Linker, 2004: Managing for water clarity in Chesapeake Bay. *Journal of Environmental Engineering-ASCE*, **130 (6)**, 631–642, doi: 10.1061/(ASCE)0733-9372(2004)130:6(631).
- Chen, S.-N., L. P. Sanford, and D. K. Ralston, 2009: Lateral circulation and sediment transport driven by axial winds in an idealized, partially mixed estuary. *Journal of Geophysical Research-Ocean*, **114**, doi: 10.1029/2008JC005014.
- Csanady, G., 1977: Intermittent Full Upwelling in Lake-Ontario. *Journal of Geophysical Research-Ocean*, **82 (3)**, 397–419, doi: 10.1029/JC082i003p00397.
- Das, P. and J. Middleton, 1997: Obliquely incident Poincare waves on a sloping continental shelf. *Journal of Physical Oceanography*, **27 (7)**, 1274–1285, doi: 10.1175/1520-0485(1997)027<1274:OIPWOA>2.0.CO;2.
- Fairall, C., E. Bradley, D. Rogers, J. Edson, and G. Young, 1996: Bulk parameterization of air-sea fluxes for Tropical Ocean Global Atmosphere Coupled Ocean Atmosphere Response Experiment. *Journal of Geophysical Research-Oceans*, **101 (C2)**, 3747–3764.



- Fong, D. and W. Geyer, 2001: Response of a River Plume During an Upwelling Favorable Wind Event. *Journal of Geophysical Research-Oceans*, **106 (C1)**, 1067–1084.
- Fong, D. and W. Geyer, 2002: The alongshore transport of freshwater in a surface-trapped river plume. *Journal of Physical Oceanography*, **32 (3)**, 957–972, doi: 10.1175/1520-0485(2002)032<0957:TATOFI 2.0.CO;2.
- Galperin, B., L. Kantha, S. Hassid, and A. Rosati, 1988: A Quasi-Equilibrium Turbulent Energy-Model For Geophysical Flows. *Journal of Atmospheric Sciences*, **45 (1)**, 55–62.
- Gan, H. and J. Allen, 2005: On Open Boundary Conditions for a Limited-Area Coastal Model off Oregon. Part 1: Response to Idealized Wind Forcing. *Ocean Modelling*, **8 (1-2)**, 115–133, doi: 10.1016/j.ocemod.2003.12.006.
- Garvine, R., 1985: A Simple-Model of Estuarine Subtidal Fluctuations Forced by Local and Remote Wind Stress. *Journal of Geophysical Research-Oceans*, **90 (NC6)**, 1945–1948, doi: 10.1029/JC090iC06p11945.
- Garvine, R., 1999: Penetration of Buoyant Coastal Discharge onto the Continental Shelf: A Numerical Model Experiment. *Journal of Physical Oceanography*, **29 (8, Part 2)**, 1892–1909.
- Geyer, W., 1997: Influence of wind on dynamics and flushing of shallow estuaries. *Estuarine Coastal and Shelf Science*, **44 (6)**, 713–722, doi: 10.1006/ecss.1996.0140.
- Hansen, D. and M. Rattray, 1965: Gravitational circulation in straits and estuaries. *Journal of Marine Research*, **23**, 104–122.
- Hickey, B., L. Pietrafesa, D. Jay, and W. Boicourt, 1998: The Columbia River Plume Study: Subtidal Variability in the Velocity and Salinity Fields. *Journal of Geophysical Research-Oceans*, **103 (C5)**, 10 339–10 368.
- Kantha, L. and C. Clayson, 1994: An Improved Mixed-Layer Model for Geophysical Applications. *Journal of Geophysical Research-Oceans*, **99 (C12)**, 25 235–25 266.
- Lentz, S., 2008: Observations and a model of the mean circulation over the Middle Atlantic Bight continental shelf. *Journal of Physical Oceanography*, **38 (6)**, 1203–1221, doi: 10.1175/2007JPO3768.1.
- Lentz, S., M. Carr, and T. Herbers, 2001: Barotropic Tides on the North Carolina Shelf. *Journal of Physical Oceanography*, **31 (7)**, 1843–1859.
- MacCready, P., 1999: Estuarine adjustment to changes in river flow and tidal mixing. *Journal of Physical Oceanography*, **29 (4)**, 708–726, doi: 10.1175/1520-0485(1999)029<0708:EATCIR 2.0.CO;2.

- Mellor, G. and T. Yamada, 1982: Development of a Turbulence Closure-Model for Geophysical Fluid Problems. *Reviews of Geophysics*, **20** (4), 851–875.
- Millero, F., R. Feistel, D. Wright, and T. McDougall, 2008: The composition of Standard Seawater and the definition of the Reference-Composition Salinity Scale. *Deep-Sea Research Part I-Oceanographic Research Papers*, **55** (1), 50–72, doi: 10.1016/j.dsr.2007.10.001.
- Officer, C., R. Biggs, J. Taft, L. Cronin, M. Tyler, and W. Boynton, 1984: Chesapeake Bay Anoxia-Origin, Development, and Significance. *Science*, **223** (4631), 22–27, doi: 10.1126/science.223.4631.22.
- Pickett, M. and F. Schwing, 2006: Evaluating upwelling estimates off the west coasts of North and South America. *Fisheries Oceanography*, **15** (3), 256–269, doi: 10.1111/j.1365-2419.2005.00400.x.
- Pringle, J. M. and E. P. Dever, 2009: Dynamics of Wind-Driven Upwelling and Relaxation between Monterey Bay and Point Arena: Local-, Regional-, and Gyre-Scale Controls. *Journal of Geophysical Research-oceans*, **114**.
- Scully, M., 2010: The Importance of Climate Variability to Wind-Driven Modulation of Hypoxia in Chesapeake Bay. *Journal of Physical Oceanography*, **40** (6), 1435–1440, doi: 10.1175/2010JPO4321.1.
- Song, Y. and D. Haidvogel, 1994: A semi-implicit ocean circulation model using a generalized topography-following coordinate system. *Journal of Computational Physics*, **115** (1), 228–244.
- Stacey, M., S. Monismith, and J. Burau, 1999: Observations of turbulence in a partially stratified estuary. *Journal of Physical Oceanography*, **29** (8, Part 2), 1950–1970, doi: 10.1175/1520-0485(1999)029<1950:OOTIAP>2.0.CO;2.
- Waldorf, B. W., J. L. Largier, S. Rennie, J. A. Austin, and G. C., 1995: Coastal Ocean Process (CoOP) Pilot Project Data Report: R/V Hatteras Shipboard Measurements. Underway, CTD and ADCP Data August 1994. *Scripps Inst. of Oceanog. Tech. Rept.*, **SIO-95-29** (-), -.

# CHAPTER 4

## How Weather-Band Fluctuations in the Wind Alter the Steady State of an Estuary.

### 4.1 Abstract

As an estuary adjusts to fluctuating winds, the estuary reaches a new steady state. For timescales longer than the adjustment time of an estuary, fluctuating winds have little influence on the stratification or the exchange of an estuary, but instead alter the salt intrusion length of the estuary.

In stratified estuaries, fluctuating winds increase the vertical mixing, which initially reduces the salt exchange (Rao, 2012), but the net salt flux into the estuary must return to zero over long timescales, as the average salinity in the estuary reaches a new steady state. A stratified estuary influenced by winds adjusts and returns to steady state by reducing the salt intrusion length. When the estuary is well-mixed or sheltered, fluctuating winds alter the coastal salinity drawn into the estuary mouth, so the estuary adjusts by increasing the salt intrusion length.

However, when the time taken for an estuary to reach the new steady state is short compared to the time of the initial change caused by the vertical mixing, the influence of fluctuating winds in a stratified estuary reduces the stratification and the exchange.

A simplified predictor for the adjustment time is used to determine when the estuary adjusts to fluctuating winds by altering the salt intrusion length, and when

the estuary adjusts by altering its stratification and exchange. The adjustment time is reasonably predicted by a function of the salt intrusion length and the depth-averaged velocity caused by the river discharge, for a range of estuarine and coastal conditions.

## 4.2 Introduction

Estuaries are regions where the salt water from the ocean mix with the fresh water of a river, thus setting the circulation in the estuary and the exchange between an estuary and a coastal ocean. The exchange depends on the along-estuary salinity gradient and the vertical stratification in an estuary, which are ultimately set by the freshwater inflow, oceanic salinity and the vertical mixing in the estuary (Hansen and Rattray, 1965; MacCready, 1999, 2007; Bowen and Geyer, 2003). In stratified estuaries, the circulation is exchange-dominated, where the salt water enters the estuary at depth, mixes vertically into the surface layers and is discharged out of the estuary.

The mixing in an estuary is largely influenced by the wind-stress, tides, and surface cooling. In several studies of estuaries, mixing due to tides have been shown to be dominant (Bowen and Geyer, 2003; MacCready and Geyer, 2010; Stacey et al., 1999). However, over seasonal, annual, or climate change timescales the tidal mixing is largely unaltered, while the wind fluctuations can be altered over these timescales. Thus the variation in the wind-driven mixing can be an important source of estuarine variability.

The fluctuations in winds can have periods of a few days (Austin and Lentz, 1999, East coast of US) to a few weeks (Dever and Lentz, 1994, West coast of US, their Fig. 9), and are referred to as weather-band fluctuations in the wind. When weather-band fluctuations in the wind force an exchange-dominated estuary and its adjacent coastal ocean, two things initially happen that alter the net salt flux out of an estuary: there is increased vertical mixing in the estuary that reduces the vertical

estuarine stratification, and there is a change in the salinity of the source coastal water drawn into the estuary (Rao, 2012; MacCready, 1999). On timescales shorter than the adjustment time of an estuary to fluctuating winds, the net salt flux out of an estuary is significantly changed, causing the estuary to lose or gain salt (Rao, 2012; MacCready, 1999). On timescales longer than the adjustment time of an estuary, the net salt flux must return to zero, so the parameters governing the salt exchange have to adjust until the steady state balance is restored.

We examine how an exchange-dominated estuary adjusts over timescales longer than the time taken for an estuary to reach a new steady state. In large estuaries like the Chesapeake Bay, the steady state is reached in about 90 days (Austin, 2002). In small estuaries, the steady state is reached in 1-10 days (Kranenburg, 1986). When the adjustment time is short, the initial changes in the estuary are followed by the adjustment of estuarine properties, thus the steady state dynamics are important. When the adjustment time is long, the estuary is still adjusting so the initial changes due to mixing are the relevant dynamics, until the seasonal weather changes become more important. This adjustment is examined for conditions typical of the Mid Atlantic Bight (MAB), and other regions such as the West coast of US and estuaries oriented oblique to the coast. This work is an extension of previous studies of increased mixing in the estuary due to tides (MacCready, 1999, 2007; Bowen and Geyer, 2003; Hetland and Geyer, 2004).

The wind influence on the estuary can alter the exchange and residence time in the estuary, which can alter the estuarine salinity and the concentration of nutrients, pollutants and other fluvial and oceanic inputs to the estuary. The changes in these concentrations are of great importance to the health of the estuarine ecosystems. These changes can cause long term water quality problems (Cerco et al., 2004) and anoxic zones in the estuaries (Scully, 2010).

This paper is organized as follows: section 2 describes the setup of the base case

numerical experiment which was modeled after the Chesapeake Bay and the MAB. This includes a description of the different forcings applied to the permutations of the base case experiment to model the wind influence for a range of observed estuarine and coastal conditions. In section 3, the steady state balance is derived to help to identify the important parameters influenced by the wind fluctuations. Section 4 discusses how wind fluctuations influence the salt exchange for a range of estuarine and coastal conditions, and in section 5 the implications of our results are discussed and extended to other regions.

### 4.3 Description of the Numerical Model

Our base case numerical experiment is modeled after the Chesapeake Bay and the MAB coastal ocean (Fig. 4-1). The parameters and forcings used in the base case experiment are described. The permutations of this base case experiment used to model the range of topography, estuarine, and coastal conditions are described as well.

The numerical model used in this study is the Regional Ocean Modeling System (ROMS). It is a primitive equation finite difference numerical model (Song and Haidvogel, 1994). The vertical momentum balance is hydrostatic and a free surface is included. A constant horizontal eddy viscosity,  $A_H$  of  $5.0 \text{ m}^2 \text{ s}^{-1}$  and a horizontal diffusivity,  $K_H$  of  $0 \text{ m}^2 \text{ s}^{-1}$  are set. The background minimum vertical eddy viscosity is  $K_V = 1.0 \times 10^{-5} \text{ m}^2 \text{ s}^{-1}$ . Diurnal tides are included in the model and is a major source of vertical mixing in the background. The Coriolis parameter is  $f = 10^{-4} \text{ s}^{-1}$ . The vertical eddy viscosity  $K_V$  is computed by the Mellor-Yamada level 2.5 turbulence closure scheme (Mellor and Yamada, 1982) using the non-dimensional stability functions from Galperin et al. (1988) and Kantha and Clayson (1994). Some studies, e.g., Garvine (1999); Stacey et al. (1999); Fong and Geyer (2001), have shown

that in strongly stratified conditions, the MY2.5 scheme underestimates the vertical eddy viscosity, while overestimating in weakly stratified conditions. Nevertheless, the MY2.5 scheme resolves the mixing accurate to first order. The density is computed by a linear equation of state using a saline contraction coefficient  $k$  is  $7.6 \times 10^{-4}$  and is a function of salinity alone. Temperature is kept constant in the model.

**Model Grids** The model utilizes a terrain-following  $\sigma$  coordinate system to resolve the vertical structure. The horizontal grid is a finite difference scheme with grid size ranging from  $1 \text{ km} \times 1 \text{ km}$  (near the western and northern boundaries) to  $4 \text{ km} \times 4 \text{ km}$  (near the eastern and southern boundaries). The higher resolution at the northern boundary minimizes the formation and downwave propagation of numerical artifacts into the study area. The highest horizontal resolution of  $1 \text{ km} \times 1 \text{ km}$  is used in the estuary and the coastal region near the estuary mouth to resolve the salt and volume fluxes being examined.

The domain in the base case numerical experiment has 384 points in the cross-shore direction, 96 points in the alongshore direction, and 20 vertical  $\sigma$  levels. The location of the boundaries are southern  $y = -100 \text{ km}$ , northern  $y = 50 \text{ km}$ , western  $x = -320 \text{ km}$ , and eastern  $x = 100 \text{ km}$ . A right-handed ‘east coast’ coordinate system is used where  $+x$  direction is offshore (‘seaward’),  $+y$  direction is northward (‘upwave’), and  $+z$  direction is upwards (‘skyward’). In the numerical model, the baroclinic time step is 90 s and the model output is saved every 120 time steps to temporally resolve the tides used in our model. The barotropic time step is  $1/20$  of the baroclinic time step. The model was run for half and double the grid spacing, and our results did not change significantly.

**Boundary Conditions** The surface momentum boundary conditions are,

$$K_V \frac{\partial (u, v)}{\partial z} \Big|_{z=0} = \frac{(\tau^{sx, sy})}{\rho_0} \quad (4.1)$$

where  $\tau^{sx}$  and  $\tau^{sy}$  are cross-shore and alongshore surface wind stresses. In this study,  $\tau^{sx} = 0$  Pa while the alongshore wind stress is varied. The bottom momentum boundary condition is a linear bottom drag,

$$K_V \frac{\partial (u, v)}{\partial z} \Big|_{z=-H} = (Ru_b, Rv_b) \quad (4.2)$$

where the bottom drag coefficient is  $R = 5 \times 10^{-4} \text{ m s}^{-1}$  and  $(u_b, v_b)$  are the bottom velocity in the cross-shore and alongshore directions respectively. The bottom drag is within the range observed by Lentz et al. (2001) for the North Carolina coast.

The northern open boundary conditions (OBC) are determined from numerical experiments using the same winds as the 3D model but in a 2D alongshore-uniform topography model. This 2D model is a cross-shore section of the 3D model and has no alongshore variations. The northern OBC implies that the ocean outside the northern boundary can be approximated as an infinite coast with no alongshore variations in forcings or topography, as described in Gan and Allen (2005) and Pringle and Dever (2009). The southern and eastern edges are open boundaries with Sommerfeld radiation conditions. This radiation condition has the least reflection at the boundary for the dominant wave mode but the other wave modes have higher reflection. To overcome this, the southern boundary also has a six grid-point wide sponge layer where the horizontal viscosity gradually increases in the southward direction. The sponge layer helps dissipate the energy of reflected waves preventing them from propagating along the southern open boundary. The western boundary is the coastal wall with free-slip condition. The free-slip imposes no friction between horizontal boundaries and the flow, and there is no normal flow into the wall.

**Bathymetry** The model domain is an idealized representation of the Mid-Atlantic Bight and has a large estuary connected to a uniform alongshore bathymetry coastal ocean (Fig. 4-2). The coastal ocean bathymetry is given by

$$H(x) = H_o + \alpha x \quad 0 \leq x \leq 100 \times 10^3 \text{ m} \quad (4.3)$$



where  $H_o = 10$  m is the coastal wall depth,  $x$  is the cross-shore distance, and  $\alpha$  is the bottom slope. In the base case experiment,  $\alpha$  was  $1 \times 10^{-3}$ , typical of the MAB.

Our model estuary has idealized dimensions similar to large estuaries such as Chesapeake Bay and Delaware Bay (Fig. 4-2B). The estuary mouth is centered at  $[x, y] = [0, 0]$  km with a length of 300 km and a width of 20 km. The length of the estuary is varied from 50-300 km. The lengths of the estuary are selected to prevent tidal resonance in the estuary. The estuary has 10 m deep walls. In the base case experiment, the estuarine thalweg was 30 m and the estuary thalweg was varied between 11-45 m to examine the influence of winds for different thalweg depths. The angle of the estuary was varied between  $-60^\circ$  to  $60^\circ$  to examine the influence of fluctuating winds for different estuary orientations. In the base case experiment, the estuary was perpendicular to the coastal ocean, i.e.,  $\theta = 0^\circ$ . Positive angles mean the head of the estuary is northward of the estuary mouth.

**Coastal Stratification** The stratification is modeled after the summer conditions at Duck, NC as a two layer system separated by a halocline centered at a depth of  $h_{hc}$  and has a halocline thickness of  $\Delta z = 11$  m (Waldorf et al., 1995; Alessi et al., 1996). The  $h_{hc}$  was varied between 15-45 m to examine the influence of winds at different pycnocline depths; in the base case experiment, the  $h_{hc}$  was 15 m. The initial density field is uniform alongshore and is a function of depth and salinity,

$$s(z) = 33 - \Delta s_{hc} \tanh\left(\frac{z + h_{hc}}{3}\right) \text{ g kg}^{-1} \quad (4.4)$$

where the salinity is  $33 \text{ g kg}^{-1}$  at the halocline center,  $z$  is the depth in metres,  $\Delta s_{hc} = 2 \text{ g kg}^{-1}$  (Fig. 4-3A). The denominator of the  $\tanh()$  function sets the  $\Delta z$  and is kept constant for all model runs. The salinity of the top layer of the coastal ocean is near  $31 \text{ g kg}^{-1}$ . The numerical experiment salinity is reported using absolute salinity in units of  $\text{g kg}^{-1}$  (Millero et al., 2008).

### 4.3.1 External Model Forcing

Each numerical experiment starts from an initial condition where the flow is at rest. The experiments run with tides and river discharge but no winds, until day 200 to reach steady state. Then the wind forcing is applied to the model for another 210 days by when the estuary has reached its new steady state. Our analysis will focus on how the estuarine dynamics adjust during the 210 days of fluctuating winds.

**Wind Forcing** The surface forcing consists of alongshore wind-stress,  $\tau^{sy}$  which is uniform across the numerical domain and fluctuates between upwelling and downwelling (Fig. 4-3B). The winds begin with an upwelling wind-stress of  $\tau^{sy}$  lasting for a period of  $t_{UW}$  days, followed by a downwelling wind-stress of  $-\tau^{sy}$  lasting  $t_{DW}$  days. A wind-stress of  $\tau^{sy} = 0.1 \text{ Pa}$  is a wind speed of about  $8 \text{ m s}^{-1}$  measured at height of 10 m (Fairall et al., 1996). Both the periods  $t_{UW}$  and  $t_{DW}$  include one day for the wind to ramp to  $\tau^{sy}$  and another day to ramp back to zero wind-stress. Only complete wind-reversal cycles,  $t_{UW} + t_{DW}$ , that fit in the 210 day duration are used. The wind-stress amplitude and period was varied between 0.05-0.2 Pa and 6-30 days respectively; in the base case experiment these were 0.1 Pa and 6 days. The time-averaged wind-stress over the 210 days is zero for all the experiments presented in this study, unless otherwise stated.

**River Forcing** The freshwater discharge enters the model at the head of the estuary and is applied evenly over the depth. The freshwater discharge has a salinity of  $0 \text{ g kg}^{-1}$ . The river discharge range of  $(0.2 - 20) \times 10^3 \text{ m}^3 \text{ s}^{-1}$  is used to examine the influence of winds at different discharge rates; the base case discharge rate was  $2 \times 10^3 \text{ m}^3 \text{ s}^{-1}$ , similar to Austin (2002). This inflow initiates at the start of the model simulation and is kept constant with time. In order to reduce the computer time for each model run, the estuary salinity is initiated closer to the steady state. The initial

salinity along the estuary is,

$$s(x) = s_{co} + \frac{\partial s}{\partial x} x, \quad -300 \text{ km} \leq x \leq 0 \text{ km} \quad (4.5)$$

where the surface salinity of the coastal ocean,  $s_{co} = 31 \text{ g kg}^{-1}$  and the along-estuary salinity gradient,  $\frac{\partial s}{\partial x} = 0.1 \text{ g kg}^{-1} \text{ km}^{-1}$  ( $\frac{\partial \rho}{\partial x} = 0.08 \text{ kg m}^{-3} \text{ km}^{-1}$ ). The exchange flow at the estuary mouth has stabilized by 200 days.

**Tides** The inclusion of tides in the numerical model sets a more realistic background estuarine mixing. Tidal forcing included in the numerical model is achieved by imposing the fluctuations of the sea surface height and current associated with a 12-hour tide at the offshore (eastern) boundary of the domain. The fluctuations of the sea surface height and current at this offshore boundary is the sum of the initial coast-ward moving tidal wave and the tidal wave reflected from the coast, as described by Das and Middleton (1997). Their solution was used to determine the magnitude of the fluctuations in the sea surface height and currents at the offshore boundary. These offshore tidal boundary conditions are then tuned to get the tides at the coastal wall to be similar to observed tidal fluctuations along the MAB coast.

## 4.4 Steady State Balance

The fluctuating winds alter the steady state of the estuary by increasing the vertical mixing in the estuary and changing the salinity of the water drawn into the estuary. In the derivation below, we show how these changes alter the steady state.

The along-estuary momentum equation for an exchange-dominated estuary is written as

$$\frac{\partial u}{\partial t} = -\frac{\partial}{\partial x}(uu) - \frac{\partial}{\partial z}(wu) - \frac{1}{\rho_o} \frac{\partial p}{\partial x} + \frac{\partial}{\partial z} \left( A_V \frac{\partial u}{\partial z} \right) \quad (4.6)$$

where  $u$  is the along-estuary velocity,  $w$  is the vertical velocity,  $p$  is the pressure, and  $A_V$  is the vertical eddy viscosity. Similarly, the conservation of salt can be described

as

$$\frac{\partial s}{\partial t} = -\frac{\partial}{\partial x}(us) - \frac{\partial}{\partial z}(ws) + \frac{\partial}{\partial z} \left( K_V \frac{\partial s}{\partial z} \right) \quad (4.7)$$

where  $s$  is the salinity, and  $K_V$  is the vertical eddy diffusivity. In both equations (4.6) and (4.7), we have assumed that the estuary is exchanged-dominated, i.e., the horizontal eddy viscosity and diffusivity are very small, and there are no lateral variations in the salinity or velocity. In wide estuaries such as the Chesapeake Bay, there are significant lateral variations (Guo and Valle-Levinson, 2008) but this simplification provides a simplified system that allows us a qualitative understanding of the most important dynamics. In addition, we assumed that the vertical eddy diffusivity and viscosity are the same.

The estuary is assumed to have two layers of equal thickness,  $h = H/2$ , where  $H$  is the total depth (Fig. 4-4). The equations (4.6) and (4.7) are rewritten as depth-averaged equations for each layer: the surface layer,  $\partial u_1/\partial t$  and  $\partial s_1/\partial t$ , and the bottom layer,  $\partial u_2/\partial t$  and  $\partial s_2/\partial t$ . The  $u_1, u_2, s_1, s_2$  are the vertically-averaged velocity and salinity for each layer.

$$\bar{u} = \frac{(u_1 + u_2)}{2} \quad u' = \frac{(u_1 - u_2)}{2} \quad (4.8)$$

$$\bar{s} = \frac{(s_1 + s_2)}{2} \quad s' = \frac{(s_1 - s_2)}{2} \quad (4.9)$$

Using the above algebraic simplification, similar to MacCready (1999), the along-estuary momentum and salt conservation equations for each depth-averaged layer is reduced to the cross-sectional averaged velocity and salinity across the estuary mouth ( $\bar{u}, \bar{s}$ , denoted by bars), and the deviation of the velocity from the cross-sectional average ( $u', s'$ , denoted by primes). The parameter  $u'$  is the volume exchange velocity, while  $s'$  is the vertical estuarine stratification.

The parameter  $\bar{u}\bar{s}$  (hereafter referred as the depth-averaged salt flux) describes the salt removed from the estuary by the river volume discharge, and  $u's'$  (hereafter referred as the exchange salt flux) describes the salt added into the estuary by the

estuarine volume exchange and the salinity difference of the water entering and leaving the estuary. This derivation gives the following simplified forms,

$$\frac{\partial u'}{\partial t} = (|u_1| - 2\bar{u})\frac{\partial u'}{\partial x} + \frac{gkh}{2}\frac{\partial \bar{s}}{\partial x} + \frac{\partial}{\partial x}\left(\frac{2A_V}{h^2} + \frac{R}{2}\right)u' + \frac{R}{2}\bar{u} \quad (4.10)$$

$$\frac{\partial \bar{s}}{\partial t} = -\bar{u}\frac{\partial \bar{s}}{\partial x} - \frac{\partial}{\partial x}(u's') \quad (4.11)$$

$$\frac{\partial s'}{\partial t} = -\bar{u}\frac{\partial s'}{\partial x} - \frac{\partial u'}{\partial x}(\bar{s} - |s_1|) - u'\frac{\partial \bar{s}}{\partial x} - \frac{2K_V}{h^2}s' \quad (4.12)$$

In steady state, the  $\bar{s}$ ,  $s'$ , and  $u'$  do not change with time or distance along the estuary. The depth-averaged velocity is much smaller than the deviation of the velocity from the depth-averaged velocity,  $k$  is the conversion factor from salinity to density, total depth is twice the layer thickness,  $H = 2h$ , and the bottom friction,  $R = 8A_V/H^2$ , which is roughly equivalent to a no-slip bottom boundary (MacCready, 1999). These assumptions simplify equations (4.10), (4.11), and (4.12) to

$$0 = \frac{gkH}{4}\frac{\partial \bar{s}}{\partial x} - \frac{12K_V}{H^2}u' \quad (4.13)$$

$$0 = -\bar{u}\bar{s} - u's' \quad (4.14)$$

$$0 = -u'\frac{\partial \bar{s}}{\partial x} - \frac{8K_V}{H^2}s' \quad (4.15)$$

These equations describe the steady state of the estuary, and our goal is to examine how fluctuating winds alter this. Equation (4.13) describes the exchange velocity,  $u'$ , depends on the along-estuary salt gradient and vertical mixing,  $K_V$ . Equation (4.14) describes the net salt flux is zero, i.e., the depth-averaged salt flux out of the estuary,  $\bar{u}\bar{s}$ , is balanced by the exchange salt flux into the estuary,  $u's'$ . Equation (4.15) describes the balance between the generation of vertical stratification by the vertical shear in the velocity acting on the along-estuary salt gradient and the loss of vertical stratification due to vertical mixing.

The depth-averaged salt flux is simple to determine since  $\bar{u} = (\text{river discharge rate})/(\text{area of estuary mouth})$  and  $\bar{s}$  is the depth-averaged salinity at the estuary mouth. The exchange salt flux is determined by rewriting (4.13) with  $u'$  as the

subject, then substituting  $u'$  into (4.15). This gives the steady state relation between the exchange salt flux, the vertical eddy diffusivity, and the along-estuary salinity gradient.

$$u's' = \frac{-g^2 k^2 H^8}{8(48)^2 K_V^3} \left( \frac{\partial \bar{s}}{\partial x} \right)^3 \quad (4.16)$$

In steady state,  $\bar{u}\bar{s} = -u's'$ , so (4.16) can be re-written as

$$\left( \frac{\partial \bar{s}}{\partial x} \right)^3 = \frac{-8(48)^2 K_V^3}{g^2 k^2 H^8} (\bar{u}\bar{s}) \quad (4.17)$$

In the following sections, the above relations are used to examine how the fluctuating winds alter the steady state of the estuary.

## 4.5 Results

When fluctuating winds force an exchange-dominated estuary and its adjacent coastal ocean, the vertical mixing by fluctuating winds cause a decrease in the vertical stratification  $s'$ , and the exchange salt flux,  $u's'$  (Rao, 2012; MacCready, 1999). On timescales longer than the adjustment time of an estuary, the estuarine net salt flux must return to zero, so the parameters from equation 4.14 ( $\bar{s}, u', s'$ ) must change until the steady state salt flux balance is restored. This section examines how the net salt flux returns to zero for different estuarine and coastal conditions, starting with the base case. The fluctuating winds in the base case have an amplitude of 0.1 Pa and period of 6 days, described in section 4.3.

### 4.5.1 Base Case with Winds both in the Estuary and Coastal Ocean

On timescales shorter than the time taken for an estuary to reach its new steady state, the initial vertical mixing in an estuary by fluctuating winds increase the vertical eddy viscosity  $A_V$  and diffusivity  $K_V$ , while the along-estuary salt gradient  $\partial \bar{s} / \partial x$  has

not had time to change. This reduces the magnitude of the exchange velocity  $u'$  and then the stratification  $s'$  reduces. Rao (2012) shows that the fractional change in  $s'$  is greater than the fractional change in  $u'$ . The combined reduction in  $u'$  and  $s'$  results in a decrease in the magnitude of the exchange salt flux  $u's'$ , and leads to the average estuarine salinity,  $\bar{s}$ , becoming fresher (Rao, 2012; MacCready, 1999) (Fig. 4-5).

For timescales longer than the adjustment time of an estuary, the estuary must adjust to this initial decrease in  $u's'$ . Since the fractional change in  $\bar{u}\bar{s}$  is small because the river discharge remains constant and the change in  $\bar{s}$  is small, the  $u's'$  must increase to its initial magnitude until the net salt flux is zero. This adjustment to steady state is caused by the along-estuary salt gradient increasing in magnitude to adjust to the increased  $K_V$  (Eq. 4.17). This increase in the along-estuary salt gradient is a result of the freshening in the estuary and the nearly constant depth-averaged salinity  $\bar{s}$  at the estuary mouth, so the along-estuary salinity difference becomes larger, thus  $\partial\bar{s}/\partial x$  increases.

The increase in  $\partial\bar{s}/\partial x$  increases the magnitude of the exchange velocity  $u'$  and the stratification  $s'$  almost to its initial magnitude (Eq. 4.13 & 4.15). The combined increase in  $u'$  and  $s'$  cause the exchange salt flux  $u's'$  to increase in magnitude until the net salt flux is zero (Eq. 4.14) and the estuary reaches the new steady state. The evolution of the along-estuary salt gradient with time for the base case is shown using solid lines in figure (4-6A). The along-estuary salt gradient  $\partial\bar{s}/\partial x$  is determined using the depth-averaged salinity along the thalweg of the entire estuary and using the least squares fit. The change in depth-averaged salinity along the estuary is largely uniform so determining the  $\partial\bar{s}/\partial x$  over the entire estuary length or only over the salt intrusion length yield similar results. The above adjustment dynamics for wind-induced mixing are consistent with those of vertical tidal mixing by MacCready (1999, 2007).

In the above section, the fluctuating winds start in the upwelling phase causing the coastal pycnocline to upwell, bringing deep salty water to the estuary mouth,

thus changing the net salt flux. However, if the winds start in the down-welling phase, then the coastal pycnocline is initially pushed away from the estuary and the upwelling winds would bring the coastal pycnocline back to its initial condition. The consequence of the phase shift is that upwelling no longer brings deep salty water to the estuary, but brings the coastal pycnocline close to its initial condition.

For timescales longer than the time taken for the estuary to adjust, whether the fluctuating winds cause the coastal pycnocline to upwell to the surface or down-well below its initial depth does not matter when the wind-induced mixing in the estuary is significant. This is shown in Fig 4-7A, which shows the experiments with and without the phase shift have very similar change in the along-estuary salt gradient to reach the new steady state. There is no significant difference in the adjustment between the experiments because the wind-induced mixing in the estuary, which causes the largest change in the net salt flux, remains similar. The starting phase of the fluctuating wind only matters when the wind-induced mixing in the estuary is not significant, e.g., well-mixed estuaries. This is discussed in the next section.

#### 4.5.2 Base Case with Winds only in the Coastal Ocean

In estuaries that are sheltered from winds, wind-induced mixing in the estuary is not significant and only the changes in the coastal salinity drawn into the estuary during coastal upwelling and down-welling alter the net salt flux of the estuary. During upwelling, the salinity drawn into the estuary increases as the coastal pycnocline upwells deep salty water at the estuary mouth.

The upwelling initially increases the  $s'$  at the estuary mouth, while  $u'$  and  $\partial\bar{s}/\partial x$  have not had the time to change. This increases the exchange salt flux  $u's'$ , causing the average estuarine salinity to become saltier (Fig. 4-5). For timescales longer than the adjustment time of an estuary, the estuary must adjust to this initial increase in  $u's'$ . Since the fractional change in  $\bar{u}\bar{s}$  is small (for the same reasons discussed in previous



section), the  $u's'$  must decrease to its initial magnitude until the net salt flux is zero. This adjustment to the new steady state is caused by the along-estuary salt gradient,  $\partial\bar{s}/\partial x$ , decreasing in magnitude. This change in the  $\partial\bar{s}/\partial x$  is a result of the increase in the depth-averaged salinity in the estuary and the nearly constant depth-averaged salinity  $\bar{s}$  at the estuary mouth, so the along-estuary salt difference decreases, thus the  $\partial\bar{s}/\partial x$  decreases.

The decrease in  $\partial\bar{s}/\partial x$ , reduces the magnitude of the exchange velocity  $u'$  (Eq. 4.13), and reduces the stratification  $s'$  almost to its initial magnitude (Eq. 4.15). The combined decrease in  $u'$  and  $s'$  causes the exchange salt flux  $u's'$  to decrease in magnitude until the net salt flux is zero (Eq. 4.14) and the estuary reaches the new steady state. The evolution of the along-estuary salt gradient with time for the base case with only winds in the coastal ocean are shown using dashed lines in figure (4-6A).

When the wind-induced mixing in the estuary is not significant, the influence of the coastal ocean when forced by fluctuating winds depends on how the fluctuating winds vertically displace the coastal pycnocline. In our experiments, the starting phase of the fluctuating winds in the coastal ocean is important because it controls the position of the coastal pycnocline, which governs if the coastal ocean adds or removes salt from the estuary, as the estuary adjusts to the fluctuating winds (Fig. 4-7B).

When the starting phase is upwelling winds, the coastal ocean adds salt into the estuary, as discussed earlier in this section. However, when the starting phase of the fluctuating winds is down-welling winds, the coastal ocean removes salt from the estuary. This is because the salinity at the estuary mouth decreases as the deep salty water is moved away from the estuary by the down-welling winds. This causes the estuary to lose salt and the average salinity of the estuary decreases. This decrease in the average estuarine salinity should lead to an increase in the along-estuary salt gradient as the estuary adjusts, but the decrease in the salinity at the estuary mouth

due to down-welling winds is much larger. This larger decrease in salinity at the estuary mouth leads to a decrease in the along-estuary salt gradient, similar to the other experiments with winds only in the coastal ocean (Fig. 4-7B).

In the field, fluctuating winds are always present and there are no phase shifts in wind observations (phase shift in winds is a numerical analysis tool). Our results show that how the coastal pycnocline moves vertically when forced by these fluctuating winds determine the influence of the ocean on the estuary, i.e., if the estuary loses or gains salt.

### 4.5.3 Well-Mixed Estuaries

The results in the previous section (sec. 4.5.1) suggest that the stratification in the estuary has an important role in determining the influence of fluctuating winds on the exchange. In this section, the effect of fluctuating winds is examined for estuaries that are already well-mixed. A well-mixed estuary is obtained by increasing the background vertical eddy diffusivity to  $0.001 \text{ m}^2\text{s}^{-1}$ .

In our experiments, the influence of fluctuating winds in well-mixed estuaries is similar to stratified estuaries, but the magnitude of fractional change in the  $\partial\bar{s}/\partial x$  is much smaller (Fig. 4-6C). The initial change in the salt exchange is small because the wind-induced mixing does not significantly change the vertical salinity structure of an already well-mixed estuary.

Since the role of wind-induced mixing is diminished in well-mixed estuaries, the influence of upwelling of salty coastal water at the estuary mouth (due to winds in the coastal ocean) is now significant. For timescales longer than the adjustment time of the estuary, the fluctuating winds on a coastal ocean adjacent to a well-mixed estuary (Fig. 4-6C) has similar effects on the along-estuary salt gradient and exchange, similar to a stratified estuary discussed in sec. 4.5.2).

In the absence of winds, the wide estuaries have reduced vertical stratification, so

the influence of wind-induced mixing is smaller than the influence of coastal upwelling on the salt exchange. As a result, the net salt flux is the coastal upwelling adding salt into the estuary, similar to only coastal winds experiments (section 4.5.2). However, a wide estuary adjusts to the fluctuating winds by increasing its along-estuary salt gradient (Figure 4-8), in contrast to the experiments with only coastal winds (dashed lines in Fig. 4-6A) and for narrower well-mixed estuaries (dashed lines in Fig. 4-6C). The addition of salt into the estuary increases the average salinity of the estuary, but in wide estuaries (which have larger volume) the increase in the average salinity is smaller than the increase of salinity at the estuary mouth due to upwelling. This results in the along-estuary salt gradient in wide estuaries to increase to adjust to fluctuating winds.

#### 4.5.4 Other Estuarine and Coastal Conditions

Permutations from the base case are used to examine if fluctuating winds influence the steady state of different coastal and estuarine conditions by adjusting the along-estuary salt gradient, and bringing the estuary to the new steady state. The permutations of the model that are used are largely determined from equation (4.17). These permutations include (Table 4.1): (i) wind-stress amplitude and period, which alter the vertical mixing,  $K_V$ , (ii) the river discharge, which alters the depth-averaged velocity,  $\bar{u}$ , (iii) the estuary thalweg depth, which alters the average depth of the estuary,  $H$ , (iv) the coastal pycnocline depth, which alters the depth-averaged salinity at the estuary mouth,  $\bar{s}$ , and (vi) the length of the estuary, which alters the along-estuary salt gradient.

For the above model permutations, the fluctuating winds are applied simultaneously to both the estuary and the coastal ocean. When the wind-induced mixing in the estuary is significant (in any permutation), then we expect the along-estuary salt gradient to adjust by increasing in magnitude, similar to base case with winds

on both the estuary and coastal ocean (sec. 4.5.1). When the change in the coastal salinity drawn into the estuary is significant, then we expect the along-estuary salt gradient to adjust by decreasing, similar to base case with only winds on the coast (sec. 4.5.2).

When fluctuating winds are applied to the above permutations, nearly all the experiments have similar response; the along-estuary salt gradient  $\partial\bar{s}/\partial x$  increases in magnitude causing the exchange salt flux  $u's'$  to increase, thus bringing the estuary to the new steady state. The evolution of the along-estuary gradient with time for the permutations of each parameter are shown in figure (4-6).

The exceptions to the above described dynamics are estuaries with fast adjustment times (the adjustment time is discussed in the next section), such as estuaries with high river discharge ( $R = 20 \times 10^3 \text{ m}^3\text{s}^{-1}$ , Fig. 4-6D) or short estuary lengths ( $L = 50 \text{ km}$ , Fig. 4-6F). On the onset of fluctuating winds, the vertical mixing in the estuary causes the exchange salt flux,  $u's'$ , to initially reduce in magnitude. In estuaries with rapid adjustment times, the along-estuary salt gradient has already decreased in magnitude and adjusted by the end of the initial decrease in  $u's'$  (Eq. 4.16). The quick adjustment of the along-estuary salt gradient is due to the rapid decrease in the depth-averaged salinity at the estuary mouth. The rapid adjustment in the along-estuary salt gradient are seen in figure (4-6 D& F).

## 4.6 Discussion

On timescales shorter than the time taken for an estuary to reach its new steady state, wind-induced mixing reduces the estuarine stratification (Rao, 2012). However, on timescales longer than the adjustment time of an estuary, wind-induced mixing caused by fluctuating winds has little influence on the magnitude of the estuarine stratification. Instead the estuary adjusts to fluctuating winds by changing its salin-

ity intrusion length into the estuary. The freshwater and salt water regions of an estuary is demarcated by the salt intrusion length; thus the wind-induced variability in the salt intrusion length is critical to managers of irrigation systems of large farming communities, aqueducts supplying municipal drinking water reservoirs, and freshwater fisheries. The adjustment to fluctuating winds is described below.

When fluctuating winds cause the stratification of the estuary to initially decrease, the exchange salt flux decreases, and the estuary loses salt and becomes fresher. The freshening in the estuary means the salt intrusion length is retreating towards the ocean as the estuary adjusts. This increases the  $\partial\bar{s}/\partial x$  which leads to the stratification and exchange increasing back to its initial magnitude. This adjustment applies to regions where fluctuating winds are observed over stratified estuaries, such as Chesapeake Bay during summer (Officer et al., 1984).

When fluctuating winds cause the exchange salt flux to initially increase, the estuary gains salt and becomes saltier. The increased average salinity in the estuary means the salt intrusion length is advancing further into the estuary as the estuary adjusts. This decreases the  $\partial\bar{s}/\partial x$  which leads to the stratification and exchange to decrease to its initial magnitude. This adjustment is applicable to regions where the estuary is sheltered from winds such as the Merrimack River estuary and when fluctuating winds over the adjacent coastal ocean is sufficiently strong enough to upwell the coastal pycnocline.

However, when an estuary adjusts very rapidly, the estuary is already in steady state by the end of the initial change in the exchange. Thus, fluctuating winds alter the stratification and the exchange. In the following section, a simple predictor of the adjustment time is used to determine which steady state estuarine dynamics discussed above are relevant for a range of estuarine and coastal conditions influenced by fluctuating winds.

### 4.6.1 Adjustment Time

When the along-estuary salt gradient has adjusted to the fluctuating winds, the estuary has reached its new steady state. In large estuaries, the time taken for the estuary to reach the new state is essentially the time taken for the along-estuary salt gradient to adjust to the increased vertical mixing. In smaller estuaries, the time taken for the estuary to reach the new steady state depends on the time taken for the initial decrease in the salt exchange to happen.

A simple adjustment predictor is used to examine when the salt intrusion length has adjusted and the estuary has reached its new steady state. Bowen and Geyer (2003) noted that the steady state salt intrusion length depends on the river discharge rate, thus the depth-averaged velocity,  $\bar{u}$  is the appropriate velocity scale to determine the adjustment time. The time to adjust to vertical mixing for exchange-dominated estuaries is

$$T_{adj} = \frac{L_{salt}}{6\bar{u}} \quad (4.18)$$

where  $L_{salt}$  is the salt intrusion length into the estuary and  $\bar{u}$  is velocity due to the river discharge rate, similar to MacCready (2007); Bowen and Geyer (2003). The use of  $\bar{u}$  is also supported in Kranenburg (1986); MacCready (1999). The numerical constant 6 is obtained when the equation governing the length of the estuarine salt intrusion are reduced to a 1<sup>st</sup> order linear ODE, in the limits of an exchange-dominated estuary as discussed in (MacCready, 2007, pp.2139-2140).

The salt intrusion length is determined from the numerical experiments as the distance that the  $30 \text{ g kg}^{-1}$  isohaline is located from the estuary mouth, and  $\bar{u} = (\text{river discharge})/(\text{sectional area of estuary})$ . The  $30 \text{ g kg}^{-1}$  isohaline is used to indicate the oceanic salinity. This prediction of the adjustment time is compared to the numerical model adjustment time, which is the time taken for the initial average salinity of the estuary to change by  $(1 - e^{-1})(\bar{s}_f - \bar{s}_i)$ , where  $\bar{s}_i$  and  $\bar{s}_f$  are the initial and final

cross-sectional averaged salinities across the estuary mouth.

This simple adjustment timescale for an exchange-dominated estuary is tested for fluctuating winds in the same estuarine and coastal conditions discussed in section 4.5.4. The adjustment times for these variations in the estuarine and coastal conditions are plotted in figure (4-9). Even with the simplification used, the predicted and numerical model adjustment times are mostly within a factor of 1/2 – 2 from the 1:1 proportionality line for the range of conditions modeled. However, there are some coastal and estuarine conditions where the adjustment time predicted are significantly different than those determined from the numerical model (Fig. 4-9). These outliers are discussed next.

In figure 4-9, the adjustment times from the numerical experiments are mostly larger than those predicted by our theory (Eq. 4.18). The larger adjustment times derived from the numerical experiments are likely due to the numerical experiments being configured as an exchange-dominated estuary, where the horizontal diffusion has little or no contribution to the exchange. While this is a reasonable assumption for large stratified estuaries like Chesapeake Bay, when the parameters governing the salt exchange, such as mixing, estuary depth, or estuary orientation are modified, the horizontal eddy diffusivity can play a larger role in transporting salt in the estuary.

When fluctuating winds in an estuary increase the steady state salt intrusion length (as discussed early in sec. 4.6), the inclusion of horizontal diffusivity can cause the salt intrusion to reach the new steady state length faster. When the state steady adjusts faster, the adjustment times derived from the numerical model is shorter, providing a better fit with theory predictions.

#### **4.6.2 Extension to other Estuaries**

The results discussed above were derived for wind-stress conditions typical of the East coast of US. In the East coast, the fluctuating winds are such that time-integrated

upwelling and down-welling wind-stress have similar magnitudes, so the time-averaged wind-stress amplitude is weak or zero (Austin and Lentz, 1999). However, there are regions where the time-integrated upwelling and down-welling wind-stress are not of similar magnitudes, so the time-averaged wind-stress amplitude is strong (Pickett and Schwing, 2006, their Fig.3). Two such regions examined are: (i) where the upwelling wind is followed by weak or cessation of wind, such as the West coast of US, and (ii) where the upwelling winds persist longer than the adjustment time of an estuary.

As the time-averaged wind-stress is increased towards upwelling, the numerical model shows the change in the along-estuary salt gradient is similar for all the three different types of wind forcings (Fig. 4-6H). This is because the change in the along-estuary salt gradient, is proportional to the change in the vertical eddy diffusivity (Eq. 4.17). To first order,  $K_V$  is proportional to the wind-stress amplitude, which remains the same for the three different wind forcing types.

There are other regions where an estuary orientation is oblique to the coast such as the Chesapeake Bay, Delaware Bay, and Long Island Sound. For the same freshwater fluxes, Garvine (2001) shows that the coastal plume (and thus the estuarine salt structure) varies with the orientation of the estuary. In the absence of winds, estuaries with negative orientation angle (Fig. 4-2) in steady state have a weak along-estuary salt gradient and are well-mixed. Thus for estuaries with negative orientations, wind-induced mixing in the estuary is not significant, and the coastal upwelling is significant in altering the salt exchange. The exchange salt flux,  $u's'$ , initially increases in magnitude when coastal upwelling brings deep salty water to the estuary mouth, but as the average estuarine salinity in the estuary becomes saltier, the along-estuary salt gradient decreases until the exchange salt flux is balanced by the depth-averaged salt flux (Fig. 4-6I), similar to the adjustment described for the base case with winds only in the coastal ocean (sec. 4.5.2).

In the absence of winds, estuaries with positive orientation angle (Fig. 4-2) in



steady state have a strong along-estuary salt gradient and a strong stratification. Thus, wind-induced mixing in the estuary is significant in altering the salt exchange. The wind-induced mixing initially reduces the magnitude of the exchange salt flux,  $u's'$ , but as the average estuarine salinity in the estuary becomes fresher, the along-estuary salt gradient increases until the exchange salt flux is balanced by the depth-averaged salt flux (Fig. 4-6I), similar to the adjustment described for the base case with winds both in the estuary and the coastal ocean (sec. 4.5.1).

**Residence Times** As the estuary adjusts to the fluctuating winds by changing its salt intrusion length, the average salinity of the estuary also changes (Fig. 4-5) to the extent we can ignore changes in the mean salinity at the estuary mouth. The change in the average salinity of the estuary indicates that the residence time of the estuary is also changing. When the  $\bar{s}$  is getting fresher, it indicates that freshwater is residing longer in the estuary.

When the residence time of an estuary increases, the fluvial pollutants carried into the estuary by the freshwater runoff from land also reside longer in the estuary, before being discharged and diluted in the coastal ocean. Thus, when weather-band fluctuations in the wind last longer than the adjustment timescales of an estuary, the fluctuating winds cause nutrients and pollutants to accumulate in the estuary, degrading the water quality.

## 4.7 Conclusions

On timescales longer than the adjustment time of an estuary, fluctuating winds influence the estuary by altering the salt intrusion length, while the stratification and exchange remain largely unchanged. Fluctuating winds in the estuary initially reduce the stratification and exchange, but the estuarine salinity becomes fresher, the along-estuary salt gradient increases. This brings the stratification and exchange back to

their initial magnitudes but reduced the salt intrusion length.

However, when the adjustment time is short enough that is comparable to the timescale of the initial change in the stratification and exchange, the fluctuating winds influence the new steady state stratification and the exchange of the estuary.

A adjustment timescale predictor was used to show when the fluctuating winds alter the steady state dynamics in an estuary by (i) altering the stratification, or (ii) altering the salt intrusion length.

**Table 4.1:** The range of parameters varied in the permutations of the numerical experiment.

Parameter	Range	Base Case
Wind-stress amplitude	0.05, 0.1, 0.2, 0.3 Pa	0.1 Pa
Wind-stress period	6, 10, 30 days	6 days
River discharge	$(0.2, 1.5, 2, 20) \times 10^3 \text{ m}^3\text{s}^{-1}$	$2 \times 10^3 \text{ m}^3\text{s}^{-1}$
Estuary thalweg depth	11, 30, 45 m	30 m
Coastal pycnocline depth	15, 30, 45 m	15 m
Estuary length	50, 150, 300 km	300 km
Well-mixed Estuary	$K_V = 1 \times 10^{-3} \text{ m}^2\text{s}^{-1}$	$K_V = 1 \times 10^{-5} \text{ m}^2\text{s}^{-1}$
Estuary angle	$-60^\circ, 0^\circ, +60^\circ$	$0^\circ$

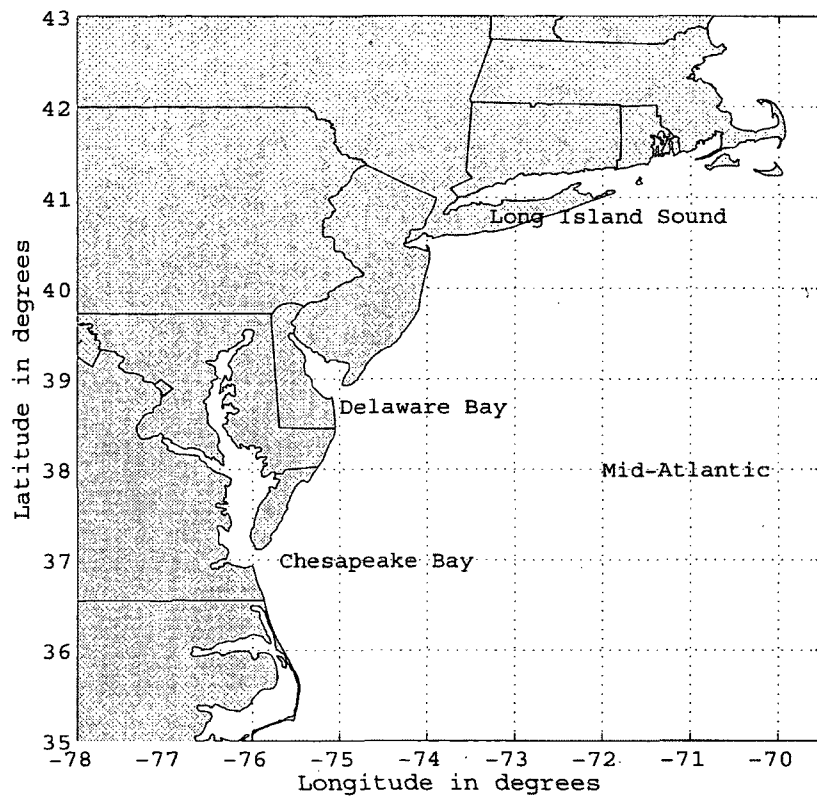


**Figure 4-1:** Our numerical experiments are modeled after the large estuaries and coastal ocean of the Mid-Atlantic Bight, including the Chesapeake Bay and Delaware Bay.

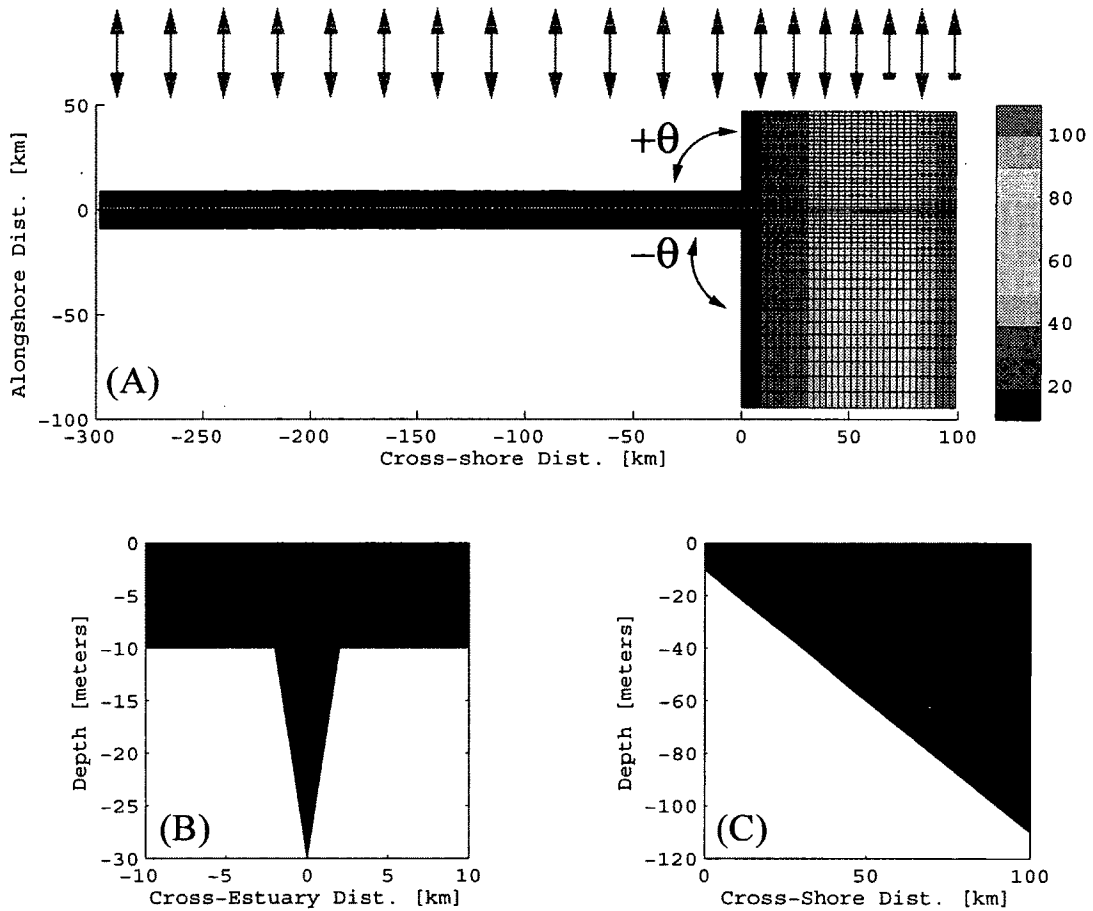


**Figure 4-2:** The numerical domain used in our experiments (A) the plan view of the numerical domain; colors indicate the depth and the lattice structure shows the depth grid points. The blue arrows show spatially uniform fluctuating winds in the estuary and the coastal ocean, and the red arrows show spatially uniform fluctuating wind only in the coastal ocean. (B) The cross-sectional view into the estuary mouth, and (C) the cross-shore view of the coastal ocean; black is water and white is estuary bottom.

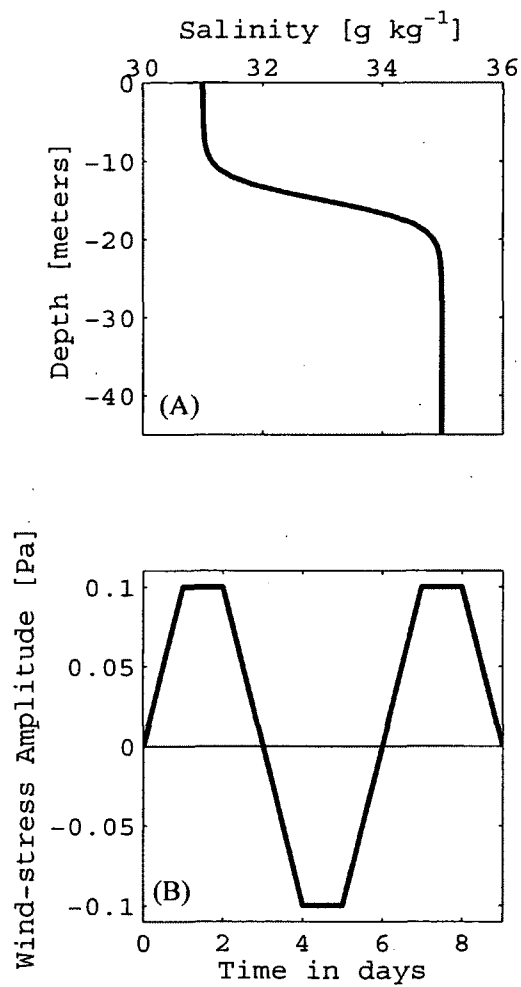


**Figure 4-3:** (A) The salinity profile for the coastal ocean in the base case numerical experiment. The profile represents summer conditions in the MAB. (B) The winds used in the base case numerical experiment. The winds ramp to maximum amplitude over a duration of a day. The winds are applied for a duration of 210 days, and has a time-averaged wind-stress amplitude of zero.

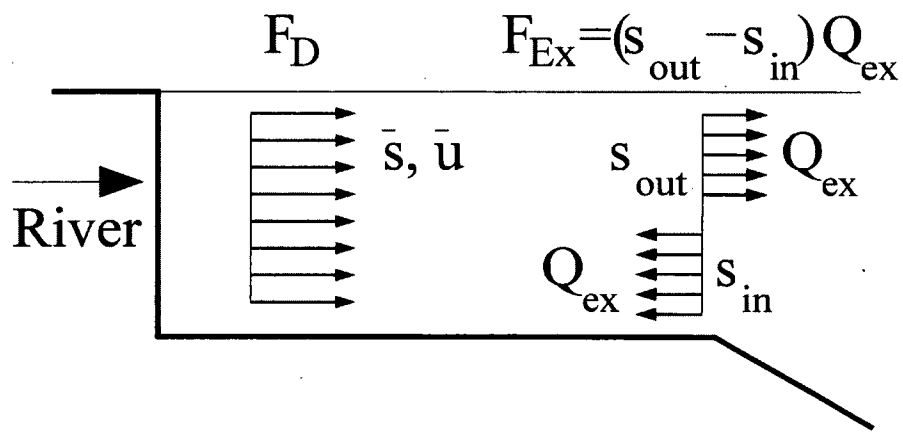


**Figure 4-4:** A cartoon of the along-estuary section. The salt exchange, i.e., net salt flux of the estuary is decomposed into two components; the depth-averaged salt flux,  $F_D$  and the exchange salt flux,  $F_{Ex}$ .

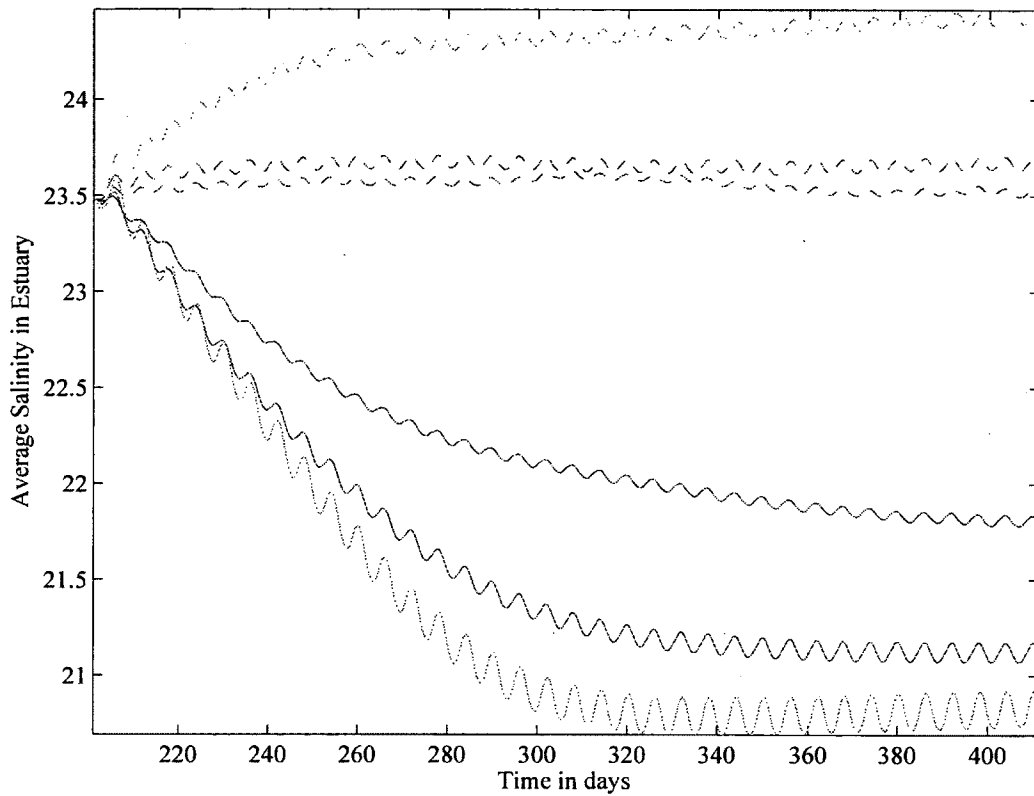


**Figure 4-5:** The tidally-averaged salt for the range of wind-stress amplitude in Table (4.1). The dotted lines are for winds only in coastal ocean and solid lines are winds on estuary and coastal ocean. The colored lines show the wind-stress for 0.05 Pa (red), 0.1 Pa (blue), 0.2 Pa (green). The influence of winds in the estuary shows a much larger change in average salinity than coastal winds alone. The fluctuations in the average salt are due the coastal winds fluctuating between upwelling and downwelling.



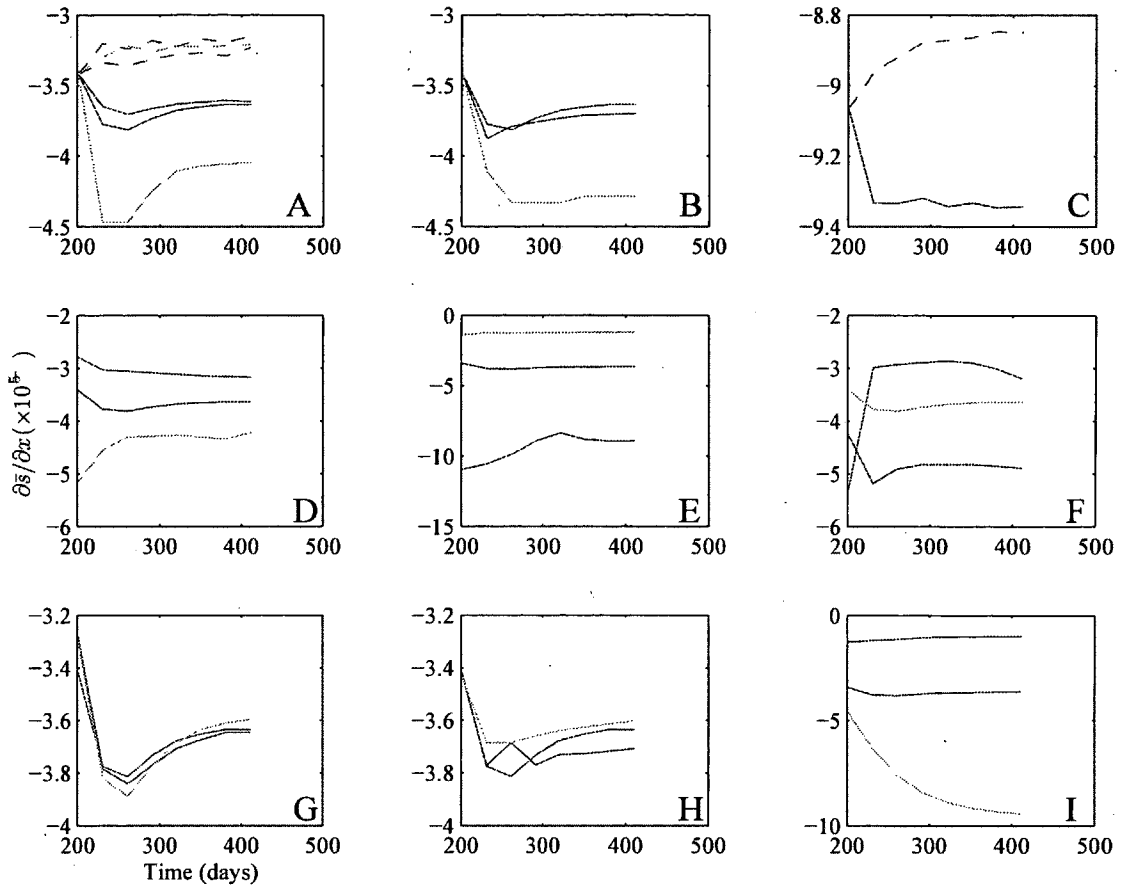


**Figure 4-6:** The along-estuary salt gradients ( $\times 10^{-5} \text{g kg}^{-1} \text{m}^{-1}$ ), when forced by fluctuating winds, as function of time. Solid line are winds applied both on estuary and coastal ocean, dashed lines are the winds applied only to the coastal ocean. (A) wind-stress amplitude (0.05Pa-red, 0.1Pa-blue, 0.2Pa-green), (B) wind-stress period (6day-red, 10day-blue, 30day-green), (C) well-mixed estuary (0.1Pa-red), (D) river discharge ( $200 \text{m}^3 \text{s}^{-1}$ -red,  $2 \times 10^3 \text{m}^3 \text{s}^{-1}$ -blue,  $20 \times 10^3 \text{m}^3 \text{s}^{-1}$ -green), (E) estuary thalweg depth (11m-red, 30m-blue, 45m-green), (F) estuary length (50km-red, 150km-blue, 300km-green), (G) coastal pycnocline depth (11m-red, 15m-blue, 45m-green), (H) time-integrated wind-stress amplitude (east-red, west-blue, steady-green), and (I) estuary orientation ( $-60^\circ$ -red,  $0^\circ$ -blue,  $60^\circ$ -green).

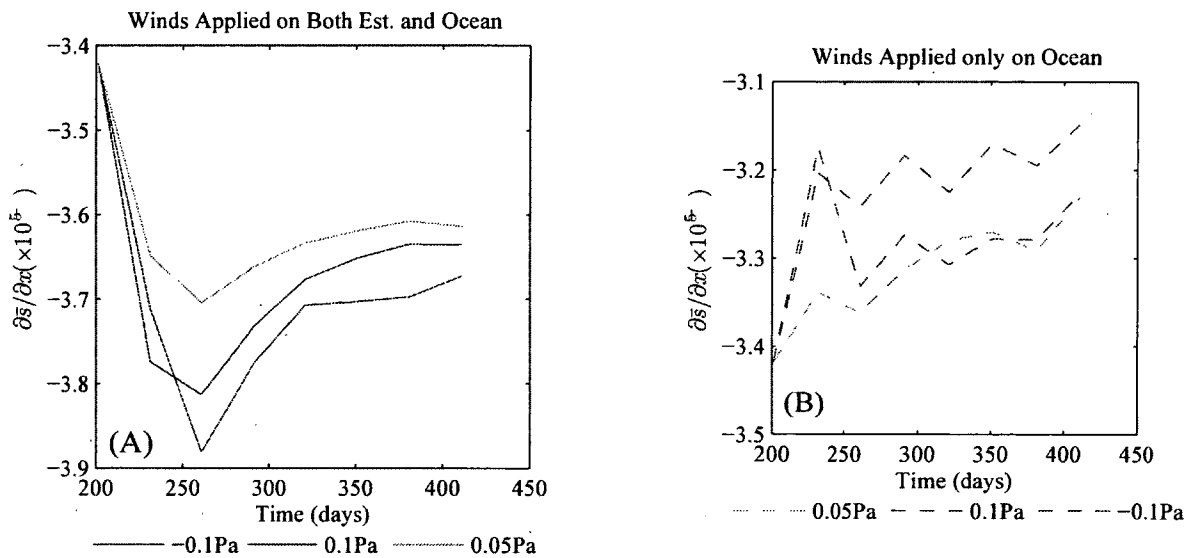


**Figure 4-7:** The evolution of the along-estuary salt gradient as a function of time. The starting phase of the fluctuating winds is upwelling when the legend label is positive, and down-welling when the legend label is negative. (A) Fluctuating winds applied both in estuary and coastal ocean for different wind-stress amplitude. (B) Fluctuating winds applied only in coastal ocean for different wind-stress amplitudes. The starting phase of the fluctuating has no significant influence on the adjustment.

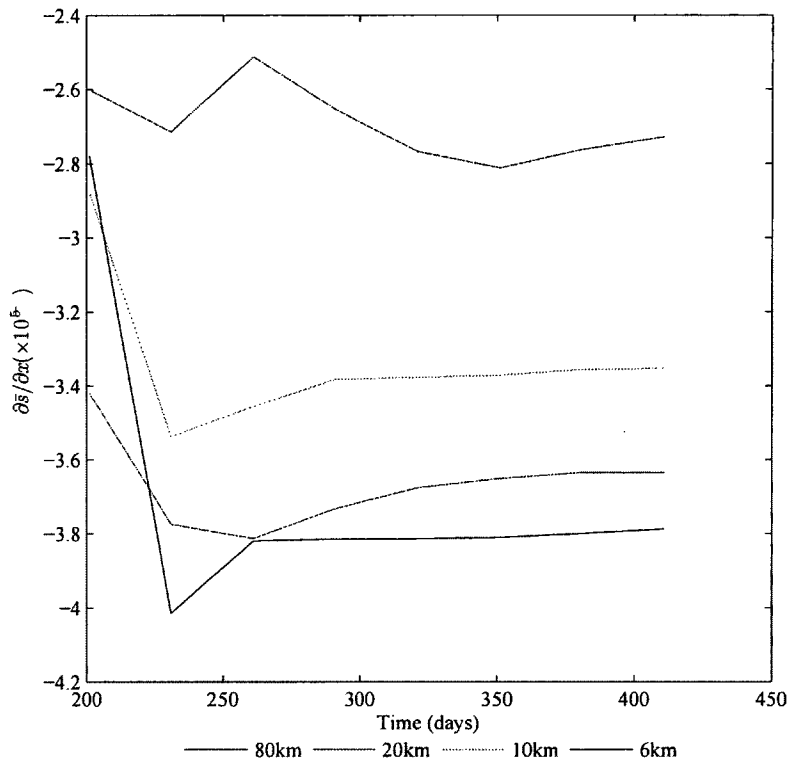


**Figure 4-8:** The evolution of the along-estuary salt gradient as function of time, for different estuary widths. The fluctuating winds are applied both in the estuary and the coastal ocean.

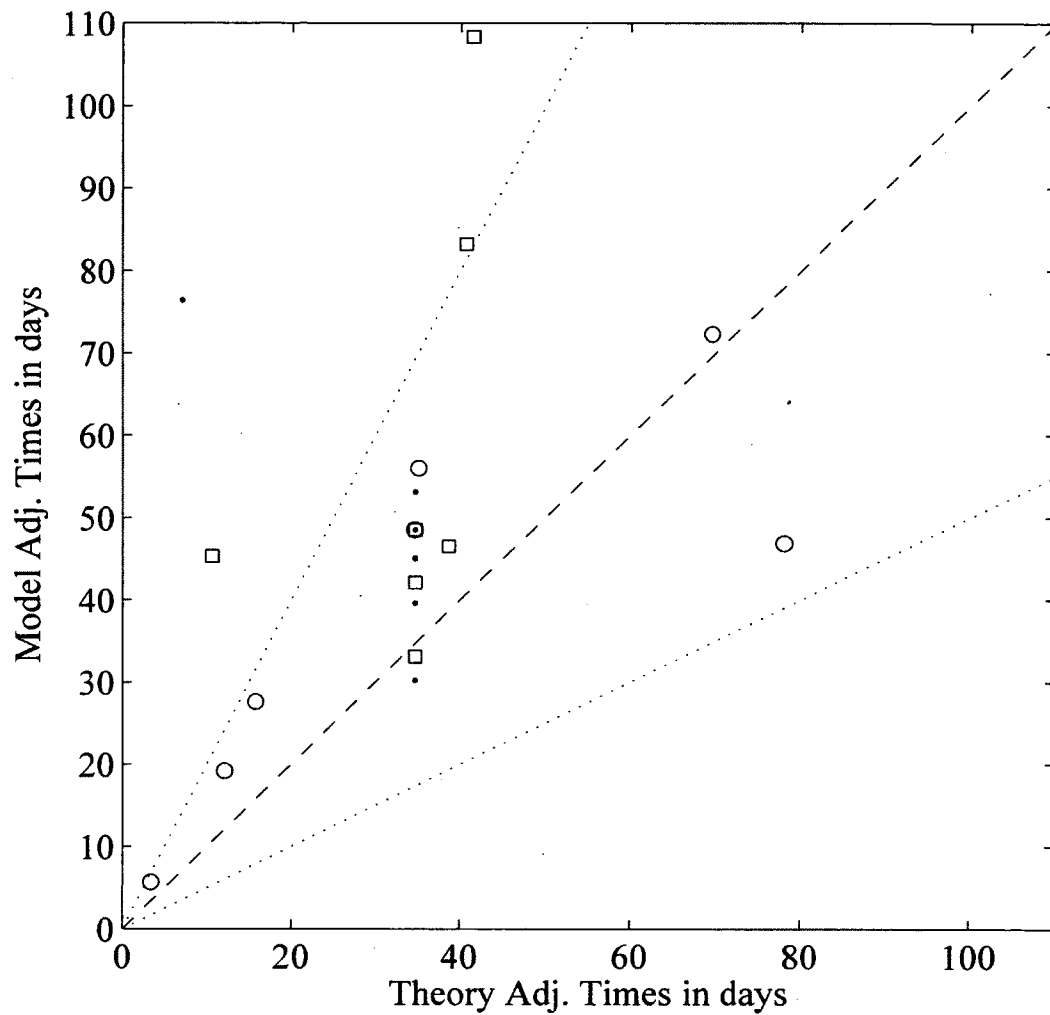


**Figure 4-9:** The adjustment times for the range of conditions in Table (4.1). The dotted lines show the 1:2 and 2:1 proportionality lines. The predictions of the adjustment times are in line with numerical experiments.

## Bibliography

- Alessi, C. A., S. J. Lentz, and J. A. Austin, 1996: Coastal Ocean Processes Inner-Shelf Study: Coastal and Moored Physical Oceanographic Measurements. *Woods Hole Oceanog. Inst. Tech. Rept.*, **WHOI-96-06 (-)**, 142.
- Austin, J., 2002: Estimating the mean ocean-bay exchange rate of the Chesapeake Bay. *Journal of Geophysical Research-Oceans*, **107 (C11)**, doi: 10.1029/2001JC001246.
- Austin, J. and S. Lentz, 1999: The Relationship Between Synoptic Weather Systems and Meteorological Forcing on the North Carolina Inner Shelf. *Journal of Geophysical Research-Oceans*, **104 (C8)**, 18 159–18 185.
- Bowen, M. and W. Geyer, 2003: Salt transport and the time-dependent salt balance of a partially stratified estuary. *Journal of Geophysical Research-Oceans*, **108 (C5)**, doi: 10.1029/2001JC001231.
- Cerco, C., M. Noel, and L. Linker, 2004: Managing for water clarity in Chesapeake Bay. *Journal of Environmental Engineering-ASCE*, **130 (6)**, 631–642, doi: 10.1061/(ASCE)0733-9372(2004)130:6(631).
- Das, P. and J. Middleton, 1997: Obliquely incident Poincare waves on a sloping continental shelf. *Journal of Physical Oceanography*, **27 (7)**, 1274–1285, doi: 10.1175/1520-0485(1997)027<1274:OIPWOA>2.0.CO;2.
- Dever, E. and S. Lentz, 1994: Heat and Salt Balances Over the Northern California Shelf in Winter and Spring. *Journal of Geophysical Research-Oceans*, **99 (C8)**, 16 001–16 017, doi: 10.1029/94JC01228.
- Fairall, C., E. Bradley, D. Rogers, J. Edson, and G. Young, 1996: Bulk parameterization of air-sea fluxes for Tropical Ocean Global Atmosphere Coupled Ocean Atmosphere Response Experiment. *Journal of Geophysical Research-Oceans*, **101 (C2)**, 3747–3764.
- Fong, D. and W. Geyer, 2001: Response of a River Plume During an Upwelling Favorable Wind Event. *Journal of Geophysical Research-Oceans*, **106 (C1)**, 1067–1084.
- Galperin, B., L. Kantha, S. Hassid, and A. Rosati, 1988: A Quasi-Equilibrium Turbulent Energy-Model For Geophysical Flows. *Journal of Atmospheric Sciences*, **45 (1)**, 55–62.

- Gan, H. and J. Allen, 2005: On Open Boundary Conditions for a Limited-Area Coastal Model off Oregon. Part 1: Response to Idealized Wind Forcing. *Ocean Modelling*, **8** (1-2), 115–133, doi: 10.1016/j.ocemod.2003.12.006.
- Garvine, R., 1999: Penetration of Buoyant Coastal Discharge onto the Continental Shelf: A Numerical Model Experiment. *Journal of Physical Oceanography*, **29** (8, Part 2), 1892–1909.
- Garvine, R., 2001: The impact of model configuration in studies of buoyant coastal discharge. *Journal of Marine Research*, **59** (2), 193–225, doi: 10.1357/002224001762882637.
- Guo, X. and A. Valle-Levinson, 2008: Wind effects on the lateral structure of density-driven circulation in Chesapeake Bay. *Continental Shelf Research*, **28** (17), 2450–2471, doi: 10.1016/j.csr.2008.06.008.
- Hansen, D. and M. Rattray, 1965: Gravitational circulation in straits and estuaries. *Journal of Marine Research*, **23**, 104–122.
- Hetland, R. and W. Geyer, 2004: An idealized study of the structure of long, partially mixed estuaries. *Journal of Physical Oceanography*, **34** (12), 2677–2691, doi: 10.1175/JPO2646.1.
- Kantha, L. and C. Clayson, 1994: An Improved Mixed-Layer Model for Geophysical Applications. *Journal of Geophysical Research-Oceans*, **99** (C12), 25 235–25 266.
- Kranenburg, C., 1986: A Time Scale For long-term salt Intrusion in Well-Mixed Estuaries. *Journal of Physical Oceanography*, **16** (7), 1329–1331.
- Lentz, S., M. Carr, and T. Herbers, 2001: Barotropic Tides on the North Carolina Shelf. *Journal of Physical Oceanography*, **31** (7), 1843–1859.
- MacCready, P., 1999: Estuarine adjustment to changes in river flow and tidal mixing. *Journal of Physical Oceanography*, **29** (4), 708–726, doi: 10.1175/1520-0485(1999)029<0708:EATCIR>2.0.CO;2.
- MacCready, P., 2007: Estuarine adjustment. *Journal of Physical Oceanography*, **37** (8), 2133–2145, doi: 10.1175/JPO3082.1.
- MacCready, P. and W. R. Geyer, 2010: Advances in Estuarine Physics. *Annual Review of Marine Science*, **2**, 35–58, doi: 10.1146/annurev-marine-120308-081015.
- Mellor, G. and T. Yamada, 1982: Development of a Turbulence Closure-Model for Geophysical Fluid Problems. *Reviews of Geophysics*, **20** (4), 851–875.
- Millero, F., R. Feistel, D. Wright, and T. McDougall, 2008: The composition of Standard Seawater and the definition of the Reference-Composition Salinity Scale. *Deep-Sea Research Part I-Oceanographic Research Papers*, **55** (1), 50–72, doi: 10.1016/j.dsr.2007.10.001.

- Officer, C., R. Biggs, J. Taft, L. Cronin, M. Tyler, and W. Boynton, 1984: Chesapeake Bay Anoxia-Origin, Development, and Significance. *Science*, **223 (4631)**, 22–27, doi: 10.1126/science.223.4631.22.
- Pickett, M. and F. Schwing, 2006: Evaluating upwelling estimates off the west coasts of North and South America. *Fisheries Oceanography*, **15 (3)**, 256–269, doi: 10.1111/j.1365-2419.2005.00400.x.
- Pringle, J. M. and E. P. Dever, 2009: Dynamics of Wind-Driven Upwelling and Relaxation between Monterey Bay and Point Arena: Local-, Regional-, and Gyre-Scale Controls. *Journal of Geophysical Research-oceans*, **114**.
- Rao, S., 2012: Wind Influence on the Interactions between Estuaries and the Coastal Ocean. *Ph.D dissertation, University of New Hampshire, Chapter 2, [In prep. for submission]*.
- Scully, M., 2010: The Importance of Climate Variability to Wind-Driven Modulation of Hypoxia in Chesapeake Bay. *Journal of Physical Oceanography*, **40 (6)**, 1435–1440, doi: 10.1175/2010JPO4321.1.
- Song, Y. and D. Haidvogel, 1994: A semi-implicit ocean circulation model using a generalized topography-following coordinate system. *Journal of Computational Physics*, **115 (1)**, 228–244.
- Stacey, M., S. Monismith, and J. Bureau, 1999: Observations of turbulence in a partially stratified estuary. *Journal of Physical Oceanography*, **29 (8, Part 2)**, 1950–1970, doi: 10.1175/1520-0485(1999)029<1950:OOTIAP>2.0.CO;2.
- Waldorf, B. W., J. L. Largier, S. Rennie, J. A. Austin, and G. C., 1995: Coastal Ocean Process (CoOP) Pilot Project Data Report: R/V Hatteras Shipboard Measurements. Underway, CTD and ADCP Data August 1994. *Scripps Inst. of Oceanog. Tech. Rept., SIO-95-29 (-)*, –.

# CHAPTER 5

## Conclusions

This thesis addresses how fluctuating winds alter the salt structure in the near-shore coastal ocean, the estuary, and to the net salt flux between these regions. In particular, these studies show how important the changes in one region are to setting the state of the adjacent region.

In chapter 2, idealized numerical experiments and field observations are used to examine the physics of an upwelled plume front after the coastal plume has upwelled and the upwelling winds stop or reverse. After the upwelling winds cease or reverse, the upwelled front moves shoreward as an ageostrophic buoyant gravity current for an inertial period (Csanady, 1971). The onshore movement of the upwelled front stops after the shoreward ageostrophic pressure gradient is balanced by the Coriolis force (Austin and Lentz, 2002). But, when the upwelling winds reverse to downwelling, the shoreward surface Ekman flow can force the upwelled front until the coast (Dale et al., 2008). In the absence of a nearby estuary, the return of the upwelled front to the coast brings back the less dense surface water, initially moved offshore during upwelling, to the coast as the upwelled isopycnals return to their pre-upwelling state. However, near estuaries, an estuarine plume can arrive along the coast, in the direction of a coastal Kelvin wave, from the source estuary (Garvine, 1999; Fong and Geyer, 2001) before the return of the upwelled front. This study shows when the time-integrated upwelling and downwelling wind stresses are comparable, there exists a region downwave of an estuary where the arrival of the plume in the nearshore region prevents the upwelled front from returning to the coast. This happens because the vertical stratification in the plume weakens during downwelling winds and allows vertical mixing, so the



weak cross-shore flow in the plume stops the front from returning to the coast. The spatial extent of this region along the coast is predicted and successfully tested against numerical experiments and field observations from the CoOP experiment at Duck, NC. The near-shore region predicted delimits the region most directly under the influence of the estuary, and where both the estuarine and coastal processes influence the nearshore water properties.

In chapter 3 and 4, the influence of fluctuating winds on the net salt flux of an estuary is examined. Winds can alter the net salt flux, salt structure, and circulation of an exchange-dominated estuary (Hansen and Rattray, 1965), which depends on the along-estuary salinity gradient and the vertical stratification in an estuary, which are ultimately set by the freshwater inflow, oceanic salinity and the vertical mixing in the estuary (Hansen and Rattray, 1965; MacCready, 1999, 2007; Bowen and Geyer, 2003). Observations of wind forcing along the coast show fluctuations in the wind, and our study examines how these fluctuating winds influence the estuary. This improves our understanding of wind influence beyond the separate upwelling and down-welling winds (Austin and Lentz, 2002; Hansen and Rattray, 1965). Our analyses focus on two timescales of fluctuating winds. The first timescale is much shorter than the time taken for the estuary to adjust; this is useful in understanding how the fluctuating winds initially alter the net salt flux of an estuary, i.e., does the estuary gain or lose salt due to fluctuating winds? The second timescale is similar to the time taken for the estuary to adjust; this helps us understand how the estuary adjusts, to the initial change in the net salt flux due to fluctuating winds, and returns to steady state.

The influence on the net salt flux is examined by first simplifying it into depth-averaged salt flux and exchange salt flux. For timescales shorter than the adjustment time, the fluctuating winds influence the estuary by altering the exchange salt flux (a product of the salinity difference entering and leaving the estuary, and the volume exchange flux); the depth-averaged salt flux does not change because the average

salinity in the estuary adjusts on a much longer timescale. The change in the exchange salt flux is caused by the changes in the salinity leaving the estuary (due to wind-induced estuarine mixing) and changes in the salinity entering the estuary (due to coastal upwelling and down-welling), and not by changes in the volume exchange flux (which adjusts on a much longer timescale). The difference in the salinity leaving and entering the estuary is the stratification of the estuary.

When the estuary is stratified, wind-induced mixing in the estuary has a larger influence on the net salt flux than the vertical displacement of the coastal pycnocline due to fluctuating winds. When the estuary is well mixed, the vertical displacement of the coastal pycnocline due to fluctuating winds has a larger influence on the net salt flux than wind-induced mixing. When the fluctuating winds in the coastal ocean move the coastal pycnocline above its initial depth, the ocean adds salt to the estuary, but when the coastal pycnocline is moved below its initial depth, the ocean removes salt from the estuary.

After the initial response of the fluctuating winds on the net salt flux, the estuary starts to adjust towards its new steady state. Over the time taken for the estuary to adjust to the fluctuating winds, the net salt flux must return to zero. Over the adjustment time, the estuary adjusts by altering its salt intrusion length. The changes in the salt intrusion length are determined by whether the initial response of the estuary is to gain or lose salt. If the estuary loses salt, the interior of the estuary becomes fresher, thus the salt intrusion is pushed towards the ocean. This occurs when the estuary is stratified and wind-induced mixing is significant. If the estuary gains salt, the interior of the estuary becomes saltier, thus the salt intrusion is pushed farther into the estuary. This occurs when the estuary is well mixed and only coastal upwelling and down-welling influence the net salt flux.

The consequence of changing the salt intrusion length is that the along-estuary salt gradient is altered. The changes in the along-estuary salt gradient as the estuary

adjusts cause the exchange salt flux and the stratification (initially altered by fluctuating winds) to return to its initial magnitude. This is interesting because we expect wind mixing to destroy the stratification, but over timescales comparable to the adjustment time of the estuary, the fluctuating winds work to restore the stratification.

### 5.0.1 Future Direction of This Study

The next step in our study would be to test our findings with field observations. When fluctuating winds influence the estuary-ocean system for timescale much shorter than the adjustment time of the estuary, the important parameters are the stratification of the estuary and the volume exchange flux. We expect the stratification to change and the volume exchange to remain constant. For timescales longer than the adjustment time of the estuary, the estuary restores the stratification and alters the salt intrusion length. Thus, the important parameters to measure in the field would be the stratification in the estuary, the volume exchange flux, and the salt intrusion length.

The stratification of the estuary should be estimated by; (i) CT profiles casts across the estuary mouth, and (ii) CT profile casts along the estuary channel. This should be done on a weekly basis, because the time required for the initial change in the exchange salt flux due to fluctuating winds is determined by the vertical salt diffusion timescale (which is 2-4 days for an estuary with mean depth of 10m). The observations along these transects would provide a good estimate of the stratification in the estuary, which can help determine if the wind-induced mixing in the estuary is important. Furthermore, the cross-estuary transect would provide an estimate of how the wind-driven coastal ocean alters the salinity entering the estuary. The observations along the estuary can be used to determine the salt intrusion length. The weekly transects across-estuary and along-estuary can be used to estimate the mean salinity of the estuary. This time-series of the mean salinity can be used to

estimate the volume exchange (Austin, 2002).

These above observations can be used to estimate the changes in the exchange salt flux when forced by fluctuating winds. For timescale shorter than the adjustment, we can estimate the time-series of the exchange salt flux, the stratification and the volume exchange flux. As the estuary adjusts, these observations would allow us to observe the stratification being restored as the salt intrusion length is altered. This approach to observing changes in estuary due to fluctuating winds is valid as long as the volume exchange flux is not altered by any other forcings. The changes in the river discharge can significantly alter the volume exchange flux, so the experiment would be best conducted when river discharge fluctuations are small. The long-term mean stream flow, e.g., stream flow into Chesapeake Bay from USGS observations, suggests that the changes in the river discharge are smallest between months of August to December.

**Improvements to Modeling** The numerics used in our numerical experiment do a good job of resolving the physics related to the influence of wind variability on the estuary and the coastal ocean, such as ensuring that the southern boundary conditions do not alter the interior of the model domain. However, the results from our idealized study are less robust to bottom topography, especially in the estuaries. This can be improved by addressing the complex bathymetry that is associated with real estuaries, in particular the along-estuary variation in the bathymetry. This includes decreasing the depth of the estuary as we approach the head of the estuary, and considering that in some estuaries the deep channels do not run continuously until the head of the estuary, but are instead several disjointed deep channels.

## Bibliography

- Austin, J., 2002: Estimating the mean ocean-bay exchange rate of the Chesapeake Bay. *Journal of Geophysical Research-Oceans*, **107** (C11), doi: 10.1029/2001JC001246.
- Austin, J. and S. Lentz, 2002: The Inner Shelf Response to Wind-Driven Upwelling and Downwelling. *Journal of Physical Oceanography*, **32** (7), 2171–2193.
- Bowen, M. and W. Geyer, 2003: Salt transport and the time-dependent salt balance of a partially stratified estuary. *Journal of Geophysical Research-Oceans*, **108** (C5), doi: 10.1029/2001JC001231.
- Csanady, G., 1971: On the Equilibrium Shape of the Thermocline in a Shore Zone. *Journal of Physical Oceanography*, **1** (4), 263–270.
- Dale, A. C., J. A. Barth, M. D. Levine, and J. A. Austin, 2008: Observations of Mixed Layer Restratification by Onshore Surface Transport Following Wind Reversal in a Coastal Upwelling Region. *Journal of Geophysical Research-Oceans*, **113** (C1), doi: 10.1029/2007JC004128.
- Fong, D. and W. Geyer, 2001: Response of a River Plume During an Upwelling Favorable Wind Event. *Journal of Geophysical Research-Oceans*, **106** (C1), 1067–1084.
- Garvine, R., 1999: Penetration of Buoyant Coastal Discharge onto the Continental Shelf: A Numerical Model Experiment. *Journal of Physical Oceanography*, **29** (8, Part 2), 1892–1909.
- Hansen, D. and M. Rattray, 1965: Gravitational circulation in straits and estuaries. *Journal of Marine Research*, **23**, 104–122.
- MacCready, P., 1999: Estuarine adjustment to changes in river flow and tidal mixing. *Journal of Physical Oceanography*, **29** (4), 708–726, doi: 10.1175/1520-0485(1999)029<0708:EATCIR.2.0.CO;2.
- MacCready, P., 2007: Estuarine adjustment. *Journal of Physical Oceanography*, **37** (8), 2133–2145, doi: 10.1175/JPO3082.1.
- Rao, S., 2012: Wind Influence on the Interactions between Estuaries and the Coastal Ocean. *Ph.D dissertation, University of New Hampshire, Chapter 2, [In prep. for submission]*.